Master's Theses and Capstones

Student Scholarship

Spring 2007

I Complexation of iron(II), cobalt(II), nickel(II) and copper(II) by hexadentate tripodal aminopyridyl chelators II Binding preferences for zinc(II) relative to nickel(II) and copper(II) in novel tetradentate aminopyridyl chelators

Matthew Lloyd Childers
University of New Hampshire, Durham

Follow this and additional works at: https://scholars.unh.edu/thesis

I. COMPLEXATION OF FE(II), CO(II), NI(II) AND CU(II) BY HEXADENTATE

TRIPODAL AMINOPYRIDYL CHELATORS II. BINDING PREFERENCES FOR

ZN(II) RELATIVE TO NI(II) AND CU(II) IN NOVEL TETRADENTATE

AMINOPYRIDYL CHELATORS

BY

MATTHEW LLOYD CHILDERS

B.S., University of North Carolina at Wilmington, 2002

THESIS

Submitted to the University of New Hampshire
in Partial Fulfillment of
the Requirement for the Degree for

Master of Science

in

Chemisrty

May, 2007

UMI Number: 1443601

INFORMATION TO USERS

The quality of this reproduction is dependent upon the quality of the copy submitted. Broken or indistinct print, colored or poor quality illustrations and photographs, print bleed-through, substandard margins, and improper alignment can adversely affect reproduction.

In the unlikely event that the author did not send a complete manuscript and there are missing pages, these will be noted. Also, if unauthorized copyright material had to be removed, a note will indicate the deletion.

UMI®
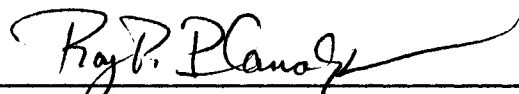
UMI Microform 1443601
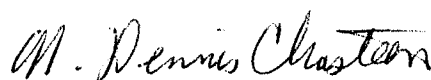
This thesis has been examined and approved.

Thesis Director, Roy P. Planalp,
Associate Professor of Chemistry

N. Dennis Chasteen
Professor of Chemistry

Vernon Reinhold,
Professor of Chemistry

April 9, 2007
Date

DEDICATION

To my parents,

Emily and Gary Childers

To my grandparents,

Elsie and Lloyd Childers and Ruby and William Wallace

To my sister,

Carrie Godwin

ACKNOWLDEGEMENTS

I would like to thank my advisor, Dr. Roy Planalp for his guidance and patience during my time at UNH. While in his research group I have grown as a scientist and enjoyed working for someone who I can call a friend.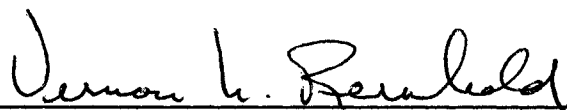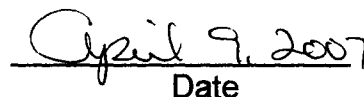 I would also like to thank Dr. Edward Wong for always smiling as he walked down the hall and showing an interest, not only in my research, but also in my life off campus. Also, I would like to thank my committee members Dr. N. Dennis Chasteen and Dr. Vernon Reinhold. I would like to acknowledge the dedicated professors in the chemistry department. I am grateful for all individuals who have educated, trained or helped me over the years. This includes, but is not limited to Cindi Rohwer, Peggy Torch, Kristin McFarlane, Bob Constantine, Amy Lindsay, Kathy Gallagher, the UIC staff and my fellow graduate students.

I am grateful for the support from my family and friends. My Mom and Dad: who have done nothing but support me and encourage me to do my best and enjoy doing what I'm doing. I couldn't have done this without them. My Sister: for being a great sister. Kaleen: for being my best friend, for always making me happy and for putting up with me being me. Dan: for being a great labmate and a better friend. Jim: for being a great friend while we became accustomed to life in New England together. All of my friends: who were always interested in what I was doing even if they didn't understand it. I couldn't have done this without you.

iv

TABLE OF CONTENTS

vii

LIST OF TABLES

x

LIST OF FIGURES

Figures   **Page**

xi

LIST OF SCHEMES

LIST OF ABBREVIATIONS

Abbreviation	Name/Definition
Δ_o	splitting energy between the t_{2g} and e_g^* orbitals in an octahedral environment
τ	value used to compare square-pyramidal and trigonal-bipyramidal geometries
Φ	twist angle
α	bite angle
ν	wavenumber
ε	molar absorptivity
MLCT	metal-to-ligand charge-transfer
LS	low spin
HS	high spin
C_{4v}	term for square-pyramidal
D_{3h}	term for trigonal bipyramidal
py	pyridine
LFSE	ligand filed stabilization energy
ppm	parts per million
VT NMR	variable temperature NMR
ESI-MS	electrospray mass spectrometry
T_d	tetrahedral
O_h	octahedral
$L^1 - L^4$	tach-x-Mepyr ($x = 3 - 6$)

Abbreviation	Name/Definition
L^5	tach-6-MeOpyr
L^6	bispicpn
L^7	bis6Mepicpn
L^8	bpdan
tach-x-Mepyr	N,N',N''-tris(x-Me-2-pyridylmethyl)-cis, cis-1,3,5-triaminocyclohexane
tach-6-MeOpyr	N,N',N''-tris(6-MeO-2-pyridylmethyl)-cis, cis-1,3,5-triaminocyclohexane
bispicpn	1,7-bis(2-pyridyl)-2,6-diazaheptane (L^6)
bis6Mepicpn	1,7-bis(6-methyl-2-pyridyl)-2,6-diazaheptane (L^7)
bpdan	1,9-bis(2-pyridyl)-3,7-diazanonane (L^8)
tptcd	1,4,7-tris(2-pyridylmethyl)-1,4,7-triazacyclononane
tptcn	1,5,9-tris(2-pyridylmethyl)-1,5,9-triazacyclododecane
lbptcn	1-[(6-methyl-2-pyridinyl)methyl]-4,7-bis(2-pyridinylmethyl)-1,4,7-triazacyclononane
tpen	N,N,N',N'-tetrakis(2-pyridylmethyl)ethylenediamine
ampy	2-(aminomethyl)-pyridine
blbpen	N,N'-bis(6-methyl-2-pyridylmethyl)-N,N'-bis(2-pyridylmethyl)ethane-1,2-diamine
(N-Me)$_3$-tachpyr	N,N',N''-trimethyl-N,N',N''-tris(2-pyridylmethyl)-1,3,5-triaminocyclohexane
tachpyrMe-trisimine	N,N',N''-tris(1-pyridin-2-yl-ethylidene)-tach
trenpyr-trisimine	N,N',N''-tris-(2-pyridylmethyl)-tren
trenpyrMe-trisimine	N,N',N''-tris(1-pyridin-2-yl-ethylidene)-tren
tachIM-trisimine	N,N',N''-tris-(1-methyl-1H-imidazol-2-ylmethylene)-tach
bipy	2,2'-bipyridine

Abbreviation	Name/Definition
phen	1,10-phenanthroline
bpdo	1,8-bis(2-pyridyl)-3,6-diazaoctane
pdan	N,N'-dimethyl-N,N'-bis[2-(2-pyridylethyl)]propylenediamine
bispicen	N,N'-bis(2-pyridinylmethyl)ethylenediamine
bis6Mepicen	N,N'-bis(6-methyl-2-pyridylmethyl)ethylenediamine
(N-Me)$_2$bispicpn	N,N'-dimethyl-N,N'-bis(2-pyridylmethyl)propylenediamine

ABSTRACT

I. COMPLEXATION OF FE(II), CO(II), NI(II) AND CU(II) BY HEXADENTATE TRIPODAL AMINOPYRIDYL CHELATORS II. BINDING PREFERENCES FOR ZN(II) RELATIVE TO NI(II) AND CU(II) IN NOVEL TETRADENTATE AMINOPYRIDYL CHELATORS

by

Matthew Lloyd Childers

University of New Hampshire, May, 2007

<u>Chapter I</u>

Effects of pyridyl-ring alkylation on complexation of Fe(II), Co(II), Ni(II) and Cu(II) by chelators based on cis,cis-1,3,5-triaminocyclohexane (tach) have been studied. The chelators studied are derivatives of tachpyr, where the ring substituents are 3-Me, 4-Me, 5-Me, 6-Me or 6-MeO (tach-x-Rpyr). Divalent complexes were synthesized for most combinations of the 4 metals and 5 chelators. Their bonding and structure were analyzed by UV/Vis/NIR spectroscopy, magnetic moment determination and single crystal X-ray crystallography. Steric repulsions between the 6-substituents result in substantially weakened metal-ligand interaction. Effects of these repulsions

xviii

include bond angle and length distortions, decrease of coordination number to five, shifts of d-d electronic transitions to lower energies and spin-free complexes of the bound metal ion.

Chapter II

Effects of iron-mediated oxidative dehydrogenation on tachpyr and derivatives were studied. Relative rates of iron-mediated oxidation were established for tachpyr and its 3-substituted derivatives as $[Fe(tach-3-Mepyr)]^{2+} >$ $[Fe(tachpyr)]^{2+} > [Fe(tach-3-MeOpyr)]^{2+}$ while no oxidation was seen for $[Fe(tach-6-Mepyr)]^{2+}$. The affinity of partially oxidized tachpyr derivatives over unoxidized derivatives towards Fe(II) was demonstrated. The lability of oxidized tachpyr derivatives was studied in an aerobic environment. Fully oxidized (trisimine) complexes were shown to be labile while partially oxidized (bisimine) complexes were determined to be inert.

Chapter III

A series of tetradentate aminopyridyl ligands was synthesized in an attempt at developing a chelator that would bind in a four-coordinate (tetrahedral) fashion and possess zinc selectivity. The resulting 1,3-diaminopropane (pn) based chelators were complexed with divalent Ni, Cu and Zn and their complexes were analyzed by UV/Vis/NIR, IR and NMR spectroscopy as well as single-crystal X-ray crystallography. It was determined that methylation of the pyridine rings at the 6-position had a greater effect on ligand affinity towards Ni(II) than homologation of the aminopyridyl arms. The crystal structures of all

the Zn(II) complexes showed the metal center to be six-coordinate with a nitrate anion bound in a bidentate fashion. However, in solution the zinc complexes showed signs of lower coordination numbers of either 4 or 5.

GENERAL INTRODUCTION

This thesis is divided into three separate chapters: I) Structural and Electronic Properties of Fe(II), Co(II), Ni(II) and Cu(II) Complexes of Pyridine-Ring Alkylated Hexadentate Aminopyridyl Ligands; II) Iron-Mediated Oxidative Dehydrogenation of Tachpyr and Tachpyr Derivatives: Correlating Biological Effects with Metal-Binding Chemistry; and III) Structural and Electronic Properties of Ni(II), Cu(II) and Zn(II) Complexes of Linear, Tetradentate, Aminopyridyl Ligands: Towards Zn(II) Selectivity. The first two chapters go with the first part of the title while the third chapter is responsible for the second part of the title. Due to the diverse nature of the material covered, each chapter is self-contained with its own introduction, results and discussion and conclusion.

1

STRUCTURAL AND ELECTRONIC PROPERTIES OF FE(II), CO(II), NI(II) AND CU(II) COMPLEXES OF PYRIDINE-RING ALKYLATED HEXADENTATE AMINOPYRIDYL LIGANDS

Introduction

Ligands that are preorganized or predisposed to bind metal ions form particularly thermodynamically or kinetically stable complexes.[1-4] The hexadentate amino/pyridyl chelator tachpyr (N,N',N''-tris(2-pyridylmethyl)-cis,cis-1,3,5-triaminocyclohexane), based on the tripodal framework tach (cis-cis-1,3,5-triaminocyclohexane), has been shown to readily complex divalent 3d transition metal ions.[5-8] Tachpyr makes metal complexes by a ring flip from an open, all-equatorial conformation, to a closed, all-axial conformation (**Scheme 1.1**), encapsulating metal ions ranging in size from Ga(III) (six-coordinate ionic radius of 0.76 Å[9,10]) to Hg(II) (ionic radius of 1.16 Å).[6,8,11,12]
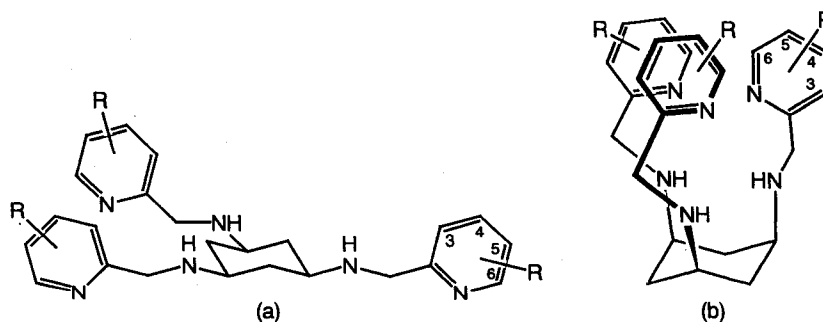
$L^1 - L^4$, R = Me, tach-x-Mepyr (x = 3 – 6)
L^5, R = MeO, tach-x-MeOPyr (x = 6)
Scheme 1.1. Structures and labeling of tach-x-Rpyr: open (a) and closed (b) conformation

2

Tachpyr and its derivatives are under consideration as chemotherapeutic agents.[13-15] Tachpyr is strongly cytotoxic to a variety of tumor cells as seen by an IC_{50} of 4.8 μM toward cultured bladder tumor cells. We have recently shown that it binds Zn(II) and Fe(II) in cells, and that the binding of Fe(II) in vitro is accompanied by redox processes.[16] We therefore pursue the hypotheses that tachpyr may affect cells by causing deprivation of essential biometals and/or that the complexes formed may go on to catalyze oxidative damage, particularly those of redox-active bioavailable metals such as Fe and Cu.
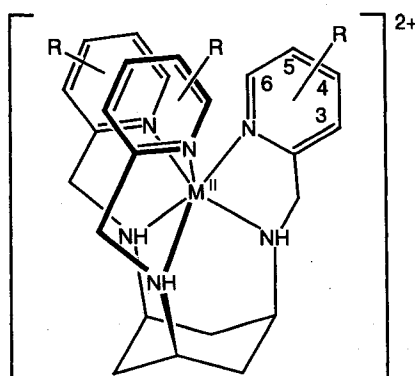
M	L^1 tach-3-Mepyr	L^2 tach-4-Mepyr	L^3 tach-5-Mepyr	L^4 tach-6-Mepyr	L^5 tach-6-MeOpyr
Fe(II)[a,b]	1a	1b	1c	1d	1e
Co(II)[c]	2a	2b	2c	-	-
Ni(II)[a]	3a	3b	3c	3d	3e
Cu(II)[a]	4a	4b	4c	4d[d]	4e[d]

[a]$X = ClO_4^-$; [b]$X = Cl^-$; [c]$X = NO_3^-$; [d]previously reported

Scheme 1.2. Structures and numbering of the metal complexes of tach-*x*-Rpyr

Study of pyridyl-ring-alkylated tachpyr variants appeared appropriate in order to change electronic properties or induce steric hindrance in tachpyr and its derivatives. Herein we focus on the ability of such derivatives to bind divalent biometals as seen from coordination geometries and the electronic properties of

3

$[M^{II}(\text{tach-}x\text{-Rpyr})]^{2+}$ (M = Fe, Co, Ni, Cu; R = Me where x = 3 – 6 and R = MeO where x = 6) (**Scheme 1.2**). The electronic structure in solution has been studied by spectroscopy, and solid-state structures have been studied by single-crystal X-ray crystallography. In toxicity studies, tach-3-Mepyr and tach-6-Mepyr emerged as most interesting, tach-3-Mepyr due to more rapid onset of toxicity and tach-6-Mepyr due to lack of toxicity, hence, these have received greater scrutiny in the present work.
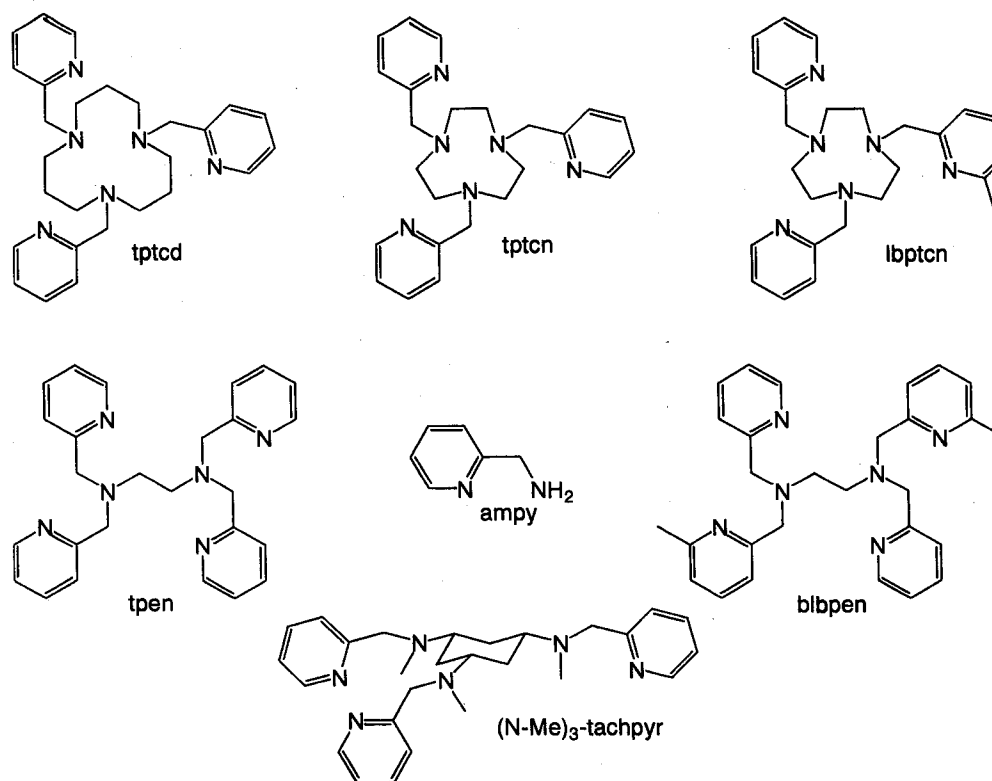
Scheme 1.3. Chelators for comparison herein

Results

Electronic Studies

To examine metal-complex structures in solution and assess effects of pyridyl substituents at various positions, the UV-Vis/Near IR spectra of the Fe(II),

4

Co(II), Ni(II) and Cu(II) complexes were measured, assigned and compared with other amino/pyridyl-metal compounds (**Tables 1.1 – 1.4**).

Iron (II). The Fe(II) complexes **1a – c** exhibit a large absorption band at 22600 – 23100 cm^{-1} with a weak, low-energy shoulder at 17400 – 18200 cm^{-1}. The intense absorption was assigned as a metal-to-ligand charge-transfer (MLCT) band. This band is due to a $d\pi - p\pi^*$ transition and is typical of low-spin (LS) Fe(II) complexes with π-acceptor ligands.[17-20] The MLCT appears to mask all d – d transitions except the low-energy shoulder that is generally assigned as the $^1A_{1g} \rightarrow {}^1T_{1g}$ transition in LS Fe(II) complexes.[18,21]

Fe(II) complexes **1d** and **1e** contain a considerably weaker MLCT band that has blue-shifted to around 28500 cm^{-1} with a slight shoulder to low-energy. The weaker MLCT band is typical for high-spin (HS) Fe(II) complexes.[18] Additionally, there is a very weak absorption at 11100 – 11700 cm^{-1} that was assigned as the $^5T_{2g} \rightarrow {}^5E_g$ transition that is seen in HS Fe(II) complexes.[17,18,20]

Table 1.1. Spectral data for **1a** – **e** and other Fe(II) amino/pyridyl complexes

Complex	v (cm^{-1})[a]	Assignments	Δ_0 (cm^{-1})	color
[FeL^1]Cl$_2$	22700 (7000)	MLCT	-	bronze
	18200 sh (290)	$^1A_{1g} \rightarrow {}^1T_{1g}$		
[FeL^2]Cl$_2$	23100 (6600)	MLCT	-	bronze
	17800 sh (95)	$^1A_{1g} \rightarrow {}^1T_{1g}$		
[FeL^3]Cl$_2$	22600 (4200)	MLCT	-	bronze
	17400 sh (500)	$^1A_{1g} \rightarrow {}^1T_{1g}$		
[FeL^4](ClO$_4$)$_2$	28800 (650)	MLCT		
	19600 sh (36.6)	unassigned	11700	red-brown
	11700 (9.4)	$^5T_{2g} \rightarrow {}^5E_g$		
[FeL^5]Cl$_2$	28200 (790)	MLCT	11100	yellow
	11100 (5.0)	$^5T_{2g} \rightarrow {}^5E_g$		
[Fe(tachpyr)]$^{2+}$	23100 (5500)	MLCT	-	bronze
	18400 (330)	$^1A_{1g} \rightarrow {}^1T_{1g}$		
[Fe(tptcn)]$^{2+19}$	23100 (12400)	MLCT	-	red
[Fe(tptcd)]$^{2+22}$	27600 (1270)	MLCT	11500	lt. brown
	11500 (9)	$^5T_{2g} \rightarrow {}^5E_g$		

^{a}spectra for complexes **1a** – **e** were measured in MeCN

Cobalt (II). Complexes **2a** – **c** produced spectra typical of HS Co(II) with two absorptions at 21500 – 21000 cm^{-1} and 10700 – 10500 cm^{-1} assigned as the $^4T_{1g} \rightarrow {}^4T_{1g}$ and $^4T_{1g} \rightarrow {}^4T_{2g}$ transitions, respectively. A shoulder was observed on the high-energy transition and has been attributed to spin-orbit splitting of the $^4T_{1g}$ state (**Table 1.2**).[23]

Table 1.2. Spectral data for **2a** – **c** and other Co(II) amino/pyridyl complexes

Complex	v (cm^{-1})[a]	Assignments	Δ_0 (cm^{-1})	color
[CoL^1](NO$_3$)$_2$	10660 (8.0)	$^4T_{1g} \rightarrow {}^4T_{2g}$		
	18430 sh (27)		-	beige
	21460 (73)	$^4T_{1g} \rightarrow {}^4T_{1g}$		
[CoL^2](NO$_3$)$_2$	10540 (12)	$^4T_{1g} \rightarrow {}^4T_{2g}$		
	18430 sh (14)		-	beige
	21300 (57)	$^4T_{1g} \rightarrow {}^4T_{1g}$		
[CoL^3](NO$_3$)$_2$	10460 (5.5)	$^4T_{1g} \rightarrow {}^4T_{2g}$		
	18050 sh (19)		-	beige
	21050 (61)	$^4T_{1g} \rightarrow {}^4T_{1g}$		
[Co(tachpyr)]$^{2+}$	10787 (3.8)	$^4T_{1g} \rightarrow {}^4T_{2g}$		
	18315 sh		-	brown
	21552 (49)	$^4T_{1g} \rightarrow {}^4T_{1g}$		

^{a}spectra for complexes **2a** – **c** were measured in MeOH

6

Nickel (II). The Ni(II) complexes **3a – e** all produced two principal bands, at $18100 - 19700$ cm^{-1} and $10800 - 12900$ cm^{-1}. The high-energy absorption was assigned as the $^3A_{2g} \rightarrow {}^3T_{1g}$ transition while the two components of the low-energy band were assigned as the $^3A_{2g} \rightarrow {}^3T_{2g}$ transition and the spin-forbidden $^3A_{2g} \rightarrow {}^1E_g$ transition (**Table 1.3**). All of these transitions are typical of octahedral Ni(II) complexes.[24]

Table 1.3. Spectral data for **3a – e** and other Ni(II) amino/pyridyl complexes

Complex	ν (cm^{-1})[a]	Assignments	Δ_0 (cm^{-1})	color
[NiL^1](ClO$_4$)$_2$	11300 sh (10.8)	$^3A_{2g} \rightarrow {}^1E_g$		
	12900 (15.9)	$^3A_{2g} \rightarrow {}^3T_{2g}$	12900	pink
	19700 (11.7)	$^3A_{2g} \rightarrow {}^3T_{1g}$		
[NiL^2](ClO$_4$)$_2$	11300 sh (12.7)	$^3A_{2g} \rightarrow {}^1E_g$		
	12800 (15.9)	$^3A_{2g} \rightarrow {}^3T_{2g}$	12800	pink
	19500 (14.2)	$^3A_{2g} \rightarrow {}^3T_{1g}$		
[NiL^3](ClO$_4$)$_2$	11200 sh (12.7)	$^3A_{2g} \rightarrow {}^1E_g$		
	12800 (17.0)	$^3A_{2g} \rightarrow {}^3T_{2g}$	12800	pink
	19500 (14.2)	$^3A_{2g} \rightarrow {}^3T_{1g}$		
[NiL^4](ClO$_4$)$_2$	10800 (25.4)	$^3A_{2g} \rightarrow {}^3T_{2g}$		
	12400 sh (11.4)	$^3A_{2g} \rightarrow {}^1E_g$	10800	pale brown
	18100 (9.28)	$^3A_{2g} \rightarrow {}^3T_{1g}$		
[NiL^5](ClO$_4$)$_2$	10900 (17.5)	$^3A_{2g} \rightarrow {}^3T_{2g}$		
	12400 sh (11.4)	$^3A_{2g} \rightarrow {}^1E_g$	10900	violet
	18100 (7.28)	$^3A_{2g} \rightarrow {}^3T_{1g}$		
[Ni(tptcn)]$^{2+}$[19]	11300 (24)	$^3A_{2g} \rightarrow {}^3T_{2g}$		
	12300 (36)	$^3A_{2g} \rightarrow {}^1E_g$	11300	violet
	19400 (27)	$^3A_{2g} \rightarrow {}^3T_{1g}$		
[Ni(tachpyr)]$^{2+}$	11400 (11.8)	$^3A_{2g} \rightarrow {}^3T_{2g}$		
	12500 (16.0)	$^3A_{2g} \rightarrow {}^1E_g$	11400	violet
	19600 (16.6)	$^3A_{2g} \rightarrow {}^3T_{1g}$		
[Ni(ampy)$_3$]$^{2+}$[21]	11300 (-)	$^3A_{2g} \rightarrow {}^3T_{2g}$		
	12700 (-)	$^3A_{2g} \rightarrow {}^1E_g$	13300	pink
	18800 (-)	$^3A_{2g} \rightarrow {}^3T_{1g}$		

[a]spectra for complexes **3a – e** were measured in MeCN

Copper (II). The spectra of **4a – c** are composed of a single broad absorption at approximately 15200 cm^{-1} (**Table 1.4**). This absorption was assigned as the $^2E_g \rightarrow {}^2T_{2g}$ transition and is typical of tetragonally-distorted six-

7

coordinate Cu(II) complexes with an N_6 donor set.[5,25] Complexes **4d** and **4e**

each produced a spectrum with a broad absorption between 14950 – 14560 cm^{-1}

that possessed a low-energy shoulder which is indicative of a five-coordinate

Cu(II) complex. [7,25-27] Deconvolution of these spectra showed each peak to be

composed of three Gaussian peaks which were assigned as the $d_{z^2} \rightarrow d_{x^2-y^2}$,

$d_{xy} \rightarrow d_{x^2-y^2}$, and $d_{xz,yz} \rightarrow d_{x^2-y^2}$ transitions as has been shown for other square-

pyramidal Cu(II) complexes.[26,28,29]

Table 1.4. Spectral data for **4a – e** and other Cu(II) amino/pyridyl complexes

Complex	ν (cm^{-1})[a]	Assignments	Δ_0 (cm^{-1})	color
[CuL^1](ClO$_4$)$_2$	15200 (86.4)	$^2E_g \rightarrow {}^2T_{2g}$	15200	blue
[CuL^2](ClO$_4$)$_2$	15200 (87.9)	$^2E_g \rightarrow {}^2T_{2g}$	15200	blue
[CuL^3](ClO$_4$)$_2$	15200 (95.9)	$^2E_g \rightarrow {}^2T_{2g}$	15200	blue
[CuL^4](ClO$_4$)$_2$	11000 (85.0)	$d_{xz,yz} \rightarrow d_{x^2-y^2}$		
	14300 (146)	$d_{yz} \rightarrow d_{x^2-y^2}$	-	green
	16300 (105)	$d_{z^2} \rightarrow d_{x^2-y^2}$		
[CuL^5](ClO$_4$)$_2$	10300 (101)	$d_{xz,yz} \rightarrow d_{x^2-y^2}$		
	14000 (91.1)	$d_{yz} \rightarrow d_{x^2-y^2}$	-	blue
	16000 (143)	$d_{z^2} \rightarrow d_{x^2-y^2}$		
[Cu(tachpyr)]$^{2+}$	15100 (93)	$^2E_g \rightarrow {}^2T_{2g}$	15100	blue
[Cu((N-Me$_3$)-tachpyr)]$^{2+}$	13800 (81.4)	$^2E_g \rightarrow {}^2T_{2g}$	14400	blue
[Cu(tptcn)]$^{2+19}$	14400 (121)	$^2E_g \rightarrow {}^2T_{2g}$	14400	blue

[a]spectra for complexes **4a – e** were measured in MeOH

Structural Studies

^{1}H NMR. For complexes **1a – c** the ^{1}H NMR spectra were consistent with

the octahedral-enforcing nature of tach-framework chelators as previously shown

in [Zn(tachpyr)]$^{2+}$ and [Ga(tachpyr)]$^{3+}$.[8] Characteristic patterns of proton-proton

coupling between cyclohexyl H atoms indicate closed, complexed tach as

opposed to open tach.[5] The two methylene protons of the coordinated pendant

arms are diastereotopic, indicating that the arms of the complexes are twisted

8

about the metal ion in the Δ or Λ configuration, and $\Delta - \Lambda$ interconversion does not occur on the NMR time-scale at room temperature. This has been previously shown in the group with various $[M(tachpyr)]^{n+}$ (M = Fe(II), Zn(II), Ga(III), In(III)) complexes.[5,6,12]

X-ray Crystallography. Solid-state structural data was obtained for complexes **1a** and **1d** using X-ray crystallography. The average Fe-$N_{(py)}$ and Fe-$N_{(amine)}$ bond lengths for **1a** are 1.972 and 2.011 Å respectively. The twist angle (ϕ) of 54.9° possessed by **1a** indicates the trigonally distorted octahedral coordination geometry of the complex, compared to a ϕ of 60° for a perfect octahedron. The average bite angle (α) of 83.6° in **1a** is comparable to other six-coordinate LS amino/pyridyl iron complexes having 5-membered chelate rings, as seen in the upper half of **Table 1.5**.

9

Table 1.5. Structural data for **1a** and **1d** and comparisons to other six-coordinate amino/pyridyl Fe(II) complexes

	Spin-State	Fe-N$_{(amine)}$ distance (Å)	Fe-N$_{(py)}$ distance (Å)	Bite angle, α (°)	Twist angle, φ (°)
[Fe(L¹)]²⁺	LS	2.008 (1) 2.012 (1) 2.013 (1)	1.971 (1) 1.973 (1) 1.973 (1)	83.16 (5) 83.77 (6) 83.91 (5)	54.9
[Fe(tptcn)]²⁺ ³⁰	LS	2.001 (6)	1.979 (6)	83.1 (2)	48.9
fac- [Fe(ampy)₃]²⁺ ³¹	LS	2.030 (1) 2.021 (1) 2.026 (1)	1.979 (1) 1.987 (1) 1.991 (1)	82.92 (4) 83.08 (4) 80.75 (4)	53.7
[Fe(L⁴)]²⁺ ᵃ	HS	2.169 (3) 2.173 (3) 2.181 (3)	2.234 (3) 2.238 (3) 2.384 (3)	76.85 (11) 78.42 (12) 78.48 (12)	52.1
		2.151 (3) 2.173 (3) 2.190 (3)	2.219 (3) 2.223 (3) 2.376 (3)	77.50 (13) 77.70 (13) 77.99 (13)	53.9
[Fe(tptcd)]²⁺ ³²	HS	2.257 (5)	2.226 (5)	77.04 (19)	41.8
mer- [Fe(ampy)₃]²⁺ ³¹	HS	2.178 (4) 2.192 (4) 2.189 (4)	2.188 (4) 2.218 (4) 2.223 (4)	76.9 (2) 75.2 (2) 75.6 (2)	41.1
[Zn(L⁴)]²⁺ ᵃ ³³	-	2.128 (4) 2.133 (4) 2.135 (4)	2.203 (4) 2.216 (4) 2.566 (5)	80.1 (2) 80.3 (2) 74.89 (15)	53.9
		2.115 (5) 2.133 (5) 2.151 (5)	2.213 (5) 2.218 (5) 2.527 (5)	79.9 (2) 79.5 (2) 76.3 (2)	49.5

ᵃStructure has two independent molecules in the asymmetric unit and both corresponding sets of data are given.

The average Fe-N$_{(py)}$ and Fe-N$_{(amine)}$ bond lengths for **1d** are 2.279 and 2.173 Å respectively. However, each of the independent molecules in the unit cell has one Fe-N$_{(py)}$ bond that is ~0.15 Å longer than the others. Complex **1d** obtains a twist angle of 53.0°. The average bite angle of 77.9° is consistent with the elongated Fe-N bonds and is in good agreement with other HS amino/pyridyl iron complexes as seen in the middle of **Table 1.5.**

10
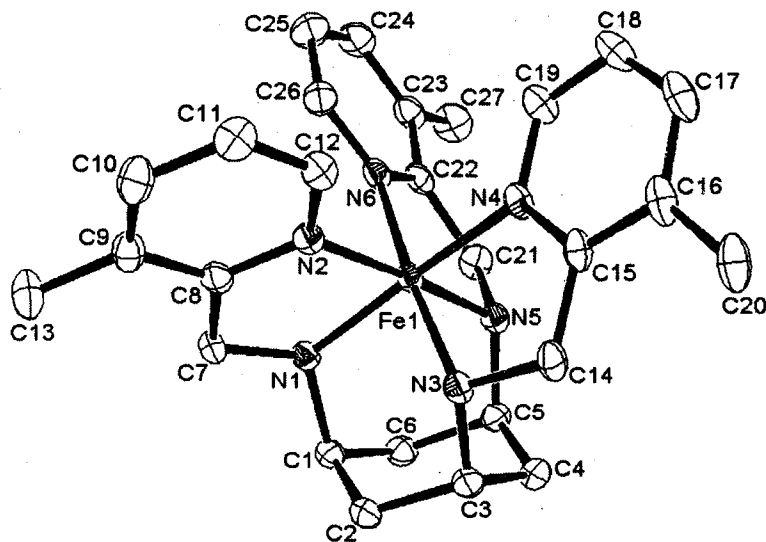
Figure 1.1. ORTEP view of the complex cation of [Fe(tach-3-Mepyr)]Cl₂ (**1a**) (50 % probability ellipsoids) with hydrogens omitted for clarity
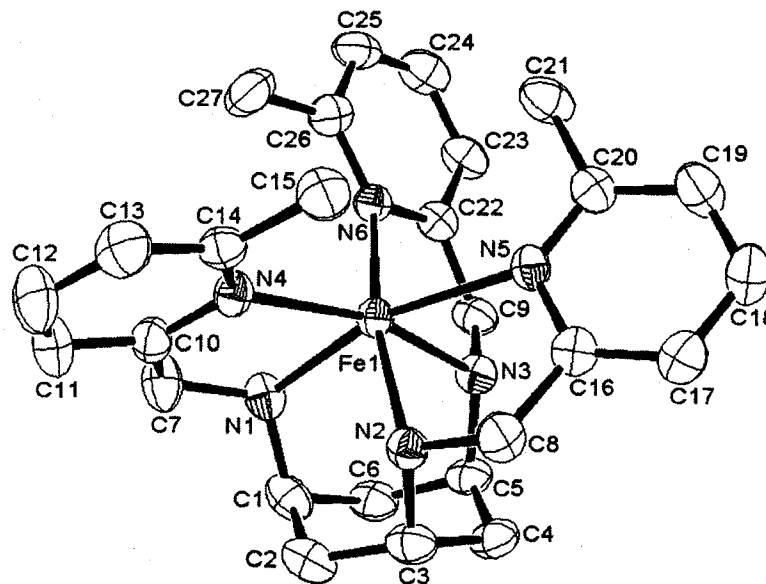
Figure 1.2. ORTEP view of the one of the complex cations of [Fe(tach-6-Mepyr)](ClO₄)₂ (**1d**) (50 % probability ellipsoids) with hydrogens omitted for clarity

Solution Reaction with Ancillary Ligands. Ancillary, monodentate

ligands (Cl⁻ and SCN⁻) were added to an acetonitrile solution of 1d and

monitored by visible spectroscopy to probe the presence of an open or

substitutable coordination site at the iron center. With the addition of one

11

equivalent of either a chloride or thiocyanate anion a red-shift of the charge-transfer band was observed (Figure 1.3). This spectral change is believed to be due to the formation of [Fe(tach-6-Mepyr)(Cl)]$^+$ and [Fe(tach-6-Mepyr)(SCN)]$^+$ respectively.[34]
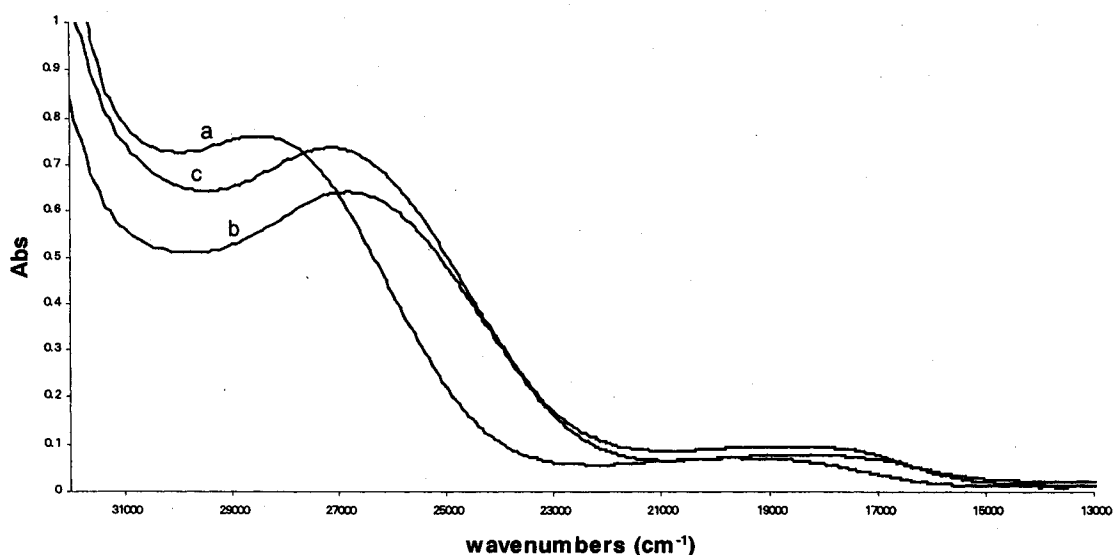
Figure 1.3. UV-Vis spectra of [Fe(tach-6-Mepyr]$^{2+}$ (**1d**) (a), **1d** plus Cl$^-$ (b) and **1d** plus SCN$^-$ (c)

Discussion

Electronic Data

Comparison across the tach-x-Mepyr series shows that 6-substituted ligands have a weaker field strength toward Fe(II), Ni(II) and Cu(II) (no 6-substituted Co(II) complexes were analyzed); while methyl substitution at the 3, 4 and 5 positions on the pyridine rings has no notable effect on the field strength relative to tachpyr for the Fe(II), Co(II), Ni(II) or Cu(II) complexes.

12

Thus, the 6-substituted Ni(II) complexes **3d** and **3e** have lower d – d transition energies as compared to the 3-, 4- and 5-substituted compounds **3a** – **c**. Similar results have been seen for Ni(II) complexes of lbptcn and blbpen, 6-substituted derivatives of tptcn and tpen.[18,35] With the octahedral enforcing nature of the metal center it is understandable that the added steric bulk at the 6-position would decrease the field strength of the ligands toward Ni(II). In an octahedral environment the 6-positions of the pyridine rings are all pointing towards the same general area, above the metal center, producing unfavorable steric interactions.

In the Fe(II) series, the 6-substitution causes a shift of Fe(II) from low-spin (**1a** – **c**) to high-spin (**1d** and **1e**). This is not surprising because LS Fe(II) metal center provides the greatest possible ligand field stabilization energy for octahedral geometry and it can π-backbond to the pyridyl donor group of amino/pyridyl chelators. To overcome the LFSE and the added stabilization of π-backbonding to adopt a HS electron configuration in **1d** and **1e**, the steric interactions between the substituents in the 6-positions must be quite substantial. Toftlund and Yde-Andersen showed this effect in their $[Fe(blbpe)]^{2+}$ complex which is HS while $[Fe(tpen)]^{2+}$ is spin-crossover.[18]

Alkylation of the pyridyl 6-position leads to five-coordinate complexes in the case of Cu(II), based on the electronic spectra of **4d** and **4e**. This result is not surprising because X-ray study showed that **4d** is five-coordinate. The τ value of 58.0% for the complex shows that, in the solid state, it adopts a

13

geometry midway between a perfect square-pyramid (τ = 0%) and that of a trigonal-bipyramid (τ = 100%).[7] The spectra of **4d** and **4e** were more closely examined to determine what five-coordinate geometry the complexes obtain in solution. Cu(II) complexes with C_{4v} symmetry will have a low-energy shoulder while D_{3h} symmetry will produce a high-energy shoulder.[7,26,29] Furthermore, a square-pyramidal (C_{4v}) complex should be composed of three absorptions while a trigonal-bipyramidal (D_{3h}) complex should only possess two absorptions. An explanation of the number of absorptions present in the different geometries can be seen in d-orbital splitting diagrams of D_{3h} and C_{4v} complexes seen in **Figure 1.4**.[29,36] Deconvolution of the spectra of **4d** and **4e** was undertaken to determine the number of transitions each possessed (**Figure 1.5**). Because spectra of **4d** and **4e** contained a low-energy shoulder and were composed of three transitions, each was assigned a square-pyramidal geometry.
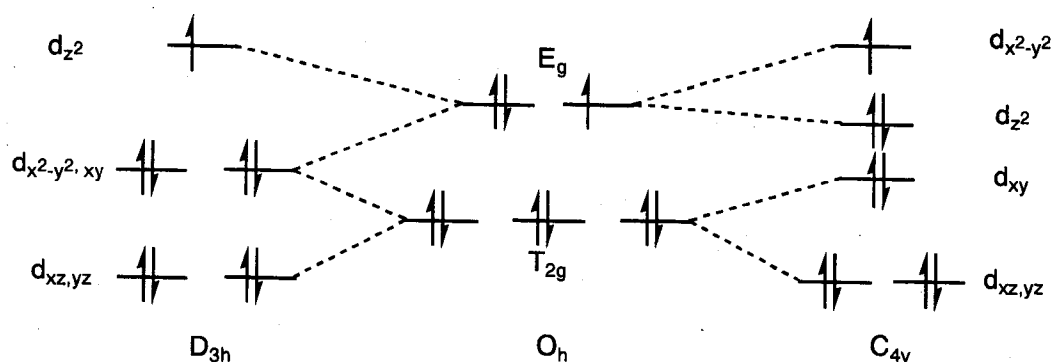
Figure 1.4. Splitting diagram for D_{3h} and C_{4v} complexes
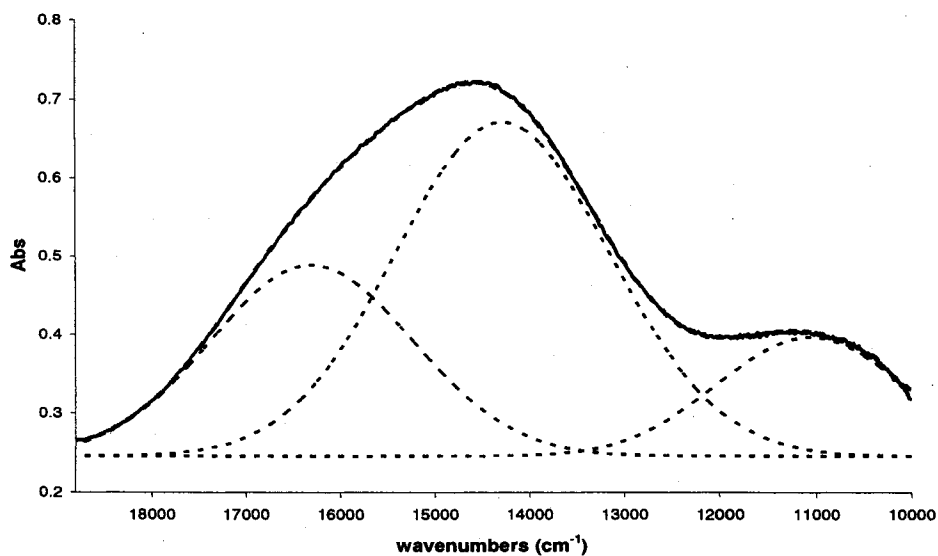
Figure 1.5. Deconvoluted electronic absorption spectrum of [Cu(tach-6-Mepyr)]$^{2+}$ (**4d**) (solid black line = experimental data, dashed red line = sum of black dashed lines)

Structural Studies

X-ray Crystallography. Complex **1a** takes on a slightly distorted octahedral geometry in the solid state. Its Fe-N$_{(amine)}$ and Fe-N$_{(py)}$ bonds are in good agreement with other LS amino/pyridyl Fe(II) complexes (**Table 1.5**). In LS Fe(II) complexes containing the aminomethyl pyridyl binding group, the Fe-N$_{(py)}$ bonds are generally shorter than the Fe-N$_{(amine)}$ bonds due to d$\pi \rightarrow$ pπ^* backbonding of Fe(II) to the ligand.[37] This was observed for **1a**. Tachpyr has shown the ability to obtain distorted octahedral geometries when binding Ni(II) and Zn(II), with twist angles of 45.5° and 43.7°, respectively.[5,8] The larger twist angle of 54.9° seen in **1a** can be attributed to the large LFSE of LS Fe(II) when in an octahedral geometry.

15

The effect of the steric interactions of the 6-methyl groups can really be seen in the crystal structure of **1d**. All of the Fe-N bonds show an elongation when compared to those of **1a**. This is attributed to the HS nature of the complex where electrons now populate the e_g^* orbitals and the six-coordinate ionic radius of Fe(II) is 0.92 Å. The steric interactions between the 6-methyl groups are most evident when examining the Fe-N$_{(py)}$ bonds. For each of the two independent molecules in the asymmetric unit there is one Fe-N$_{(py)}$ bond that is ~0.15 Å longer than the other two. The lengthening of one bond to compensate for steric interactions between 6-methyl groups was also observed in the Zn(II) and Mn(II) complexes of the same ligand, which are isostructural with **1d** (**Table 1.5**).[33] Even with these steric interactions, the complex is still able to obtain a geometry close to octahedral with an average twist angle of 53.0°. The bite angle of 77.9° is consistent with the elongated Fe-N bonds and is in good agreement with other HS amino/pyridyl Fe(II) complexes as seen in **Table 1.5**.

Solution Reaction with Ancillary Ligands. Based on the X-ray analysis of **1d** it was determined that a pyridyl group of the ligand could be either loosely bound or unbound to the metal center in solution and may be substitutable. To test this, monodentate ligands were added to acetonitrile solutions of the complex and monitored by visible spectroscopy. With the addition of one equivalent of Cl⁻ or SCN⁻ to solutions of **1d** a red-shift in the MLCT band was observed (**Figure 1.3**). We believe this red-shift is due to the formation of the species [Fe(tach-6-Mepyr)(Cl)]⁺ and [Fe(tach-6-Mepyr)(SCN)]⁺ respectively. This

16

study was utilized by Toftlund and coworker to analyze the behavior of a bulky tpen derivative, N,N'-bis(6-methyl-2-pyridylmethyl)-N,N'-bis(2-pyridylmethyl)ethane-1,2-diamine, when bound to Fe(II) and they saw the same red-shift of the charge-transfer band that we observed. They rationalize the metal-to-ligand charge transfer, MLCT, shift to lower energy by stating that the introduction of an exogenous ligand lowers the formal oxidation state of the iron due to better σ-donor abilities of the new ligand.[34]

Conclusion

The 6-position has a considerable effect on metal-binding properties in tach-6-Rpyr due to steric interactions amongst 6-substituents of the metal-bound ligand. In solution, this was evident from the lowering of d − d transition energies in Ni(II) complexes, the formation of a HS Fe(II) complex with a substitutable pyridyl group and the formation of five-coordinate Cu(II) complexes. In the solid state the steric interactions were apparent in the distorted octahedral geometry and elongated Fe-$N_{(py)}$ bond in **1d**. On the other hand, comparison to solution visible spectra of [M(tachpyr)]$^{2+}$ (M = Fe(II), Co(II), Ni(II), Cu(II)) indicate little electronic effect of 3-, 4- or 5-alkylation on ligand-field strength in the tach-x-Mepyr series, nor any steric effect of 3-alkylation.

17

IRON-MEDIATED OXIDATIVE DEHYDROGENATION OF TACHPYR AND TACHPYR DERIVATIVES: CORRELATING BIOLOGICAL EFFECTS WITH METAL-BINDING CHEMISTRY

Introduction

As mentioned in the previous chapter, it has been shown that tachpyr and

its derivatives will readily bind divalent iron in an anaerobic, aqueous or alcoholic,

environment. Previous group work has also revealed that Fe(II), once bound to

tachpyr, promotes the oxidative dehydrogenation of one or two of the amino-

methylene group(s) of the ligand when in an aerobic environment (**Scheme**

2.1).[6,16,38] This process is well known in other Fe-amino complexes.[39-43] The

product of the dehydrogenation is a so-called α,α'-diimino binding group which

has great ability to stabilize Fe(II) due to its σ-donor/π-acceptor properties.[44] The

resulting mono- and diimino Fe(II) complexes (denoted as $[Fe(tachpyr-ox-n)]^{2+}$

and $[Fe(tach-x-Rpyr-ox-n)]^{2+}$ where n = 2 or 4) are readily produced in air,

however, more forcing conditions such as H_2O_2 are required to produce the fully

oxidized product, $[Fe(tachpyr-ox-6)]^{2+}$.

18

Fe(II) or (aq or MeOH)
+
tachpyr

[Fe(tachpyr-ox-6)]$^{2+}$ [Fe(tachpyr-ox-2)]$^{2+}$ [Fe(tachpyr-ox-4)]$^{2+}$

Scheme 2.1. Oxidation of [Fe(tachpyr)]$^{2+}$
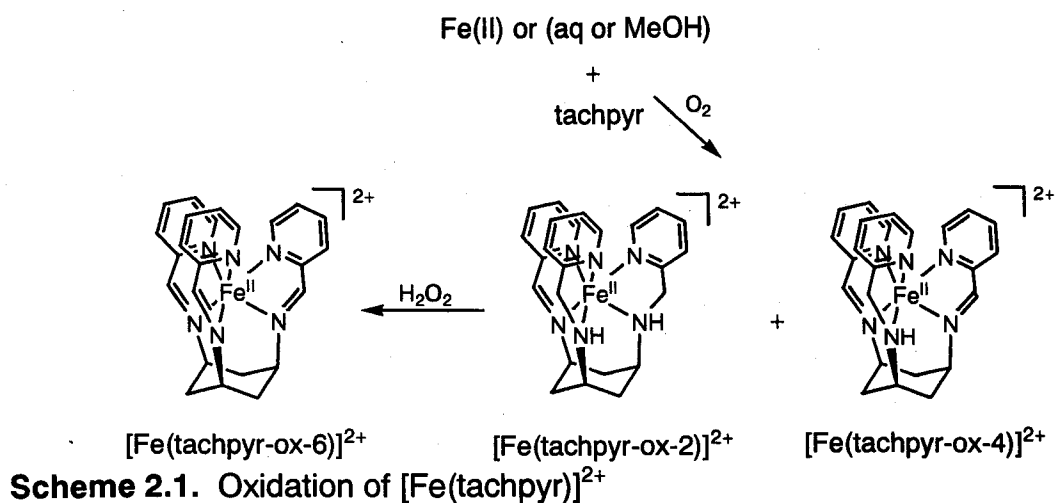
Results from biological study of tachpyr indicate a need to better understand the metal-binding chemistry of it and its derivatives. Previous results have shown also that the iron, zinc and copper complexes of tachpyr are not effective as cytotoxic agents, whereas the calcium, magnesium and manganese complexes are, relative to the free ligand. These results are in accord with the ability of tachpyr to bind Fe(II), Zn(II) and Cu(II) more strongly than Ca(II), Mg(II) and Mn(II), with the later complexes dissociating in aqueous media.[5,11,38] Further, it has been shown that iron and zinc are the principal metals targeted by tachpyr in cells[16] and that tachpyr preferentially binds Fe(II) over Zn(II).[38] The resulting oxidative dehydrogenation of the ligand when bound to iron complicates the chemistry taking place in the cell, therefore the formation of the oxidized iron complexes and their role in the biological activity of tachpyr and derivatives has not been thoroughly assessed. This chapter describes the results of several experiments performed to better understand and correlate the iron-mediated oxidative dehydrogenation of tachpyr and derivatives with their biological activity.

19

X = 3-Me (5)
X = 3-MeO (6)
X = 4-Me (7)
X = 5-Me (8)

x = 3-Me (9)
x = 3-MeO (10)
x = 4-Me (11)
x = 5-Me (12)

[Fe(tach-x-Mepyr-ox-2)]$^{2+}$

[Fe(tach-x-Mepyr-ox-4)]$^{2+}$

[Fe(tach-3-Mepyr-ox-6)]$^{2+}$ (13)

[Fe(tachpyr-ox-2)]$^{2+}$ (14)

[Fe(tachpyr-ox-4)]$^{2+}$ (15)
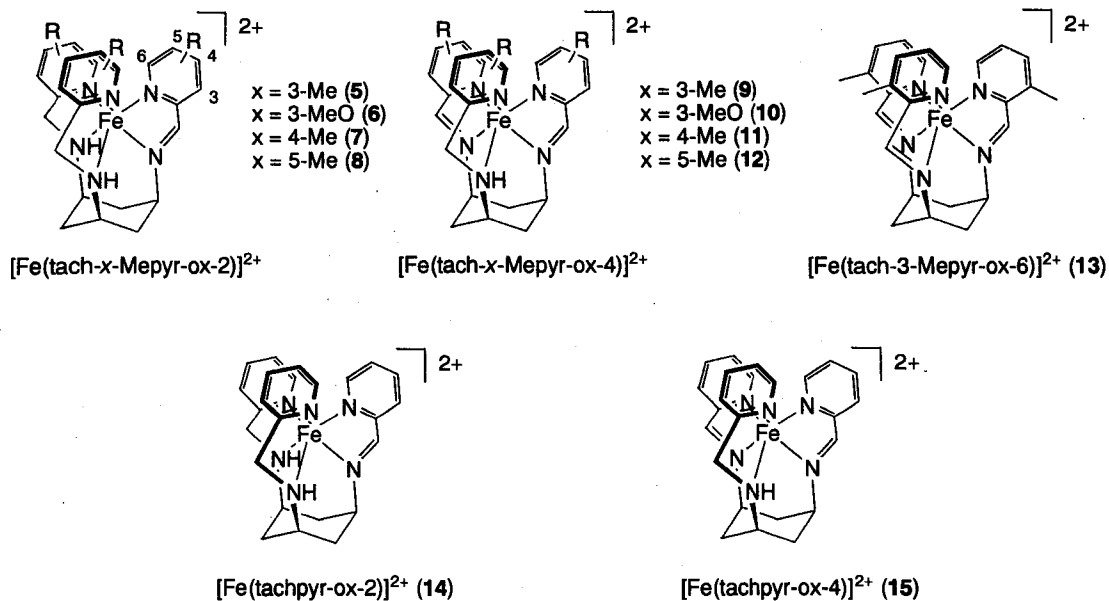
Scheme 2.2. Names and labeling of synthesized and studied complexes in the chapter

[Fe(tachpyrMe-trisimine)]$^{2+}$

[Fe(trenpy-trisimine)]$^{2+}$ (R = H)
[Fe(trenpyrMe-trisimine)]$^{2+}$ (R = Me)

[Fe(tachIM-trisimine)]$^{2+}$

[Fe(bipy)$_3$]$^{2+}$

[Fe(phen)$_3$]$^{2+}$
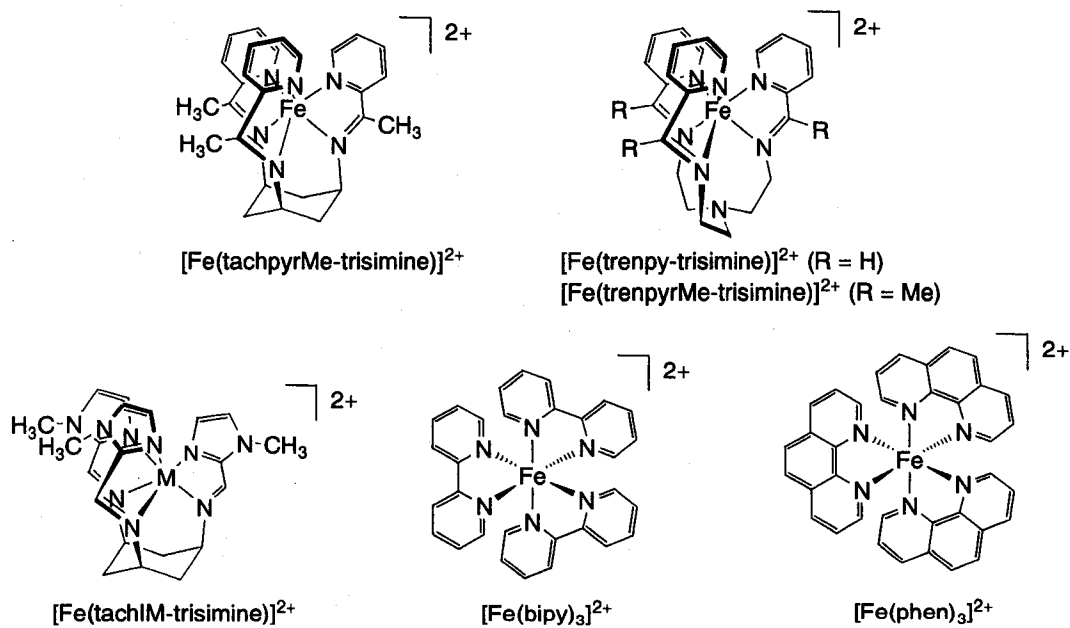
Scheme 2.3. Complexes used for comparison and discussion

20

Oxidation of [Fe(tach-*x*-Mepyr)]$^{2+}$ complexes

When exposed to air, oxidation of the Fe(II) complexes ensues resulting in

the mono- and diimino complexes except for [Fe(tach-6-Mepyr)]$^{2+}$, which shows

no signs of oxidation when monitored by low-res ESI-MS. For the [Fe(tach-*x*-

Mepyr)]$^{2+}$ (*x* = 3, 4, 5) complexes where imine formation occurs, a color change

from amber to green to blue is observed. Concomitant with the color change, a

strong charge-transfer band around 16700 cm^{-1} develops in the UV-Vis spectrum

(**Figure 2.1**), characteristic of α,α'-diimine chelating groups. The presence of

isobestic points indicates multiple species are present in the solution.
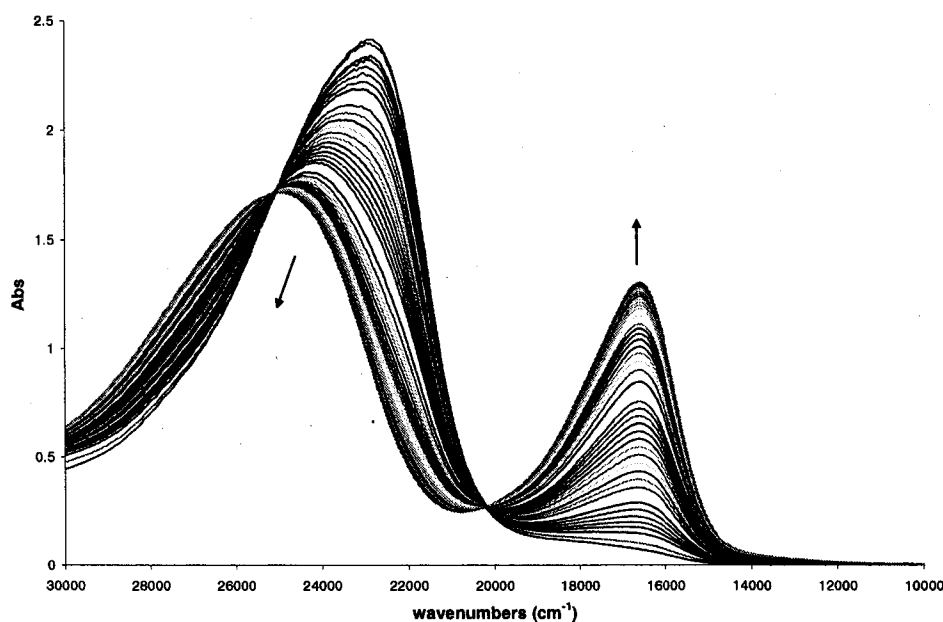
Figure 2.1. Observing the air oxidation of [Fe(tachpyr)]$^{2+}$ by UV-Vis over a 20 hour period

Relative Rates of Oxidation for Tachpyr and Tach-x-Rpyr Fe(II) Complexes

Combination of Fe(II) and unoxidized ligand in D$_2$O in the presence of air

21

produces a mixture of unoxidized and partially oxidized Fe(II) complexes. By monitoring the reactions with ^{1}H NMR (**Figure 2.2**) and ESI-MS it was shown that the rate of oxidation decreases in the order $[Fe(tach-3-Mepyr)]^{2+}$ > $[Fe(tachpyr)]^{2+}$ > $[Fe(tach-3-MeOpyr)]^{2+}$. Oxidation of $[Fe(tach-6-Mepyr)]^{2+}$ was not observed.
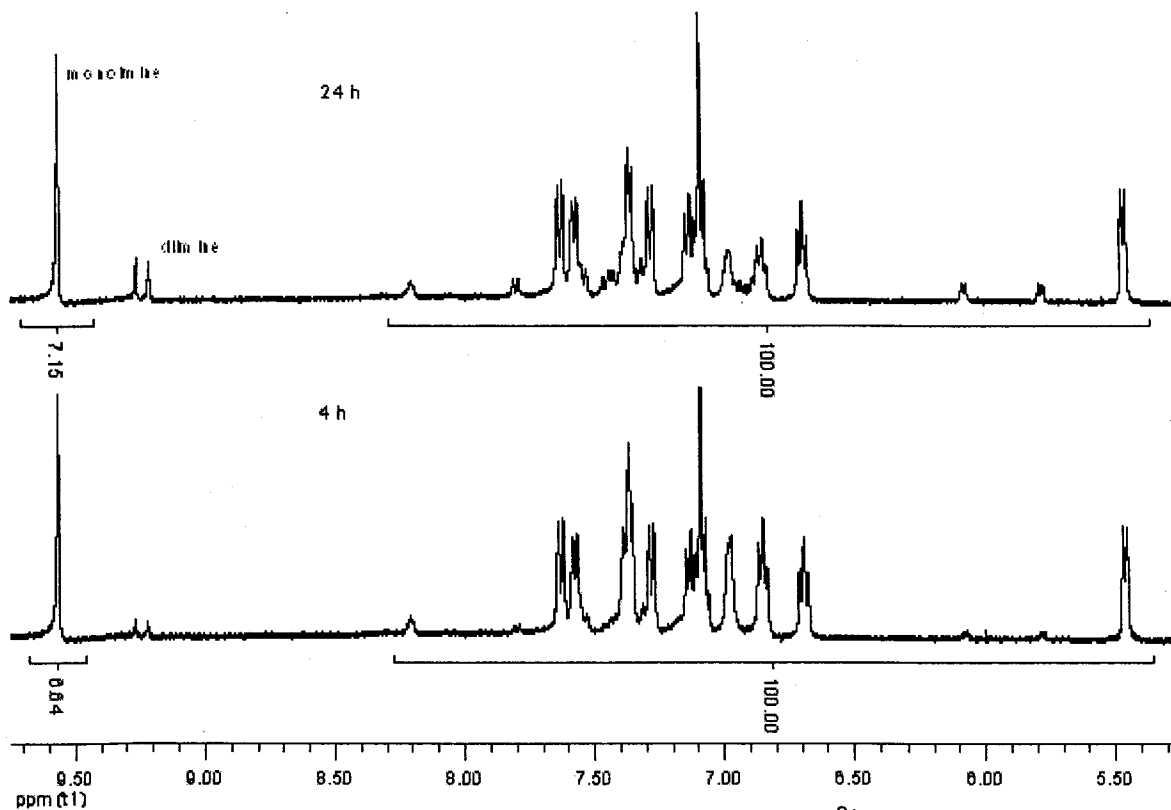
Figure 2.2. Following the oxidation of $[Fe(tach-3-Mepyr)]^{2+}$ (**1a**) to $[Fe(tach-3-Mepyr-ox-n)]^{2+}$ (n = 2 or 4; **5** and **9**, respectively) by ^{1}H NMR

Disproportionation Reaction of Fe(III) with Tach-4-Mepyr

Combination of equal amounts of Fe(III) and tach-4-Mepyr in MeOD-d_4 produced a roughly 1:1 mixture of $[Fe(tach-4-Mepyr)]^{2+}$ and $[Fe(tach-4-Mepyr-ox-2)]^{2+}$, quantified by ^{1}H NMR (**Figure 2.3**).

22
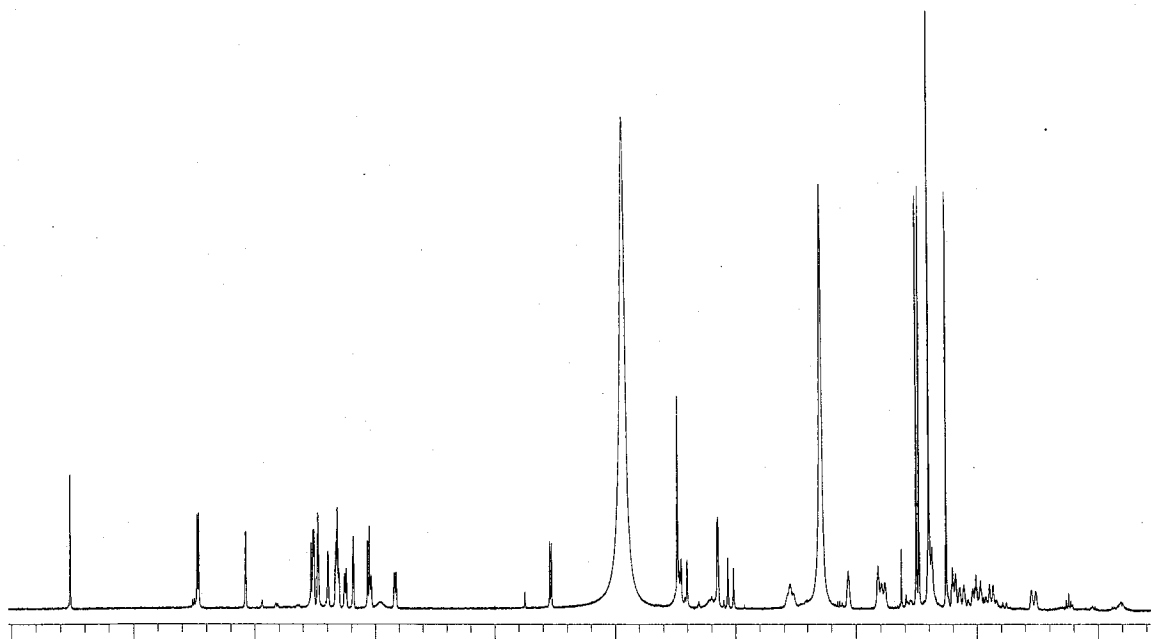
Figure 2.3. ^{1}H NMR spectrum of the disproportionation reaction between Fe(III) and tach-4-Mepyr

Affinity of Unoxidized and Ox-2 Tachpyr Derivatives Towards Fe(II)

Addition of 1.5 equivalents of either phen or bipy to a solution with approximately equal amounts of [Fe(tach-4-Mepyr)]$^{2+}$ and [Fe(tach-4-Mepyr-ox-2)]$^{2+}$ allowed for comparison of the affinity of an unoxidized tachpyr derivative and a partially oxidized derivative towards Fe(II). After addition of phen/bipy, ^{1}H NMR showed a larger decrease in the amount of [Fe(tach-4-Mepyr)]$^{2+}$ than [Fe(tach-4-Mepyr-ox-2)]$^{2+}$. Also, a single peak appeared at approximately 2.44 ppm that corresponds to the pyridyl methyl group of the free unoxidized ligand.

23
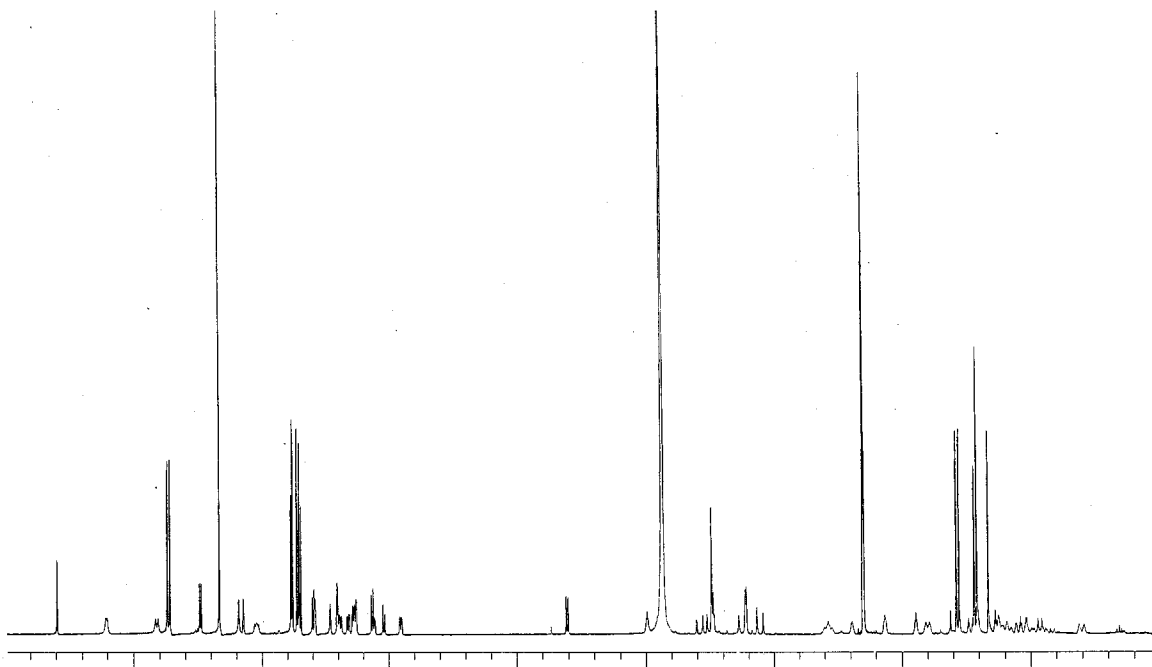
Figure 2.4. ^{1}H NMR of [Fe(tach-4-Mepyr)]$^{2+}$ (**1b**) and [Fetach-4-Mepyr-ox-2)]$^{2+}$ (**7**) from disproportionation reaction with addition of 1,10-phenanthroline to the reaction mixture

Syntheses and Characterization of Complexes

Complex **13** was synthesized by reacting Fe(ClO$_4$)$_2$•6H$_2$O and tach-3-Mepyr-ox-6 in MeOH, from which crude product was obtained by vapor-phase diffusion of Et$_2$O. Washing the crude products with Et$_2$O then drying provided 86% isolated yield. The [Fe(tach-3-Mepyr-ox-4)]$^{2+}$ complex (**9**) was prepared from the combination of FeCl$_2$•4H$_2$O and tach-3-Mepyr in MeOH, in the presence of O$_2$. The solution was allowed to sit as oxidation occurred and resulted in the presence of only the bisimine complex. Product was precipitated from solution by the addition of NH$_4$PF$_6$ as blue microcrystals. Recrystallization of the crude product from MeCN/EtOH by vapor-phase diffusion of Et$_2$O at a reduced temperature afforded the product in 60% yield. The formulations of the products

24

were confirmed by elemental analysis (for **13**), mass spectrometry, UV-Vis

spectroscopy (**Figure 2.5**) and ^{1}H NMR.
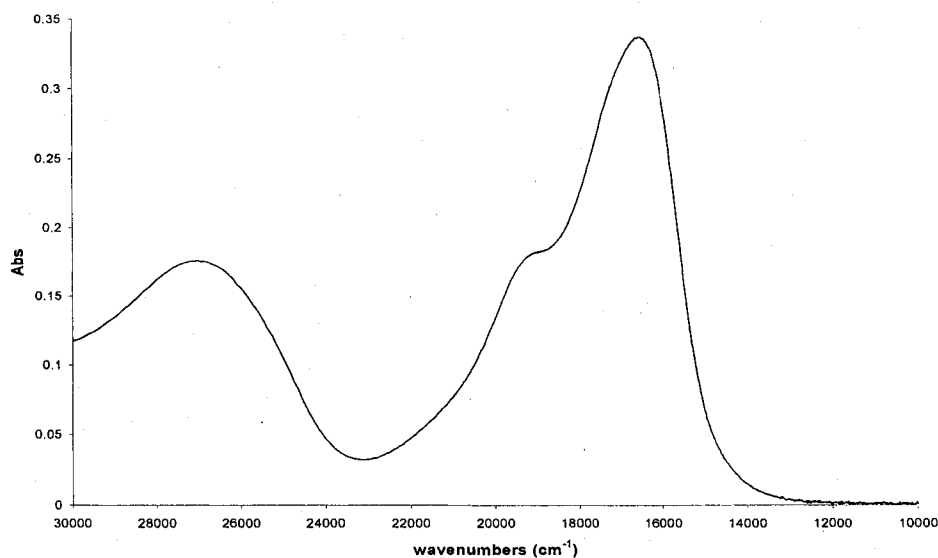
Figure 2.5. UV-Vis spectrum of **9** in MeCN

Inertness of [Fe(tach-3-Mepyr-ox-n)]$^{2+}$ (n = 4 or 6)

The inertness of [Fe(tach-3-Mepyr-bisimine)]$^{2+}$ (**9**) and [Fe(tach-3-Mepyr-

trisimine)]$^{2+}$ (**13**) were examined by heating them as buffered pH 7.4 solutions in

air at 65°C while monitoring their UV-Vis spectra. Complex **9** was unchanged

after 24 h while **13** showed a ca. 30 % decrease in the spectral intensity of the

peak at 585 nm (17100 cm^{-1}) (**Figure 2.6**) and formation of a precipitate,

indicative of decomposition.

25
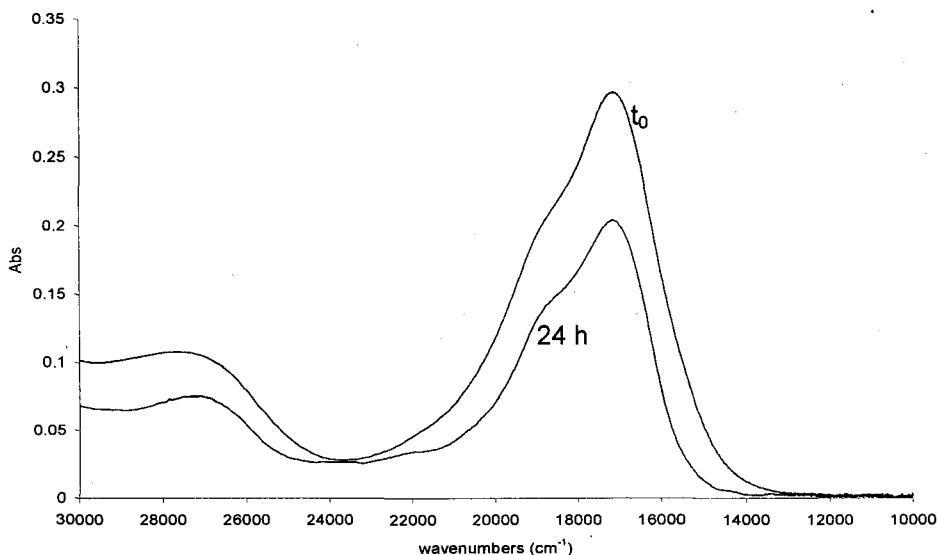
Figure 2.6. Following the degradation of [Fe(tach-3-Mepyr-ox-6)]$^{2+}$ (**13**) by UV-Vis in pH 7.4 MOPS buffer

Discussion

Tachpyr has been shown to bind Fe(II) and Zn(II) in cells, actions that our group believe to underlie its cytotoxic activity.[16,45] The binding of Fe(II) or Fe(III) by tachpyr under aerobic conditions leads to iron-mediated oxidative dehydrogenation to form [Fe(tachpyr-ox-2)]$^{2+}$ and [Fe(tachpyr-ox-4)]$^{2+}$ which have also been detected in cells.[16] Therefore, we have investigated the formation, bonding properties and lability of Fe(II) complexes of the mono-, bis- and trisimine forms of tach-x-Mepyr and tachpyr in order to compare them to the corresponding amino complexes and to other related hexadentate chelators. This was done in an effort to understand the consequences of iron-mediated oxidative dehydrogenation for biological activity of the chelators.

26

Relative Rate of Oxidation of Tachpyr and Derivatives

It has previously been observed that Fe(II), once bound to tachpyr, promoted the oxidative dehydrogenation of the amino-methylene group (**Scheme 2.1**),[6] as is well-known in other iron-amino complexes.[39-43] It has also been observed that in the presence of air [Fe(tachpyr)]$^{2+}$ readily oxidizes to the mono- and bisimine complexes [Fe(tachpyr-ox-2)]$^{2+}$ and [Fe(tachpyr-ox-4)]$^{2+}$, respectively, but not to the trisimine complex, [Fe(tachpyr-ox-6)]$^{2+}$. More forcing conditions, such as H_2O_2, are required to generate the trisimine complex (**Scheme 2.1**). The [Fe(tach-x-Mepyr)]$^{2+}$ species (x = 3, 4 or 5) have been shown to possess nearly the same physical properties as [Fe(tachpyr)]$^{2+}$,[33] including the tendency to oxidize to mono- and bisimine complexes but not to the trisimine species. Accordingly, their solutions change from amber to green to blue, but not to purple (the color associated with the trisimine species) in air. The resulting electronic absorption spectra all agree with [Fe(α,α'-diimine)]$^{2+}$ spectra reported in the literature.[44,46-48] Consistent with the low-spin, diamagnetic NMR and in analogy to other σ-donor/π-acceptor ligand Fe(II) complexes such as [Fe(phen)$_3$]$^{2+}$, the mono- and diimino derivatives of tach-x-Mepyr (x = 3, 4 or 5) interact strongly with Fe(II).

While alkylation at the 3-, 4- or 5-position of the pyridine rings of tachpyr does not affect the iron-binding ability of the chelators, it does change the rate of oxidation of the Fe(II) complexes. The rate of redox activity is substantially accelerated with 3-methylation. This observation had been made previously in

27

the group when working with these iron complexes; however, the relative rates

were not quantitated. The oxidation of the iron complexes of tachpyr, tach-3-

Mepyr and tach-3-MeOpyr was followed by ^{1}H NMR (**Figure 2.2**) or ESI-MS to

obtain relative data. Within this series of complexes no substantial ground-state

difference in chelating properties is inferred from comparison of the unoxidized

Fe(II) complexes (the [Fe(tach-3-MeOpyr)]$^{2+}$ data comes from Joon Cho,

unpublished), yet their rate of oxidation decreases in the order [Fe(tach-3-

Mepyr)]$^{2+}$ > [Fe(tachpyr)]$^{2+}$ > [Fe(tach-3-MeOpyr)]$^{2+}$. The relative rates were

determined by integrating the area under the monoimine peak in the ^{1}H NMR and

comparing it to the area under the aromatic peaks (**Table 2.1**).

Table 2.1. Ratio of area under imine peak of [Fe(L-ox-2)]$^{2+}$ to area under aromatic peaks

Time	[Fe(tach-3-Mepyr)]$^{2+}$ [a]	[Fe(tach-3-MeOpyr)]$^{2+}$ [b]	[Fe(tachpyr)]$^{2+}$ [c]	Theoretical maximum[d]
0 h	0.000	0.000	0.000	0.000
4 h	0.066	0.047	0.048	0.111
24 h	0.071	0.049	0.056	

[a]Bisimine species was seen at both 4 h and 24 h for [Fe(tach-3-Mepyr)]$^{2+}$, thus, the degree of oxidation for [Fe(tach-3-Mepyr)]$^{2+}$ at 4 h and 24 h is greater than indicated by these data. [b]Bisimine species was not observed for [Fe(tach-3-MeOpyr)]$^{2+}$ during this study. [c]Bisimine species was seen at 24 h for [Fe(tachpyr)]$^{2+}$, thus, the degree of oxidation for [Fe(tachpyr)]$^{2+}$ at 24 h is greater than indicated by these figures. [d]Maximum for total conversion to [Fe(L-ox-2)]$^{2+}$.

The rate of oxidation of this series mirrors the rates of cytotoxicity of the

chelators involved (**Table 2.2**). To expand this series to include a chelator that is

not a strong iron chelator [Fe(tach-6-Mepyr)]$^{2+}$ was exposed to air, which did not

cause oxidation as observed by ESI-MS. Again, this mirrors the cytotoxicity of

the chelator, as tach-6-Mepyr is not cytotoxic.[33]

28

Table 2.2. IC50 values (μM) of tachpyr, tach-3-Mepyr, tach-3-MeOpyr and tach-6-Mepyr after 24, 48 and 72 hours and the relative rates of oxidation of the corresponding Fe(II) complex

	24 hours	48 hours	72 hours	Relative rate of oxidation of the Fe(II) complex
Tachpyr	22	6	6	medium
tach-3-Mepyr	11	6	6	fast
tach-3-MeOpyr	130	22	12	slow
tach-6-Mepyr	-	-	-	none

Affinity of Unoxidized and Partially Oxidized Chelators for Iron

In previous group work it was shown that combining equal amounts of

Fe(III) and tachpyr produces a roughly 1:1 mixture of [Fe(tachpyr)]$^{2+}$ and

[Fe(tachpyr-ox-2)]$^{2+}$.[16] The same reaction was run between tach-4-Mepyr and

Fe(III) with the same result (**Scheme 2.4**). Due to the difficulty

$$\text{Fe(III) + tach-4-Mepyr} \xrightarrow[\text{H}_2\text{O or MeOH}]{\text{deaerated}} \quad + \quad$$

(*ca.* 1 : 1)
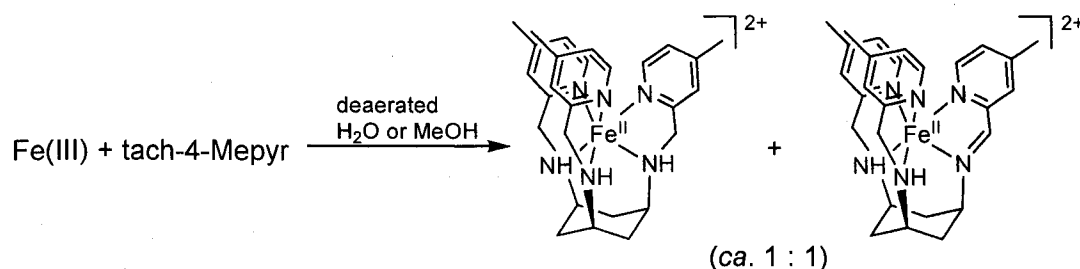
Scheme 2.4. Disproportionation reaction between Fe(III) and tach-4-Mepyr resulting in approximately a 1 : 1 mixture of [Fe(tach-4-Mepyr)]$^{2+}$ (**1b**) and [Fe(tach-4-Mepyr-ox-2)]$^{2+}$ (**7**)

of synthesizing and isolating the monoimine form of tachpyr and its derivatives,

this disproportionation reaction is the best way to generate and study the Fe(II)-

monoimino complex. A competition reaction was run under anaerobic conditions

in which an α,α'-diimine ligand, either phen or bipy, was added to a freshly

generated mixture of [Fe(tach-4-Mepyr)]$^{2+}$ and [Fe(tach-4-Mepyr-ox-2)]$^{2+}$ (ca. 1:1)

in MeOD-d_4 (**Eqn 1**). By monitoring this reaction the relative affinities towards

29

divalent iron of unoxidized and partially oxidized tachpyr derivatives could be determined and compared. Two observations were made when the reaction was followed by ^{1}H NMR. First, there was a larger decrease in the amount of $[Fe(tach\text{-}4\text{-}Mepyr)]^{2+}$ than $[Fe(tach\text{-}4\text{-}Mepyr\text{-}ox\text{-}2)]^{2+}$. Second, a signal appeared at approximately 2.44 ppm that corresponded to free unoxidized chelator (**Figure 2.4**). The disappearance of the unoxidized complex along with the appearance of free unoxidized chelator shows that Fe(II) is more easily displaced from the unoxidized ligand than the partially oxidized ligand, which is rationalized by the increased π-acceptor ability of the α,α'-diimine group of the oxidized chelator.[44]

$$[Fe(tach\text{-}4\text{-}Mepyr)]^{2+} + [Fe(tach\text{-}4\text{-}Mepyr\text{-}ox\text{-}2)]^{2+} \xrightarrow{\frac{3eq\ \alpha,\alpha'\text{-diimine}}{MeOD\text{-}d_4}}$$

(1-x)$[Fe(tach\text{-}4\text{-}Mepyr)]^{2+}$ + *(1-y)*$[Fe(tach\text{-}4\text{-}Mepyr\text{-}ox\text{-}2)]^{2+}$
+ *(x+y)*$[Fe(\alpha,\alpha'\text{-diimine})_3]^{2+}$ + *x*tach-4-Mepyr + *y*tach-4-Mepyr-ox-2

Eqn 1
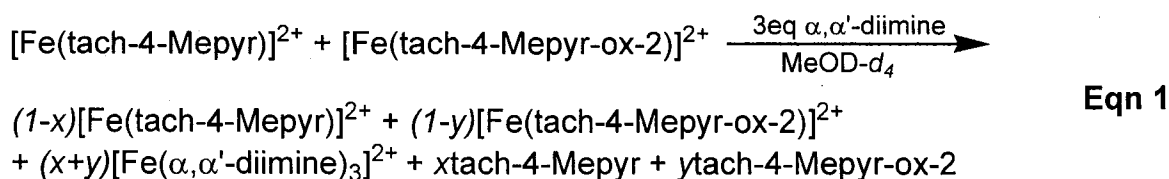
Synthesis and Characterization of $[Fe(tach\text{-}3\text{-}Mepyr\text{-}ox\text{-}n)]^{2+}$ (n = 4 or 6)

Normally, when methanolic solutions of Fe(II) and tachpyr or tach-*x*-Mepyr (*x* = 3, 4, 5) are combined in air a mixture of mono- and bisimine Fe(II) complexes results. Noticeably absent from the solution is the trisimine Fe(II) complex. It was serendipitously determined that when solutions of Fe(II) and tach-3-Mepyr were reacted on the bench top and allowed to sit, the product was exclusively the bisimine complex $[Fe(tach\text{-}3\text{-}Mepyr\text{-}ox\text{-}4]^{2+}$. The bisimine complex was isolated and its inertness and solid state structure were examined and compared to that of several tach-based trisimine Fe(II) complexes, including $[Fe(tach\text{-}3\text{-}Mepyr\text{-}ox\text{-}6)]^{2+}$, $[Fe(tachpyr\text{-}ox\text{-}6)]^{2+}$, $[Fe(tachpyrMe\text{-}ox\text{-}6)]^{2+}$ and

30

[Fe(tachIM-ox-6)]$^{2+}$ as well as several tren-based Fe(II) trisimine complexes (**Scheme 2.2**).

All tach-trisimine complexes of Fe(II) are labile in aqueous pH 7.4 medium at 65°C[49] while the tach-bisimine complex is inert under the same conditions. Clearly the trigonal-prismatic coordination geometry that a tach-trisimine chelator prefers[46,47,50,51] is unfavorable to Fe(II)-LS which strongly favors octahedral coordination, thus providing an explanation as to why tach-trisimine complexes are not observed in cells treated with tachpyr and derivatives. While the rigidity of the tach-trisimine framework enforces trigonal-prismatic geometry and leads to labile or high-spin Fe(II) complexes the same cannot be said of the tach-bisimine Fe(II) complex. The amino N of tach-3-Mepyr-ox-4 allows for some flexibility in the oxidized ligand and produces an inert, low-spin Fe(II) complex. While the bisimine complex is inert it is not free of strain. Both imino N's show a substantial deviation from the plane formed by the N, C, C and Fe atoms (**Table 2.3**). Along with the distortion of the imino N's, a rotation along the CH-C(2-pyridyl-ipso) bond in each arm of the chelator of approximately 10° directs the lone pair of the pyridyl N away from the metal center. The combination of the imino N distortions and the rotation allow the inner coordination sphere to obtain a distorted octahedral geometry. This can be seen in the crystal structure of [Fe(tach-3-Mepyr-ox-4)]$^{2+}$ (**Figure 2.7**).
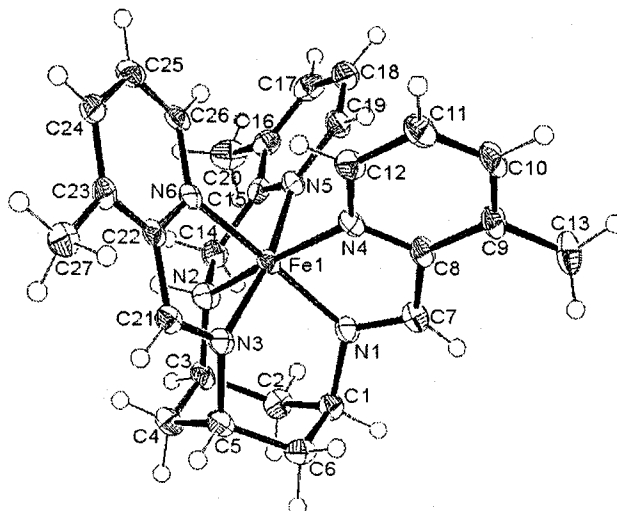
Figure 2.7. ORTEP view of the complex cation of [Fe(tach-3-Mepyr-ox-4)](PF$_6$)$_2$ **(9)** (50 % probability ellipsoids)

In contrast to the tach framework, the tren framework allows the N(R)-CH$_2$-pyridyl donor arms to remain planar but all canted in a left- or right-handed twist about the C$_3$ axis that travels through Fe and the apical N, resulting in a more inert Fe(II) complex. This was observed by Boubekeur in their structural study of of [Fe(trenpyr-trisimine)](PF$_6$)$_2$ (**Table 2.4**), in which the trigonal twist angle is 54° and distortions of the imino N atoms analogous to [Fe(tachpyrMe-trisimine)]$^{2+}$ are not observed.[52] This is consistent with previous findings in the group that [Fe(trenpyrMe-trisimine)]$^{2+}$ and [Fe(trenpyr-trisimine)]$^{2+}$ are inert in pH 7.4 media at 65°C.[49] In this case the flexibility present in the tren framework allows these complexes to obtain a more desired geometry and remain inert.

32

Table 2.3. Deviations (Å) of atoms from least-squares planes of the imino nitrogen and its three bound atoms in [Fe(tachIM-ox-6)](ClO₄)₂, [Fe(tachpyrMe-ox-6)](ClO₄)₂ and [Fe(tach-3-Mepyr-ox-4)](PF₆)₂ (9)

Compound	atoms and deviations from their least-square planes, Å		
[Fe(tachIM-ox-6)]$^{2+}$	Fe, 0.01237(5) N(1), -0.051(4) C(1), 0.018(5) C(3), 0.020(4)		
[Fe(tachpyrMe-ox-6)]$^{2+}$	Fe, 0.0255(5) N(1), -0.097(3) C(1), 0.033(4) C(7), 0.038(4)	Fe, -0.0245(5) N(2), 0.094(3) C(3), -0.033(4) C(13), -0.037(4)	Fe, -0.0273(5) N(3), 0.105(3) C(5), -0.037(4) C(19), -0.041(3)
[Fe(tach-3-Mepyr-ox-4)]$^{2+}$	Fe, 0.0014(5) N(1), -0.1255(25) C(1), 0.0739(32) C(7), 0.0843(33)	Fe, -0.0014(6) N(3), 0.1035(26) C(5), -0.0564(32) C(21), -0.0551(31)	

Table 2.4. Structural comparisons of [Fe(tachIM-ox-6)](ClO₄)₂, [Fe(tachpyrMe-ox-6)](ClO₄)₂, [Fe(tach-3-Mepyr-ox-4)](PF₆)₂ (9), [Zn(tachpyr-ox-6)](ClO₄)₂[53] and [Fe(trenpyr-trisimine)](PF₆)₂[52]

Substance	M-N$_{imine}$ bond distances (Å) or M-N$_{amine}$ distances (Å)	M-N$_{heterocycle}$ bond distances (Å)	bite angle of 5-ring, N$_{imine}$-Fe-N$_{heterocycle}$ (°)	twist angle (°)
[Fe(tachIM-ox-6)]$^{2+}$	2.197(3)	2.185(3)	75.01(12)	12.30(13)
[Zn(tachpyr-ox-6)]$^{2+}$	2.148(4), 2.142(4), 2.167(4)	2.211(4), 2.282(4), 2.258(4)		4.6(3)
[Fe(tachpyrMe-ox-6)]$^{2+}$	1.906(3), 1.924(3), 1.929(3)	1.987(3), 1.974(3), 1.981(3)	80.51(13), 80.8(2), 80.66(13)	44.6(2), 44.9(2), 44.9(2)
[Fe(tach-3-Mepyr-ox-4)]$^{2+}$	1.899(3),1.909(3) (Fe-N$_{imine}$); 1.977(3) (Fe-N$_{amine}$)	1.984(2), 1.991(3), 2.000(3)	80.66(11), 80.88(11), 82.23(11)	43.1 44.5 47.6
[Fe(trenpyr-ox-6)]$^{2+}$	1.952(4), 1.953(4), 1.946(5)	1.983(5), 1.979(4), 1.979(4)		54

33

Conclusion

From this work, multiple connections can be made between the chemistry of tach-based chelators and their biological properties. While tach-3-Mepyr, tachpyr and tach-3-MeOpyr all have similar binding properties toward Fe(II) in an oxygen-free environment, the rates of oxidative dehydrogenation of their Fe(II) complexes in air are substantially different. The rate of oxidation of the chelators appears related to their mechanism of cytotoxicity because rate of cytotoxicity correlates with the rate of oxidation. It was shown that tach-6-Mepyr does not undergo iron-mediated oxidative dehydrogenation, and that it is not cytotoxic. The affinity of a partially oxidized tachpyr derivative towards Fe(II) has been shown to be greater than the affinity of the same unoxidized derivative. This result shows how oxidation of the chelator improves its ability to act as an iron-deprivation agent by introduction of the σ-donor/π-acceptor function of an α,α'-diimine bonding group. Finally, it has been shown that tach-trisimine complexes decompose in aqueous pH 7.4 medium while a tach-bisimine Fe(II) complex is inert under the same conditions. This has been attributed to unfavorable coordination geometry imposed by the tach-trisimine chelator, while the bisimine chelator is flexible enough to obtain a suitable geometry. Several connections between the chemistry and biology of tachpyr and derivatives have been mentioned, but a full understanding of both chemical and biological aspects requires further study.

34

CHAPTER III

STRUCTURAL AND ELECTRONIC PROPERTIES OF NI(II), CU(II) AND ZN(II) COMPLEXES OF LINEAR, TETRADENTATE, AMINOPYRIDYL LIGANDS: TOWARDS ZN(II) SELECTIVITY

Introduction

The focus of this chapter is development of zinc-selective chelators. The need for Zn-selective chelators can be seen in several disciplines. Recently, the need to probe biological zinc has resulted in the development of several chelators with a chromophore or fluorophore built in that have an affinity towards divalent zinc.[54-56] While these chelators do have an affinity for zinc they might not be selective for zinc. This allows other biometals to interfere by competing for the zinc-binding site. In this case selectivity is not essential because a response can still be measured. However, chelators designed to inhibit overactive matrix metalloproteinases (MMPs) by selectively binding zinc have not made it to clinical trials despite promising in vitro results due to a lack of metal binding selectivity.[57] A similar problem has been seen in our own group's work with tachpyr. In cultured cells, tachpyr has been shown to bind both Fe(II) and Zn(II).[16,38] Our hypothesized mode of cytotoxicity, through iron deprivation, is difficult to prove if the chelator binds multiple metals. Development of a zinc-selective chelator that is chemically similar to tachpyr could provide more insight into tachpyr's mode of action and help in the determination of the cytotoxic effects of zinc deprivation along with iron deprivation. Zinc selective chelators

35

can also be used in separation chemistry. Development of a lipophilic ligand system that selectively removes zinc from acidic aqueous solutions has been thoroughly studied by Parker and coworkers who have had good results utilizing the formation of ZnL_2 or Zn_2L_2 species.[58-60] This is of commercial interest because it is a more cost-efficient means of separation than traditional pyrometallurgical methods.[59]

The difficulty in obtaining selectivity for Zn(II) is in overcoming the Irving-Williams series which states, the stability of complexes formed with divalent first row transition metals will increase in the order Fe < Co < Ni < Cu > Zn.[61,62] This series predicts that Zn(II) will complex a given ligand with lesser stability than either Ni(II) or Cu(II). The remainder of this introduction discusses several aspects of Zn(II) coordination chemistry (geometric preferences and coordination number, donor atoms and the effect of increased steric bulk) that may be manipulated to increase the affinity of a chelator for Zn(II) relative to other divalent transition metals.

Divalent zinc is a d^{10} metal and therefore has a completely filled d shell. This leads to a ligand field stabilization energy (LFSE) of zero for any geometry. LFSE represents the stabilization of the d electrons, which is qualitatively determined by binding geometry, and whose magnitude is determined by strength of donor-acceptor interactions.[63] With a LFSE of zero, Zn(II) can and will take on multiple geometries including tetrahedral. This cannot be said for most other transition metals where there is a preferred geometry other than

36

tetrahedral based on their LFSE. If a ligand with four donor atoms that can either

force or easily attain a tetrahedral binding site is made, then the chelator's affinity

for zinc relative to other metals should be enhanced. Tetrahedrally-enforcing

chelators prepared for this purpose have been published in the literature with

varied success.[58-60,64-69] The most popular approaches to tetrahedral

enforcement focus on the [2 + 2], [2 − 2]$_2$ and [3 + 1] motifs (**Figure 3.1**[64]).

[2 + 2]   [2 − 2]

[2 − 2]$_2$ [3 + 1]   [1 + 3]
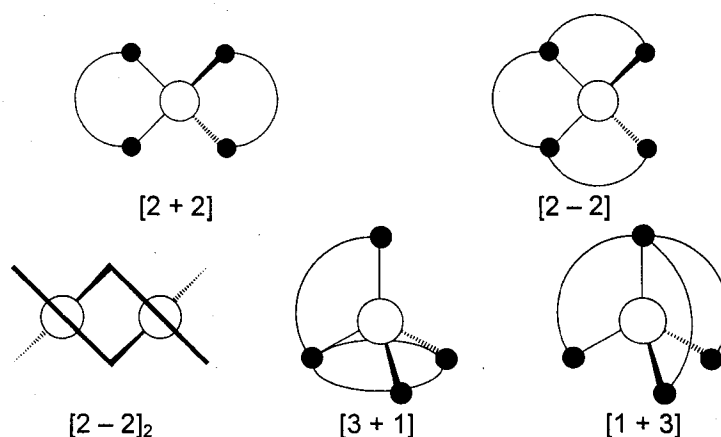
Figure 3.1. Variety of ligand structure types imposing tetrahedral coordination

It is also important to use hard-soft acid-base theory to select the donor

atoms to use for a zinc selective chelator. Zinc is considered an intermediate

acid (in hard-soft terms) so it will bind with most types of donor atoms. While this

might not be ideal, it can be used to rule out extremely hard donors such as

anionic oxygen which prefer Fe(III) or Mn(II). Several donor groups have been

investigated in the literature such as nitrogen in the forms of amines (primary,

secondary and tertiary), pyridine, imidazole or sulfonamides as well as oxygen

from carboxylates, phosphinates or phenolates.[58-60,64-69] While no combination of

donor atoms has been labeled as the best donor atoms for zinc selectivity, an N$_4$

37

donor set will readily bind zinc. This works out well since nitrogen is considered an intermediate base (in hard-soft terms) and matches up well with the intermediate acid characteristics of Zn(II).

In addition to limiting the number of donor atoms to four, use of steric bulk is another way of controlling the geometry a complex will obtain. Bulky groups can act in two different ways when binding a metal (depending on the binding motif, **Figure 3.1**). First, they can provide intra-ligand steric interactions and direct the donor atoms into the geometry that best alleviates steric strain, which is tetrahedral. An example of intra-ligand steric hindrance can be seen in our $[M(tach-6-Mepyr)]^{2+}$ (M = Cu(II), Zn(II)) complexes.[33] Second, they can prevent the binding of ancillary ligands through inter-ligand interactions, obscuring the binding sites not occupied by the donor atoms of the selective, and keeping the coordination number low.[70]

After having considered the preferred geometry of Zn(II), possible donor atoms and means of utilizing steric bulk we decided to focus our efforts on the [2 – 2] coordination motif using the known chelator, bispicpn (**Scheme 3.2**). It is an N_4 chelator with sufficient flexibility to assume tetrahedral coordination. We saw two ways to derivatize the chelator, by adding steric bulk at the 6-position of the pyridine rings or homologating the arms of the ligand. Substitution at the 6-position could provide intra- and inter-ligand steric effects. Homologation of bispicpn by adding a methylene unit to each arm would create three 6-membered chelate rings in the resulting complexes. These 6-membered chelate rings allow

38

for larger bite angles, which are favorable for tetrahedral geometry and metals with small atomic radii.[71]

In the literature it has been shown that bispicpn and its derivatives bind with varying stereochemistries. Thus, the Ni(II) complex of the N-methyl derivative formed a *cis-β* complex[72] while the Cu(II) complex of bispicpn obtained a *trans* geometry[73].
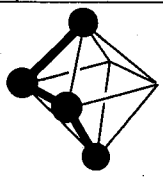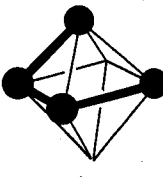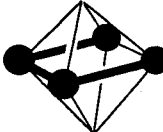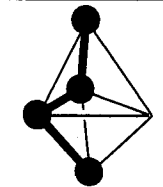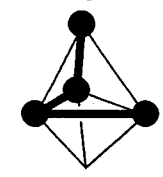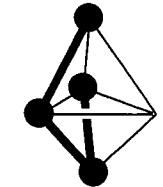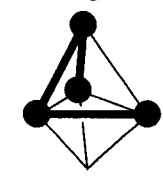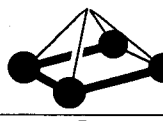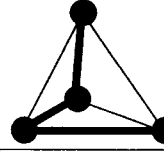
Our hope is to take advantage of the lack of LFSE of Zn(II) and determine if, by adding steric bulk, we can develop a chelator that binds in a tetrahedral geometry and ultimately is selective for divalent zinc, relative to other M(II) ions. The success of this project will rely on not only developing a chelator that has a high affinity towards zinc, but also one that has lowered affinities for other metals. As a result of this we will monitor the physical properties of other transition metal complexes (Ni(II) and Cu(II)) as we study the Zn(II) complexes. The eventual goal of this project is to develop chelators with decreased affinities towards Ni(II) and Cu(II) without decreasing affinity for Zn(II) as much, thus gaining net selectivity towards Zn(II). Herein, the Ni(II), Cu(II) and Zn(II) complexes of bispicpn and two derivatives (**Scheme 3.2** and **Scheme 3.3**) have been synthesized and characterized, and some qualitative changes in M(II) affinities that favor Zn(II) are reported. Chelators used for comparison in this chapter are in **Scheme 3.1**.
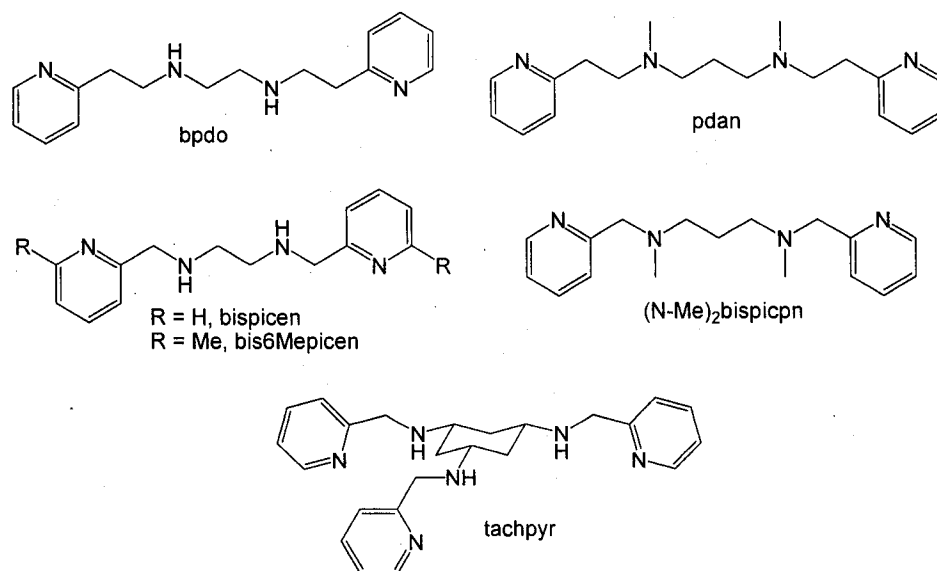
Scheme 3.1. Amino/pyridyl chelators used for comparison and discussion

The nomenclature for six-coordinate geometries obtained by linear

tetradentate chelators is dependent on the relative positions of the "open"

coordination sites. They are typically occupied by an anion or solvent molecule,

forming an overall pseudo-octahedral complex. For the five-coordinate

geometries the relative positions of the pyridyl nitrogens along with the final

geometry upon addition of an ancillary ligand (typically an anion or solvent

molecule) determines the nomenclature. When an overall trigonal-bipyramidal

geometry is attained a *cis* or *trans* label along with a Greek figure (if necessary)

assigned. However, if an overall square-pyramidal conformation is attained that

nomenclature is kept. Only one four-coordinate conformation, tetrahedral, can

be expected from this series of linear tetraamine chelators.

40

Table 3.1. Possible conformations that this series of linear tetraamine ligands could take on for coordination numbers 4, 5 and 6 for visual aid and use in discussion

Overall Coord. Number	Nomenclature	Representation
6	*cis-α*	
6	*cis-β*	
6	*trans*	
5	*trans(5)*	
5	*cis-α(5)*	
5	*cis-β(5)*	
5	*cis-γ(5)*	
5	*square-pyramidal*	
4	*tetrahedral*	

41

Ligand Synthesis

The tetraamine chelators bispicpn, L^6, and bis6Mepicpn, L^7, were

prepared using an improvement to the method of Newkome and coworkers'

method[74] providing better yields than they reported. Ligands L^6 and L^7 were

prepared by the condensation of the appropriate pyridyl aldehyde with 1,3-

diaminopropane in ethanol affording the desired diimino intermediate. Reduction

of the diimine with $NaBH_4$ in ethanol resulted in the target molecules. Yields for

L^6 and L^7 were 85.0% and 96.6% respectively.

H_2N⌒⌒NH_2 + 2 [pyridyl-CHO with R] →(a) EtOH, Δ, 2 h; b) 3 eq. NaBH₄, Δ, 18 h)→ [bis(pyridylmethylaminopropyl) product]
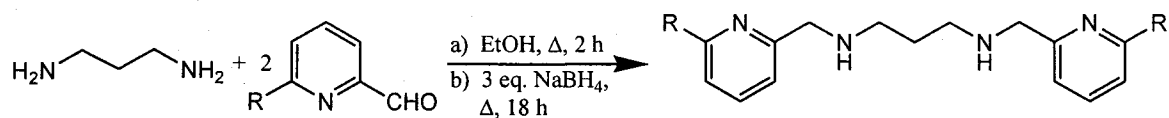
R = H, L^6, bispicpn
R = Me, L^7, bis6Mepicpn
Scheme 3.2. Synthesis of bispicpn, L^6, and bis6Mepicpn, L^7

The homologated tetraamine chelator 1,9-bis(2-pyridyl)-3,7-diazanonane

(bpdan), L^8, proved to be more difficult to obtain than L^6 and L^7. The lack of

availability of 2-pyridineacetaldehyde meant it needed to be synthesized.

Attempts at making the desired aldehyde from 2-pyridylacetic acid by

synthesizing the methyl ester, reducing it to the alcohol with $NaBH_4$ and

performing a Swern oxidation on the alcohol proved unsuccessful. Without the

desired aldehyde other routes had to be explored. Among the routes attempted

were the condensation of vinyl pyridine with 1,3-diaminopropane, coupling 2-(2-

aminoethyl)pyridine with 1,3-dibromopropane in an S_N2 manner and formation of

42

the analogous amide through an active ester. However, these routes did not produce the desired product. L[8] was successfully prepared by tosylation of the readily available starting materials 1,3-propanediol and 2-(2-aminoethyl)pyridine. Deprotonation of the pyridylsulfonamide with NaH to form the sodium salt followed by coupling with the tosyl diol afforded the protected ligand. Deprotection of the amines with concentrated H_2SO_4 generated the free amine in 33 % yield (**Scheme 3.3**).
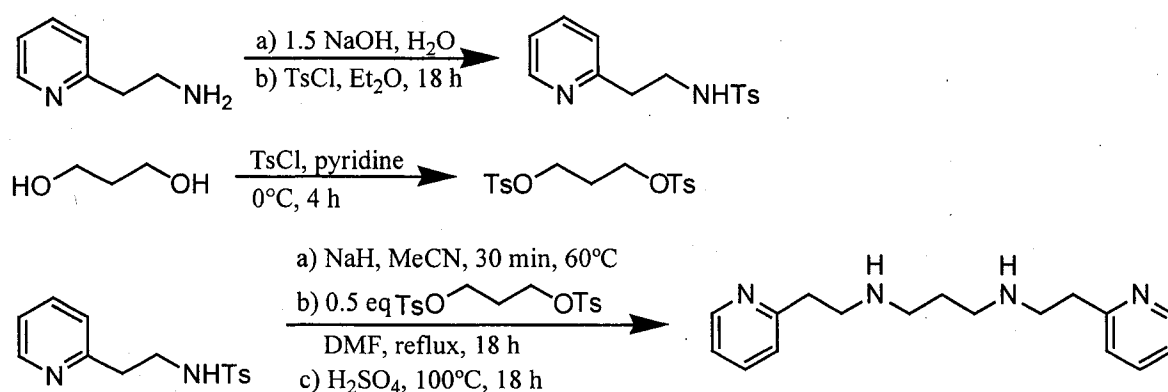
Scheme 3.3. Synthesis of bpdan, L[8]

Metal Complexation

M(II)	bispicpn (R = H, n = 1)	bis6Mepicpn (R = Me, n = 1)	bpdan (R = H, n = 2)
Ni(II)[a]	17a	17b	17c
Cu(II)[a]	18a	18b	18c
Zn(II)[b]	19a	19b	19c

[a]$X = ClO_4^-$, [b]$X = NO_3^-$
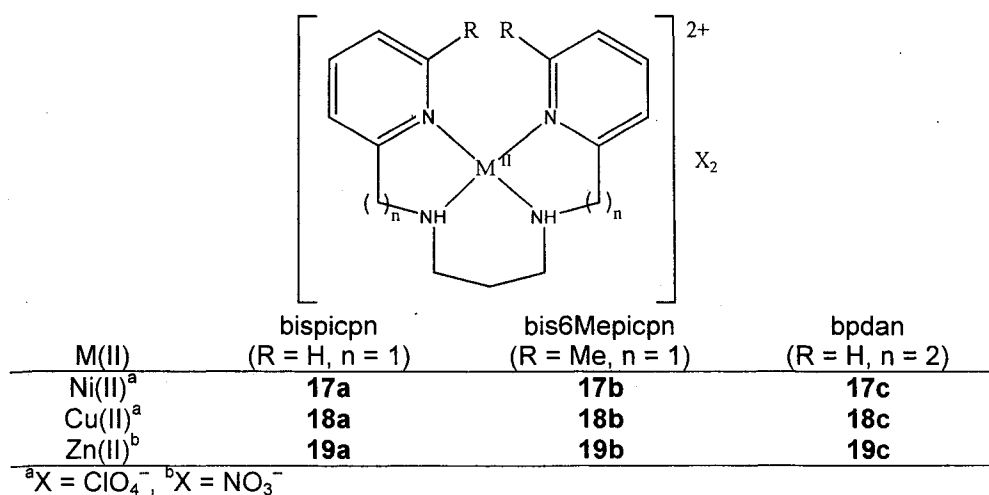
Scheme 3.4. Structures and numbering of isolated metal complexes of bispicpn, bis6Mepicpn and bpdan

43

The complexing properties of bispicpn, bis6Mepicpn and bpdan (L^6, L^7 and L^8 respectively) were evaluated by determination of reaction conditions needed to form $[ML]^{2+}$ (M = Ni(II), Cu(II) and Zn(II)) and physical characterization of the resulting complexes (**Scheme 3.4**). To investigate the steric and electronic effects of varying pyridyl substituents and changing the chelate ring size, as well as obtain the coordination geometry around the M(II) center, the series of divalent metal complexes were isolated and characterized by UV-Vis or ^{1}H and ^{13}C NMR as appropriate and IR spectroscopy. X-ray crystallography was performed for **19a – c**. Isolation of the complexes was accomplished by reaction of equimolar amounts of the respective metal ion salts and the ligands in alcohol followed by precipitation with Et$_2$O. Purification by recrystallization from appropriate solvents produced crystalline solids for all the complexes except [Ni(bispicpn)]$^{2+}$ which was isolated and analyzed as a powder. For all of the Ni(II) and Cu(II) complexes ClO$_4^-$ proved to be a suitable anion for isolation while NO$_3^-$ was the anion used for isolation of the Zn(II) species. Various anions (Cl$^-$, NO$_3^-$, ClO$_4^-$ and CF$_3$SO$_3^-$) were used to study [Zn(bispicpn)]$^{2+}$ and [Zn(bpdan)]$^{2+}$ in solution.

Electronic Structure

Solution phase UV-Vis/Near IR spectra of Ni(II) and Cu(II) complexes served to characterize their structures and to assess the effects of varying pyridyl substituents and chelate ring size. The spectra were measured, assigned and compared with other amino/pyridyl complexes with both N$_4$ and N$_6$ chelators.

44

Nickel (II). The electronic absorption spectra of all the Ni(II) complexes

produced absorptions typical of octahedral Ni(II). This suggests that in solution

the Ni(II) species exist in the form $[Ni(ligand)(X)(X')]^{n+}$, where X or X' could be

any anion or solvent molecule and n can be 0, 1, or 2 depending on the charges

of X and X'. In both water and acetonitrile, **17a** produced two principal bands at

$18000 - 19000 \text{ cm}^{-1}$ and $11000 - 12000 \text{ cm}^{-1}$ (**Figure 3.2**, **Table 3.2**). These two

bands have been assigned as the $^3A_{2g} \rightarrow {}^3T_{1g}$ and $^3A_{2g} \rightarrow {}^3T_{2g}$ transitions

respectively. The low energy band is composed of two components as is seen

by the presence of a small, high energy shoulder. The second component of the

$^3A_{2g} \rightarrow {}^3T_{2g}$ transition which produces the shoulder is commonly seen in

octahedral Ni(II) complexes and is assigned as the spin-forbidden $^3A_{2g} \rightarrow {}^1E_g$

transition. A third, spin-allowed, transition is expected to be present in octahedral

Ni(II) complexes at higher energies, however, this transition is not seen for **17a**,

as it is assumed to lie under the large charge-transfer $(\pi - \pi^*)$ band of the ligand.

45
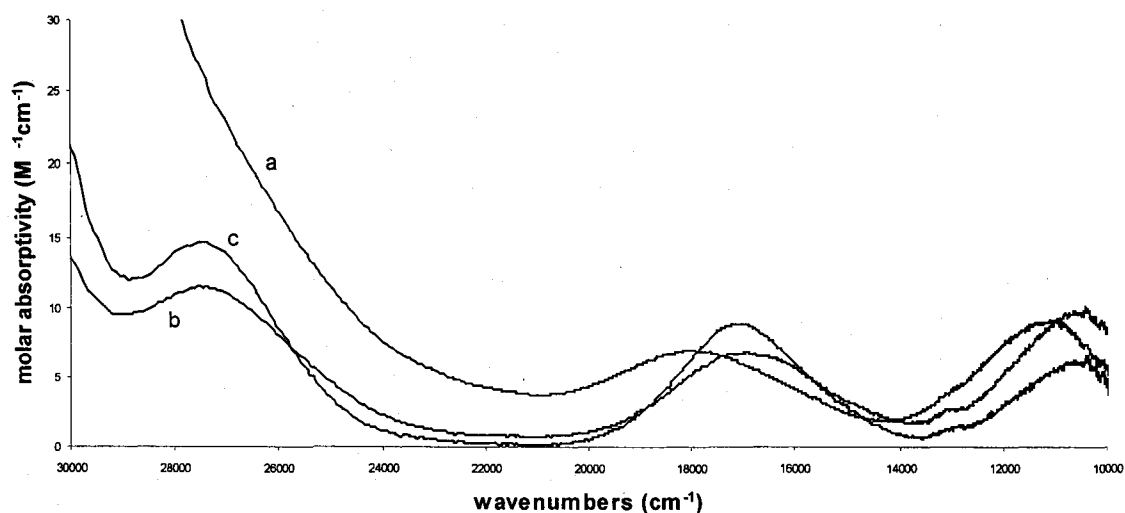
Figure 3.2. Electronic absorption spectra of: a, [Ni(bispicpn)](ClO_4)$_2$ (**17a**); b, [Ni(bis6Mepicpn)](ClO_4)$_2$ (**17b**); c, [Ni(bpdan)](ClO_4)$_2$ (**17c**) in water

The spectra of both **17b** and **17c** exhibit three bands at 27500 – 29000 cm^{-1}, 17000 – 18000 cm^{-1} and 10600 – 11400 cm^{-1} (**Figure 3.2, Table 3.2**). These bands have been assigned as the $^3A_{2g} \rightarrow {}^3T_{1g}$ (P), $^3A_{2g} \rightarrow {}^3T_{1g}$ (F) and $^3A_{2g} \rightarrow {}^3T_{2g}$ (F) transitions, respectively. Again, the low energy transition contains a small, high energy shoulder assigned as the $^3A_{2g} \rightarrow {}^1E_g$ transition. The major difference in the spectra of **17b** and **17c** when compared to **17a** is the red shift of the peaks and the resulting unmasking of the high energy d – d transition. The appearance of this band is presumably due to the decrease in ligand field strength towards the Ni(II) center as either the steric bulk or the chelate ring size increases for **17b** and **17c** respectively. When comparing all three complexes, an important trend to note is the blue shift all of the spectra (**17a** – **17c**) undergo when taken in acetonitrile verses water. In acetonitrile, every peak is shifted to

46

higher energy by ~ 1000 cm^{-1}. This shift suggests coordination by solvent molecules instead of anion (ClO_4^-) is what produces the observed octahedral geometry.

Table 3.2. Spectral data for Ni(II) tetraamine complexes

Complex	Solvent	v/cm^{-1} (ε/M^{-1} cm^{-1})	Assignments	Δ_o (cm^{-1})	color
$[Ni(L^6)]^{2+}$	H_2O	18080 (7.3)	$^3A_{2g} \to {}^3T_{1g}$	11120	violet
		13040 sh (4.3)	$^3A_{2g} \to {}^1E_g$		
		11120 (9.5)	$^3A_{2g} \to {}^3T_{2g}$		
	MeCN	18910 (9.7)	$^3A_{2g} \to {}^3T_{1g}$	11920	violet
		12840 sh (5.4)	$^3A_{2g} \to {}^1E_g$		
		11920 (6.7)	$^3A_{2g} \to {}^3T_{2g}$		
$[Ni(L^7)]^{2+}$	H_2O	27480 (11.5)	$^3A_{2g} \to {}^3T_{1g}$	10590	blue
		16980 (6.7)	$^3A_{2g} \to {}^3T_{1g}$		
		12890 sh (2.7)	$^3A_{2g} \to {}^1E_g$		
		10590 (9.7)	$^3A_{2g} \to {}^3T_{2g}$		
	MeCN	28900 (13.1)	$^3A_{2g} \to {}^3T_{1g}$	10940	violet
		17920 (8.3)	$^3A_{2g} \to {}^3T_{1g}$		
		12830 sh (5.4)	$^3A_{2g} \to {}^1E_g$		
		10940 (9.5)	$^3A_{2g} \to {}^3T_{2g}$		
$[Ni(L^8)]^{2+}$	H_2O	27470 (14.7)	$^3A_{2g} \to {}^3T_{1g}$	10610	blue
		17090 (8.8)	$^3A_{2g} \to {}^3T_{1g}$		
		12850 sh (1.5)	$^3A_{2g} \to {}^1E_g$		
		10610 (6.0)	$^3A_{2g} \to {}^3T_{2g}$		
	MeCN	28490 (28.0)	$^3A_{2g} \to {}^3T_{1g}$	11390	violet
		18050 (14.5)	$^3A_{2g} \to {}^3T_{1g}$		
		12820 sh (4.1)	$^3A_{2g} \to {}^1E_g$		
		11390 (7.0)	$^3A_{2g} \to {}^3T_{2g}$		
$[Ni(bispicen)]^{2+}$ [75]	MeOH	16530 (13.0)	$^3A_{2g} \to {}^3T_{1g}$	9860	
		9860 (9.0)	$^3A_{2g} \to {}^3T_{2g}$		
$[Ni(tachpyr)]^{2+}$ [5]	MeOH	19570 (16.6)	$^3A_{2g} \to {}^3T_{1g}$	11360	
		12550 (16.0)	$^3A_{2g} \to {}^3T_{2g}$		
		11360 sh (11.8)	$^3A_{2g} \to {}^1E_g$		
$[Ni((bpdo)]^{2+}$ [76]	H_2O	28200 (20.0)	$^3A_{2g} \to {}^3T_{1g}$	11050	
		22500 (8.0)	$^1A_{2g} \to {}^1A_{1g}$ [a]		
		17400 (16.0)	$^3A_{2g} \to {}^3T_{1g}$		
		11050 (20.0)	$^3A_{2g} \to {}^3T_{2g}$		
$[Ni((N-Me)_2bispicpn)]^{2+}$ [72]	MeOH	16920 (24.0)	$^3A_{2g} \to {}^3T_{1g}$	10290	
		10290 (27.0)	$^3A_{2g} \to {}^3T_{2g}$		

[a]The presence of this band is attributed to a square planar Ni(II) species in solution along with the solvated, distorted octahedral complex.

Copper (II). **Figure 3.3** shows the series of Cu(II) complexes (**18a** – **18c**) in water. The series in acetonitrile shows similar profiles with slight shifts to

47

higher energy (**Table 3.3**). Again, the solvent dependence of the band positions indicates a bonding interaction between the metal center and solvent molecules. However, the determination of geometry for the Cu(II) complexes is not as straightforward as it was for the Ni(II) complexes. It has been well documented that the coordination sphere of Cu(II) is quite flexible and can assume multiple coordination geometries of various coordination numbers including 4, 5 and 6.
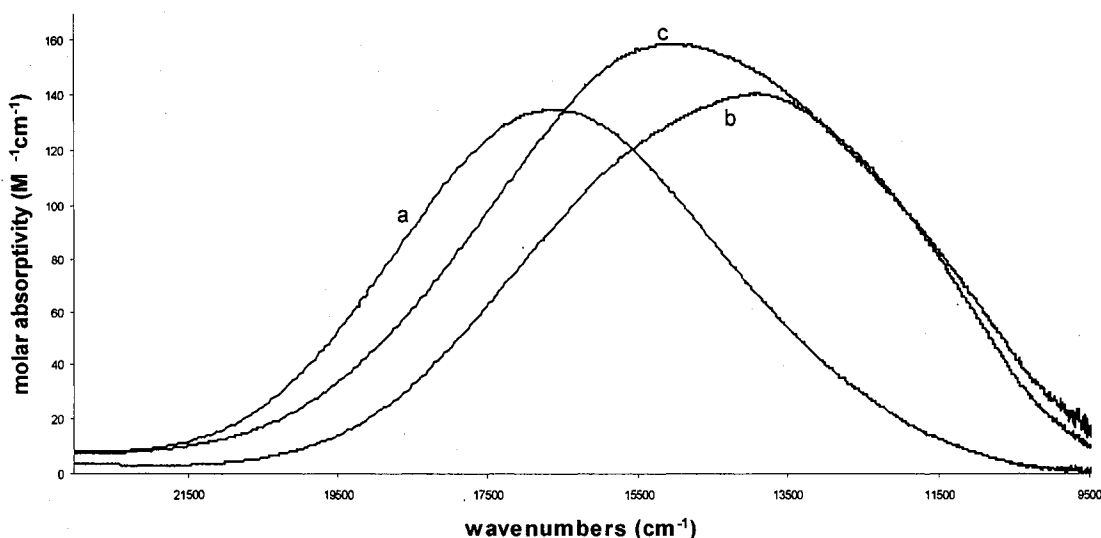
Figure 3.3. Electronic absorption spectra of: a, [Cu(bispicpn)](ClO$_4$)$_2$ (**18a**); b, [Cu(bis6Mepicpn)](ClO$_4$)$_2$ (**18b**); c, [Cu(bpdan)](ClO$_4$)$_2$ (**18c**) in water

Complex **18a** produces a large, symmetric peak around 16500 cm^{-1}. Such a peak is associated with an octahedral Cu(II) complex. Any slight asymmetry seen in the peak is attributed to tetragonal distortions present in the complex. Complexes **18b** and **18c** each produce a single, broad, asymmetric peak with maxima around 14000 and 15000 cm^{-1}, respectively. The asymmetry is due to the plasticity of the metal center, as the geometry around the metal center

48

dictates the shape of the peak. The spectra for **18b** and **18c** do not allow for unambiguous assignment of the geometry of the complex, but based on position and shape of the peaks **18b** and **18c** are most likely square-pyramidal and tetragonally distorted octahedral respectively in solution.

Table 3.3. Spectral data for Cu(II) tetraamine complexes

Complex	Solvent	ν/cm^{-1} (ε/M^{-1} cm^{-1})	Assignments	Δ_o (cm^{-1})	Color
$[Cu(L^6)]^{2+}$	H_2O	16530 (134.7)	$^2E_g \rightarrow {}^2T_{2g}$	16530	violet
	MeCN	16720 (198.7)	$^2E_g \rightarrow {}^2T_{2g}$	16720	blue
$[Cu(L^7)]^{2+}$	H_2O	13990 (139.0)	-	13990	blue
	MeCN	14350 (280.0)	-	14350	blue
$[Cu(L^8)]^{2+}$	H_2O	14950 (159.1)	-	14950	blue
	MeCN	15630 (203.3)	-	15630	blue
$[Cu(bispicen)]^{2+}$ [77]	MeCN	16690 (182.0)	$^2E_g \rightarrow {}^2T_{2g}$	16690	
$[Cu(tachpyr)]^{2+}$ [7]	MeOH	15110 (93.0)	$^2E_g \rightarrow {}^2T_{2g}$	15110	blue
$[Cu(bpdo)]^{2+}$ [78]	MeCN	17270 (180.0)	$^2E_g \rightarrow {}^2T_{2g}$	17270	
$[Cu(pdan)]^{2+}$ [79]	H_2O	15170 (274.0)	$^2E_g \rightarrow {}^2T_{2g}$	15170	

Competition Reactions

To compare the selectivity of chelators L^6, L^7 and L^8 for either Ni(II) or Cu(II) versus Zn(II), aqueous solutions of **17a – c** and **18a – c** were prepared and 1, 10 or 100 equivalents of Zn(II) was added to the solutions. The UV-Vis spectrum was followed for up to 24 hours after the addition of Zn(II) to monitor any spectral changes that would occur with exchange of the metal centers. Multiple wavelengths were monitored and used to determine that any spectral changes were due to the loss of the Ni(II) or Cu (II) complex. Only **17b** showed a decrease in spectral intensity with addition of Zn(II). For this reaction (**Eqn. 2**) the K_{eq} value was determined to be 1.67($\pm$0.07) x 10^{-2} showing little exchange, as expected from the Irving-Williams series. To ensure the reaction was at

49

equilibrium the solution was heated up and then allowed to cool down. Upon heating, the spectral intensity further decreased, but it returned when the solution cooled to its starting temperature.

$$[Ni(L^7)]^{2+} + 10\ Zn^{2+} \rightleftharpoons n\ [Zn(L^7)]^{2+} + n\ Ni^{2+} + 10\text{-}n\ Zn^{2+} \qquad \textbf{(Eqn. 2)}$$
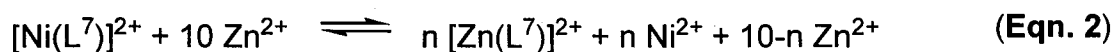
Structural Studies

To elucidate the effects of alkylation at the six-position of the pyridine rings and of increasing the chelate ring size of the chelator on the solution-state structures of the Zn(II) complexes **19a – c**, ^1H and ^{13}C NMR studies were performed. To study the effects of alkylation and homologation of the chelator on the solid-state structures, we undertook crystallographic studies on **19a – c**.

^1H and ^{13}C NMR. The NMR spectra of **19a** showed two symmetric species in solution (**Figure 3.4**). There are two distinct sets of peaks representing a major and minor species in both the ^1H and ^{13}C NMR that, from integration of the pyridyl protons in the ^1H NMR, show the two species to exist in a ratio of 1:2.2. To examine the effect of other anions on the complex, a series of spectra with Cl^-, ClO_4^- and OTf^- were collected. When Cl^- was used only one species was seen in solution, but when ClO_4^- and OTf^- were used two species were again seen.

50
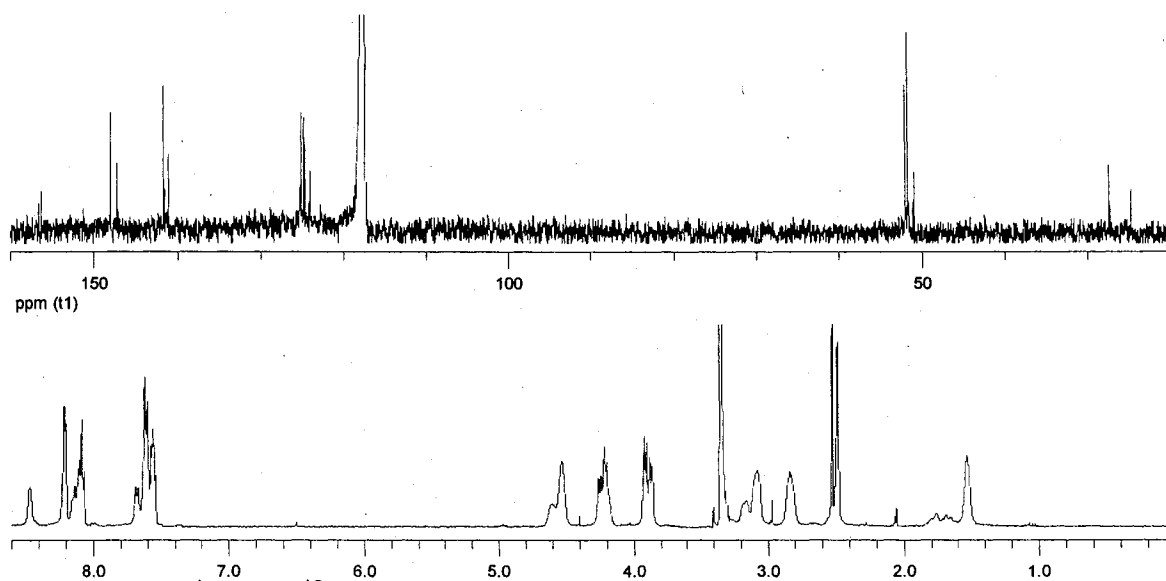
Figure 3.4. ^{1}H and ^{13}C NMR spectra of **19a**

Complex **19b** provided a ^{1}H NMR that had several broad, unassignable peaks while the ^{13}C NMR only produced eight peaks; seven sharp, well defined peaks and a short, broad peak. It was determined that some type of dynamic process was occurring and variable temperature (VT) NMR was used to interpret the spectra. By increasing the temperature to 65°C, several peaks in the ^{1}H NMR converged or sharpened up to produce a spectrum representative of one symmetric species. With an increase in temperature to 65°C, the ^{13}C NMR produced the expected nine peaks.

51
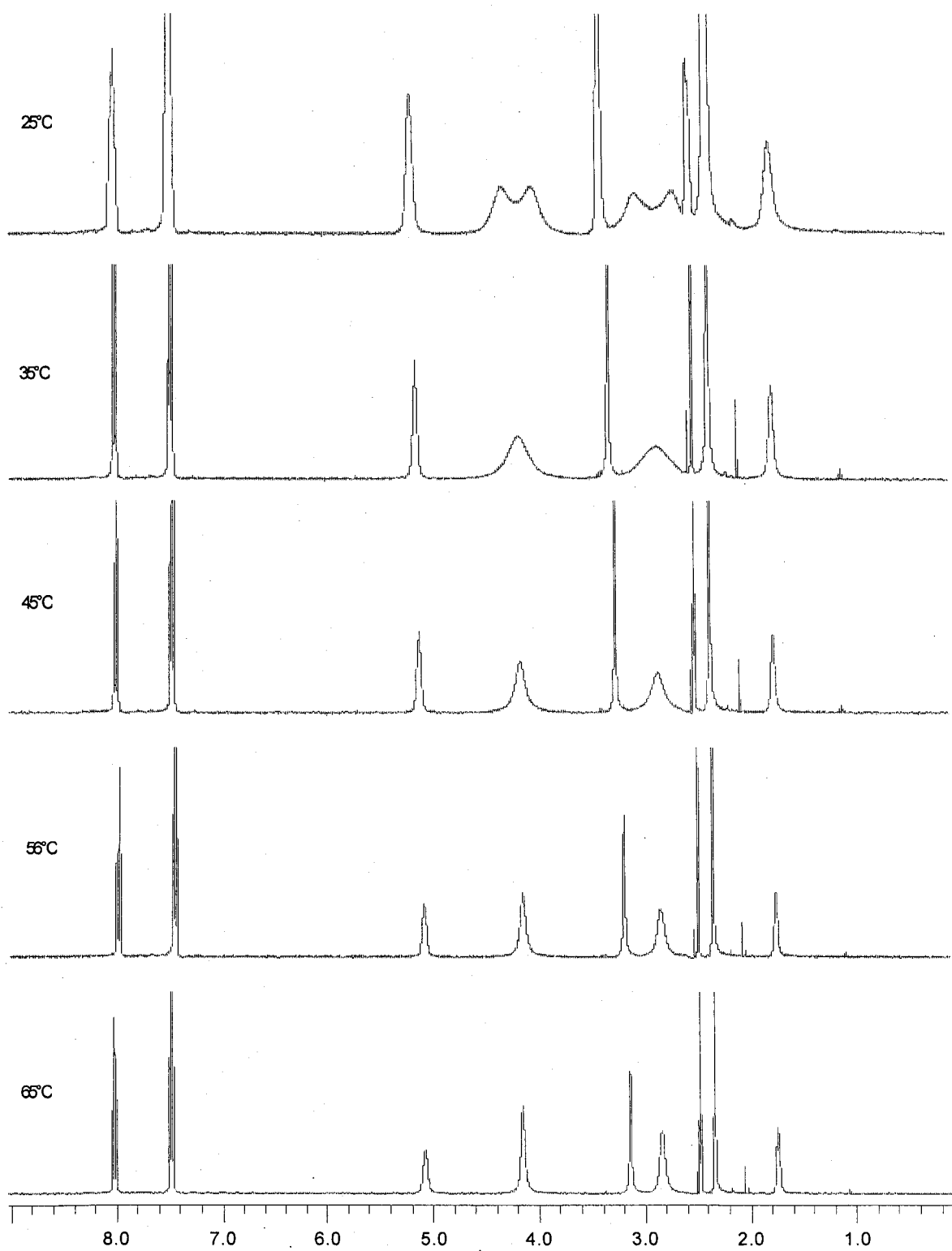
Figure 3.5. Series of high temperature ^1H NMR of **19b**

52

Complex **19c** produced ^{1}H and ^{13}C NMR spectra similar to **19a**. To analyze the association of anions to [Zn(bpdan)]$^{2+}$, a series of spectra were collected with various anions including NO_3^-, Cl^-, ClO_4^- and $CF_3SO_3^-$. When NO_3^- was used there appeared to be one species in solution. However, there was some broadening and lack of definition in the ^{1}H spectrum in the aliphatic region and not all of the carbons were accounted for in the ^{13}C spectrum. This was attributed to a dynamic process occurring in solution. The spectra of the Cl^- species clearly showed one symmetric species in solution. The spectra obtained for the ClO_4^- and $CF_3SO_3^-$ anion species provided evidence for two symmetric species in solution with ratios of 1:2.9 and 1:2.2 respectively.

X-ray Crystallography. Solid-state structural data were obtained for complexes **19a** – **c** using X-ray crystallography. The crystal data showed that all three complexes obtained a distorted *cis-β* octahedral geometry around the metal center. The axial sites of the octahedron are occupied by a nitrate oxygen and a pyridyl nitrogen for each complex. Complexes **19a**, **19b** and **19c** are depicted in **Figures 3.6 – 3.8** and selected bond lengths and angles are listed in **Table 3.4**.
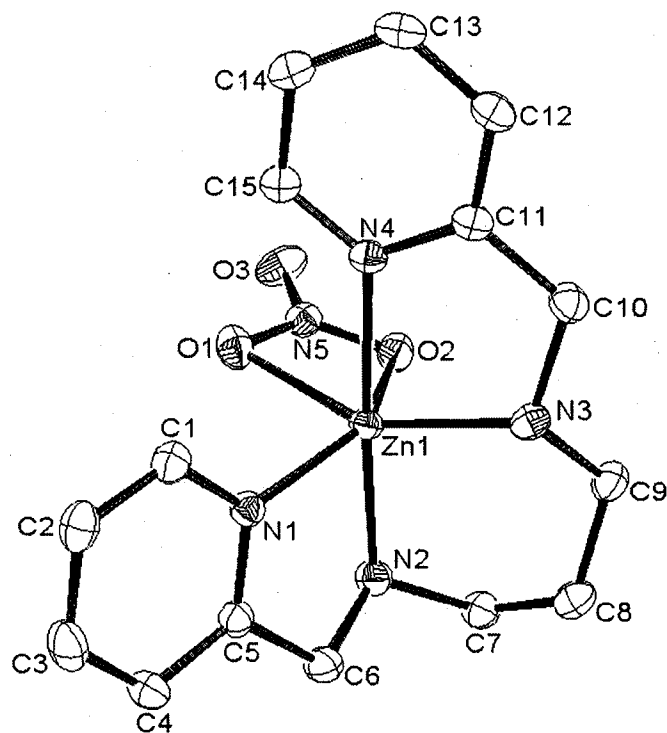
Figure 3.6. ORTEP view of the complex cation of [Zn(bispicpn)(NO$_3$)](NO$_3$) (**19a**) (50 % probability ellipsoids) with hydrogens omitted for clarity
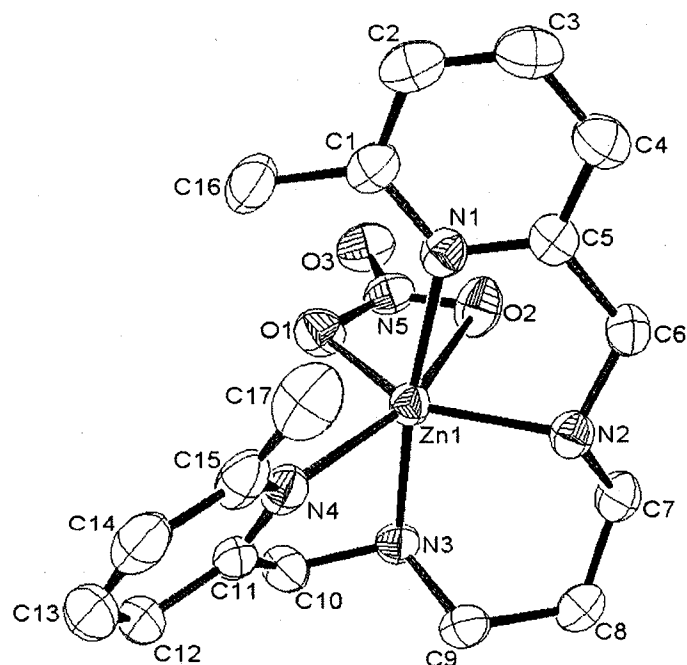
Figure 3.7. ORTEP view of the complex cation of [Zn(bis6Mepicpn)(NO$_3$)](NO$_3$) (**19b**) (50 % probability ellipsoids) with hydrogens omitted for clarity

54
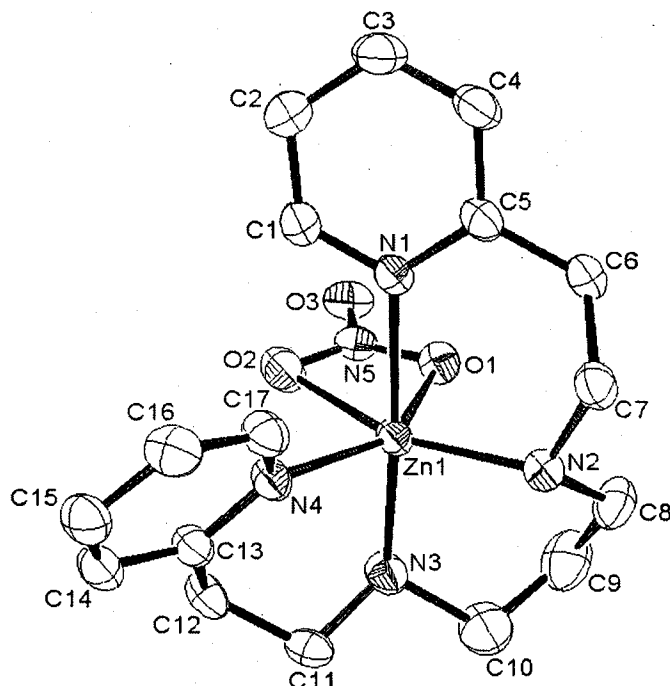
Figure 3.8. ORTEP view of the complex cation of [Zn(bpdan)(NO₃)](NO₃) **(19c)** (50 % probability ellipsoids) with hydrogens omitted for clarity

Table 3.4. Structural comparisons of [Zn(bispicpn)(NO₃)](NO₃) **(19a)**, [Zn(bis6Mepicpn)(NO₃)](NO₃) **(19b)** and [Zn(bpdan)(NO₃)](NO₃) **(19c)**

	Zn-N_{amine} distances (Å)	Zn-N_{py} distances (Å)	Zn-O distances (Å)	N_{amine}-$(CH_2)_n$-N_{py} bite angle, α (°)	N_{amine}-$(CH_2)_n$-N_{amine} bite angle, β (°)
[Zn(L⁶)(NO₃)]⁺ᵃ	2.1288 (16)	2.0709 (15)	2.2823 (14)	80.84 (6)	96.70 (6)
	2.0756 (16)	2.1493 (15)	2.2193 (14)	80.32 (6)	
	2.0818 (17)	2.1215 (15)	2.2498 (15)	81.34 (6)	96.68 (7)
	2.1214 (16)	2.0841 (15)	2.2678 (15)	81.13 (6)	
[Zn(L⁷)(NO₃)]⁺	2.0713 (17)	2.1105 (17)	2.1407 (15)	82.31 (7)	91.65 (7)
	2.0979 (18)	2.1401 (17)	2.5176 (15)	79.33 (7)	
[Zn(L⁸)(NO₃)]⁺	2.069 (2)	2.178 (2)	2.229 (2)	93.79 (8)	93.17 (9)
	2.096 (2)	2.097 (2)	2.429 (2)	93.59 (8)	

ᵃStructure has two independent molecules in the asymmetric unit and both corresponding sets of data are given.

Discussion

Electronic Structure

No surprises were encountered when characterizing the Ni(II) complexes.

The d^8 electron configuration of divalent nickel will assume an octahedral

55

geometry when there are six donor atoms available to complex with the metal and that is what was observed. All the complexes produced spectra typical of octahedral amino/pyridyl nickel with either solvent molecules or anions providing the fifth and sixth donor atoms (**Table 3.2**). Divalent copper provides a more challenging characterization. Its d^9 electron configuration allows for a more flexible coordination sphere, as seen in several reports of 4-, 5- and 6-coordinate Cu(II) compounds.

Nickel (II) Spectra. The entire series of Ni(II) spectra can be seen in **Figure 3.2**. From the positions of the transitions and the subsequent Δ_o values the relative field strengths of the ligands towards divalent nickel can be listed as bispicpn > bpdan ~ bis6Mepicpn in both water and acetonitrile. It is the larger field strength towards nickel that makes the UV-Vis spectrum of **17a** differ from those of **17b** and **17c**. With a larger field strength towards the metal center all of the electronic transitions are shifted to higher energies, placing the $^3A_{2g} \rightarrow {}^3T_{1g}$ (P) transition of **17a** under the large $\pi - \pi^*$ transition of the ligand similar to the analogous amino/pyridyl complexes [Ni(bispicen)]$^{2+}$ and [Ni((N-Me)$_2$-bispicpn)]$^{2+72,75}$ and confirming the data of McKenzie et al.[80] as well as Pandiyan et al.[75]

The reason for the weakened field strength and the appearance of the $^3A_{2g} \rightarrow {}^3T_{1g}$ transition in **17b** and **17c** is presumably different for each complex. In **17b** an element of steric bulk has been added to the ligand by incorporating a methyl group onto the pyridine ring at the 6-position, as we have previously

56

reported for tach-6-Mepyr.[33] Octahedral coordination in all of the *cis-α, cis-β* and *trans* configurations will always lead to collisions of the methyl groups. Complex **17c** differs from **17a** in the size of its chelate rings. Bispicpn offers 3 chelate rings; two 5-membered rings and one 6-membered ring for a 5-6-5 arrangement. Since the two arms of bpdan have been extended by one methylene unit it provides three 6-membered chelate rings in a 6-6-6 arrangement. The affinity of a ligand towards larger metals, such as divalent cadmium or lead, is lower for a ligand with a 6-membered chelate ring than for the same ligand with a 5-membered chelate ring.[81,82] However, it has also been pointed out that increasing the chelate ring size of more than one or sometimes two chelate rings will decrease the affinity of the ligand toward both large and small metal ions due to the introduction of steric crowding.[71] The introduction of this steric crowding explains why the 6-6-6 arrangement of L^8 provides a lower field strength toward Ni(II) than bispicpn.

One similarity between the UV-Vis spectra of all the nickel complexes is the position of the weak shoulder of the $^3A_{2g} \rightarrow {}^3T_{2g}$ (F) transition. As mentioned earlier, this absorption is assigned to the spin-forbidden $^3A_{2g} \rightarrow {}^1E_g$ (D) transition. This transition is present due to spin orbit coupling. As the other bands in this series of spectra travel to various energies depending on the complex, the $^3A_{2g} \rightarrow {}^1E_g$ (D) transition stays relatively stagnant. This can be explained by examining the Tanabe-Sugano diagram for d^8 metals (**Figure 3.9**).

57
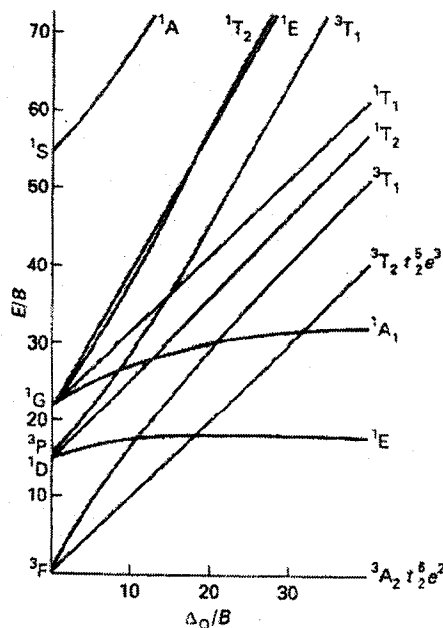
Figure 3.9. Tanabe-Sugano diagram for d^8 metals

The ^1E_g energy level is nearly parallel to the ground state $^3A_{2g}$ energy level while the other observed transitions all have energy levels with increasing slopes. This means, regardless of the ground state energy of the complex, the $^3A_{2g} \rightarrow {}^1E_g$ (D) transition will always be close to the same energy while the energy needed to facilitate the other transitions will vary depending on the system.

Copper (II) Spectra. While the electronic absorption spectra of Cu(II) amino/pyridyl complexes are relatively simple, usually containing only one, broad peak, they can be quite difficult to interpret. The difficulty of interpreting the electronic absorption spectrum of a Cu(II) complex arises from its flexible coordination sphere and ability to take on irregular geometries.[25,83] There are some general rules regarding placement and shape of the transitions in a Cu(II) UV-Vis spectrum that can lead to assignments of stereochemistry around the metal center. For 4-coordinate complexes containing square planar or distorted

58

tetrahedral geometry a transition in the region of 15,000 – 21,000 cm^{-1} is usually seen.[84,85] Complexes containing the 5-coordinate square pyramidal geometry tend to have a band in the region of 15,000 – 18,000 cm^{-1} with a low energy shoulder[25-27] while 5-coordinate trigonal bipyramidal complexes have a band at energies lower than 14,000 cm^{-1} with a high energy shoulder[27,83,86]. The splitting diagrams for square pyramidal and trigonal bipyramidal complexes can be seen in **Figure 1.4**. Finally, 6-coordinate tetragonal octahedral complexes produce a band in the region of 15,500 – 20,000 cm^{-1}.[83,84] Although these rules are very general, they can be a useful starting place for spectral interpretation.

The complex [Cu(bispicpn)]$^{2+}$ has been previously studied by several groups.[77,80,85,87] Through the use of X-ray crystallography[73], X-ray powder diffraction[80], diffuse reflectance spectroscopy[80] and UV-Vis spectroscopy[79,85] a general consensus has been reached that **18a** contains a tetragonally distorted octahedral geometry in solution. McKenzie and coworkers[73,80] have shown through X-ray techniques that, in the solid state, the ligand wraps around the metal center in a distorted in-plane fashion and adopts a distorted square-planar geometry with axial interactions between perchlorate anions and the metal center (CSD reference code, PYDCUA). Comparison of the X-ray data of **18a** reported by McKenzie, the solution state UV-Vis data of **18a** from this work (**Table 3.3**, **Figure 3.3**) and previous reports suggests that in solution the complex retains its solid state geometry, most likely with solvent molecules replacing the anions in the axial positions. It is difficult to rule out the possibility of square-pyramidal

59

geometry based on band position; however, the symmetry of the observed peak in the electronic absorption spectrum indicates our data agrees with previous reports and the complex is most likely in a tetragonally distorted octahedral environment.

McKenzie and Gibson suggested that B-strain is a contributing factor in determining the final geometry that tetradentate amino/pyridyl ligands such as bispicen and bispicpn will adopt. B-strain refers to the bulkiness of a ligand and the resulting steric interaction produced by increasing the bulk as substituents are added to a ligand or as individual chelate rings are lengthened.[88] They state that a complex obtaining a *trans* geometry will incur the greatest B-strain while the *cis-β* and *cis-α* geometries will each possess less B-strain.[80] Hancock and coworkers further demonstrated this point by performing molecular mechanics (MM) calculations on Cu(II) complexes with bispicen and bispicpn bound in a distorted square-planar geometry. Their calculations showed the distance between the 6,6'-hydrogens of the pyridine rings of the bispicpn complex were closer than those of the bispicen complex and there was greater strain in the bispicpn complex.[82] Rybak-Akimova and coworkers also contributed to the steric hindrance discussion by comparing the X-ray structures of three amino/pyridyl Cu(II) complexes with varying chelate ring sizes or 5-5-5, 5-6-5 and 6-5-6 (**Figure 3.10**). They were able to show that as the number of 6-membered chelate rings increased the more tetrahedral distortion occurred around the metal

60

center, but the ligand still adopted a distorted *trans* geometry, with all the donor atoms wrapped around the equator of the metal center.[78]
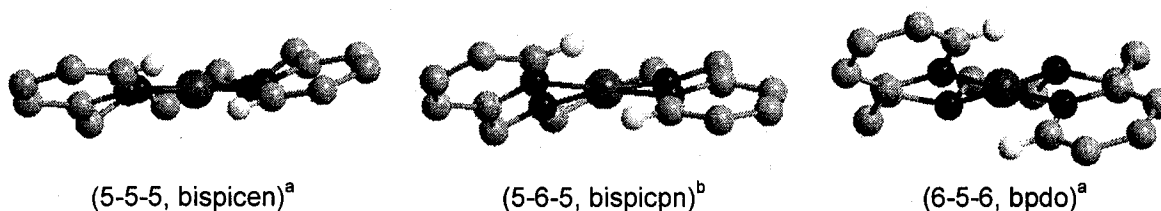

(5-5-5, bispicen)[a]   (5-6-5, bispicpn)[b]   (6-5-6, bpdo)[a]

Figure 3.10. X-ray data of a series of $[CuN_4]^{2+}$ complexes with amino/pyridyl donors and varying chelate ring sizes with all hydrogens removed except the 6,6'-hydrogens; [a]ref # 78, [b]ref # 73

As seen from the X-ray structure of $[Cu(bispicpn)](ClO_4)_2$ (**Figure 3.10**), introduction of methyl groups at the 6 and 6' positions of the pyridine rings of L^6 should introduce a large amount of steric hindrance if the chelator binds around the equator of the metal center in a *trans* fashion. Newkome and coworkers studied the effect of 6-methylation by comparing Pd(II) complexes of L^6 and L^7 by X-ray crystallography. Divalent palladium is a d^8 metal and strongly favors a square-planar geometry. It was concluded that while the presence of methyl groups caused only minor distortions of square-planar geometry in $[Pd(L^6)]^{2+}$ and $[Pd(L^7)]^{2+}$ it was probably due to the strong electronic preferences of Pd(II) and its larger ionic radius, which decreases the steric interactions.[74] McKenzie and Gibson came to a similar conclusion when studying the solid state structure of $[Cu(L^7)](ClO_4)_2$. They state that there is a large tetrahedral distortion around the metal center, but the chelator is still wrapped around the metal center in a planar fashion due to the stabilization provided by the crystal lattice.[80] While it is good to have an idea of the solid state geometry, it is important to realize that the

61

lattice stabilization McKenzie discusses will be gone in solution and the possibility of a new geometry around the metal center is quite likely.

With the introduction of methyl groups and possible steric interactions it is reasonable to expect either a drop in coordination number from 6 to 5 or a shift in octahedral binding from *trans* to either *cis-α* or *cis-β* as the pyridine rings of the chelator are forced away from each other. Unfortunately, the electronic absorption spectrum of **18b** does not provide us with distinct evidence for one situation or the other. It does show two changes when compared to the spectrum of **18a**. First, there is a shift to lower energy and second, there is an element of asymmetry introduced to the absorption. Based on the position of the peak, around 14,300 cm^{-1} (**Table 3.3**, **Figure 3.3**), it is difficult to fit the energy of the peak with any particular geometry according to the general rules mentioned above. Because of the ambiguity of the position of the peak it is necessary to focus on its shape to assign a geometry to the complex. The asymmetry of the absorbance spectrum makes it clear that multiple bands are under the peak requiring deconvolution of the spectrum. Upon deconvolution it was determined that the spectrum was composed of three peaks (**Figure 3.11**).

62

Figure 3.11. Deconvolution of [Cu(bis6Mepicpn)](ClO₄)₂ (**18b**) in water (solid black line = experimental data, dashed red line = sum of black dashed lines)

The presence of three bands in a Cu(II) UV-Vis spectrum usually suggests the complex has a square-pyramidal geometry. However, this geometry typically has a distinct low energy shoulder. The deconvolution does not allow unambiguous structural assignment, however it appears to be a five-coordinate geometry derived by adding a weakly bound ligand to the *trans* solid-state structure.

The electronic absorption spectrum of the novel complex **18c** is slightly asymmetric and shifted to lower energy relative to **18a**. This asymmetric band at 15,000 cm⁻¹ was satisfactorily decomposed to two peaks (**Figure 3.12**).

63

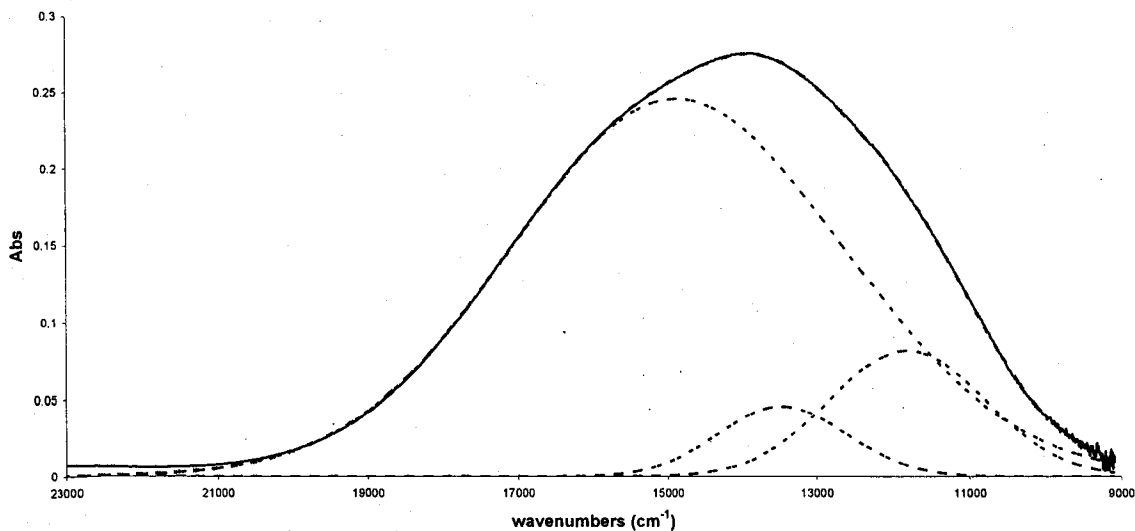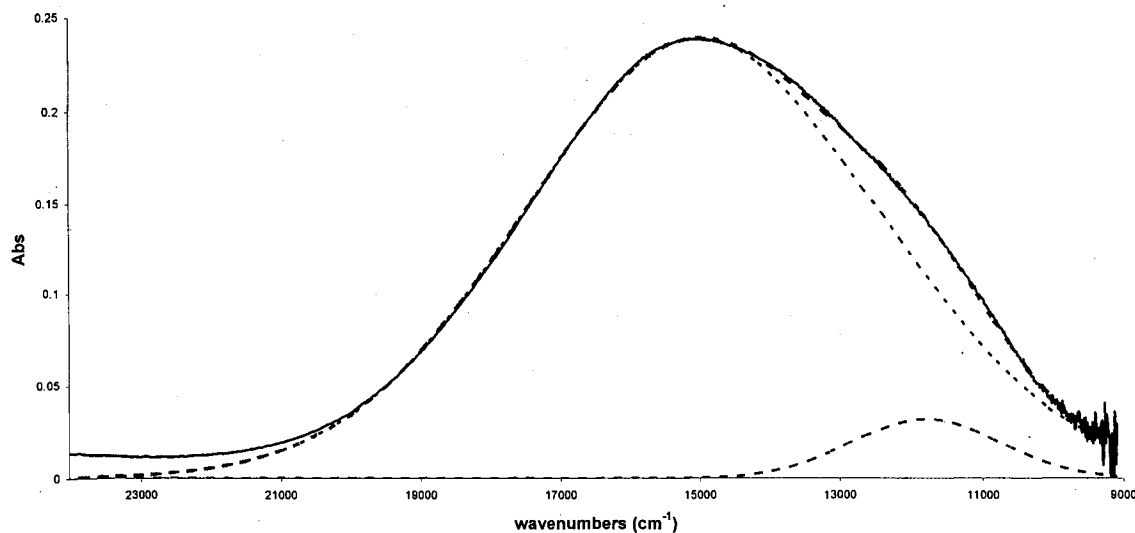**Figure 3.12.** Deconvolution of [Cu(bpdan)](ClO_4)$_2$ (**18c**) in water (solid black line = experimental data, dashed red line = sum of black dashed lines)

This spectrum cannot readily be assigned to a specific geometry; although trigonal-bipyramidal Cu(II) may consist of two peaks, the relative intensities expected are reversed from those observed. On the other hand, comparison of similar complexes such as L^8's N-methylated derivative[79] or the ethylenediamine backbone derivative[78] (6-5-6 chelate ring system seen in **Figure 3.10**) which have both been assigned as having tetragonally distorted octahedral geometry in solution have been reported as having similar spectra with a single broad absorption, at a lower and a higher energy, respectively (**Table 3.3**). It therefore appears likely that **18c** possesses a tetragonally distorted octahedral geometry.

Competition Reactions

To evaluate the affinity of L^6, L^7 and L^8 towards Ni(II) and Cu(II) relative to Zn(II), free zinc, in the form of anhydrous Zn(OTf)$_2$, was added to aqueous

64

solutions of the individual complexes **17a – c** and **18a – c**. The generic equation

for the resulting reaction is shown as **Eqn. 3**. This type of test provides a method

$$[M(L^n)]^{2+} + Zn^{2+} \rightleftharpoons [Zn(L^n)]^{2+} + M^{2+} \quad (n = 6,7,8; M = Ni, Cu) \qquad (\textbf{Eqn. 3})$$
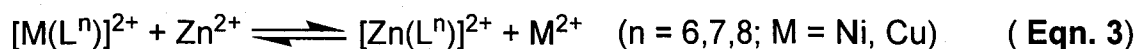
of comparing stability constants of the complexes in solution without actually

having to calculate their values. If the stability constants of the two complexes

are the same and one equivalent of Zn(II) is added to a solution of $[M(L^n)]^{2+}$,

when the reaction reaches equilibrium there should be equal amounts of both

metal complexes. Based on the Irving-Williams series the likelihood of seeing

any spectral changes due to an exchange of Ni(II) or Cu(II) with Zn(II) is very

small[61,62], and indeed a lack of exchange was observed for all complexes except

17b. This is a clear indication that the bulk introduced at the 6-position of the

pyridine rings plays a larger role in decreasing the stability of the metal complex

than the incorporation of extra 6-membered chelate rings.

The equilibrium constant of a reaction is the ratio of stability constants of

the complexes present.[89] The calculated K_{eq} value of $1.67(\pm0.07) \times 10^{-2}$ allows a

comparison of stability constants to be made between **17b** and **19b**. The stability

constant of L^7 with Ni(II) is approximately 60 times greater than with Zn(II). While

this in no way shows selectivity towards Zn(II) over Ni(II), it does show that we

can decrease the affinity of a ligand towards Ni(II) with steric bulk, which was a

goal of this project.

Structural Studies

^{1}H and ^{13}C NMR. To determine the solution state structure of the Zn(II)

complexes, a series of ^{1}H and ^{13}C NMR were taken for each complex. For **19a,**

solution reactions were run with various ZnX_2 salts (X = NO_3^-, Cl^-, ClO_4^- and

OTf^-) and L^6 to observe how the complex reacted with both coordinating (NO_3^-,

Cl^-) and non-coordinating (ClO_4^-, OTf^-) anions. When comparing these spectra,

two distinct results were seen. For the reactions with NO_3^-, ClO_4^- and OTf^- as

the anions the spectra showed signs of two symmetric species. For the reaction

using Cl^- as the anion, only one symmetric species was present in the resulting

spectra (**Figure 3.13**).

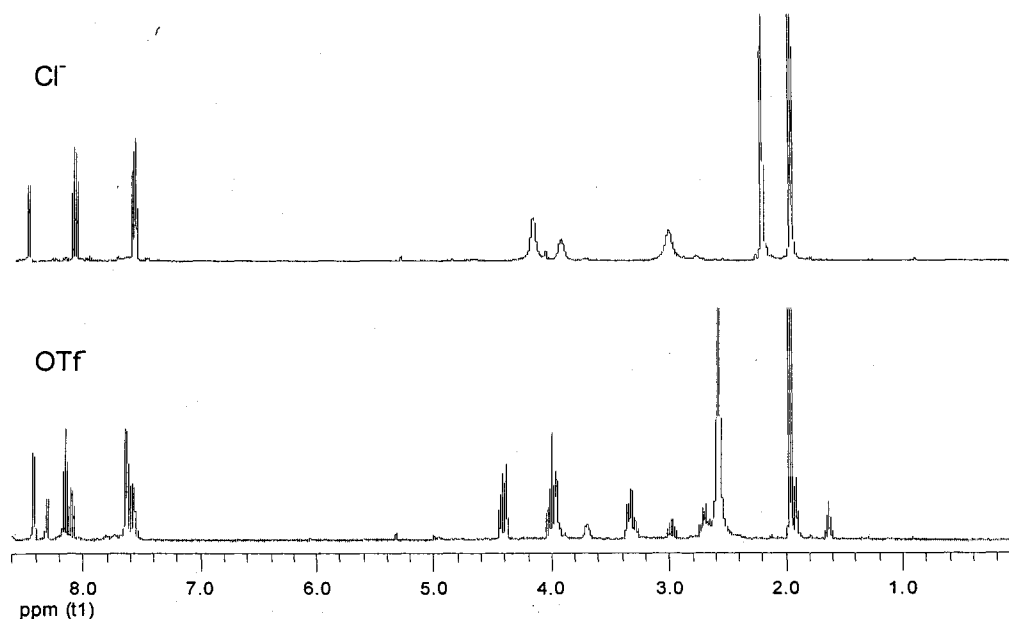**Figure 3.13.** Comparison of ^{1}H NMR spectra of [Zn(bispicpn)]$^{2+}$ (**19a**) with either
Cl^- or OTf^- as the anion

The two-species ^{1}H NMR spectra in the range of δ 1.5 – 4.5 were too

complex to interpret without use of 2D techniques, although their sharpness

66

suggested species that are not undergoing interconversions at a rate corresponding closely to the NMR timescale. The aromatic region of the spectra provides a more useful area for interpretation. Each pyridine ring should produce four peaks. If no symmetry is present in the complex there should be 8 pyridyl peaks, but if a symmetry element (axis of rotation or a mirror plane) is present only 4 pyridyl peaks will be observed. For the spectra showing two species, a series of four large peaks were present in the aromatic region of the spectrum along with a series of four smaller peaks. Each set of peaks contains nearly identical splitting patterns and each set belongs to a species with a different conformation. The ^{13}C NMR of these reactions confirms the presence of two symmetric species. For a complex with symmetry, 8 carbon peaks should be present and for these spectra 2 distinct sets of 8 peaks, one large and one small, are seen (**Figure 3.14**).
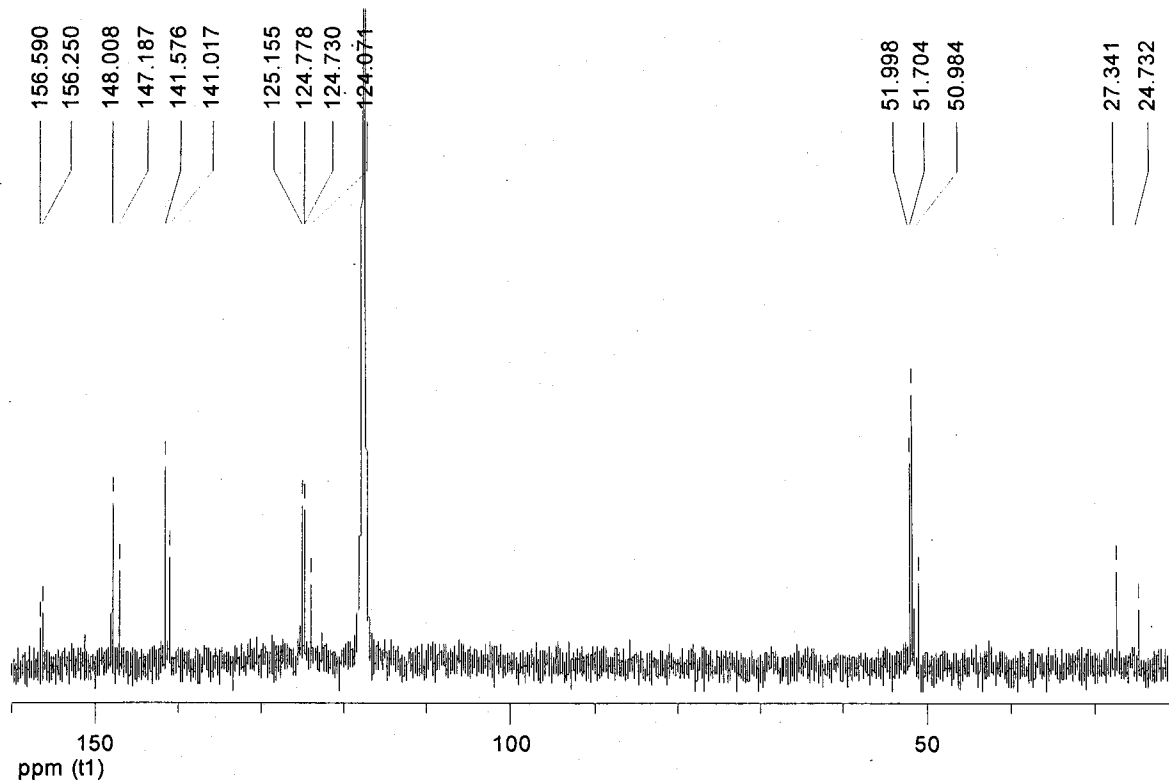
Figure 3.14. ^{13}C NMR spectrum of [Zn(bispicpn)](OTf)$_2$ (**19a**) showing two species in solution

Since it can be shown that the species present in solution are symmetric the possible geometries of the complexes can be narrowed down to a small number of options, which are shown in **Table 3.5**. Unfortunately there are no clues as to which of the six possible geometries are actually present. All that can be said about the spectra is that there are two symmetric complexes present in any combination of two of the geometries listed in **Table 3.5**.

Table 3.5. Geometries containing an element of symmetry

Coord. Number	Geometry	Coord. Number	Geometry
4	distorted tetrahedral	5	square-pyramidal
4	square-planar	6	Trans
5	trans(5)	6	cis-α

68

The ^{1}H NMR spectrum for the reaction with Cl$^-$ as the anion shows four peaks in the aromatic region as expected. It is the aliphatic protons in the complex that provide some insight as to how the complex is behaving in solution. The peaks for the methylene protons on either side of the amine show up as broad singlets at 4.16 and 3.01 ppm. The broad nature of these peaks suggests that there is some sort of dynamic process occurring. If the complex were rigid, each of the protons mentioned above would be inequivalent, and would produce unique peaks. Variable temperature (VT) NMR could be used to resolve the peaks, but was not since we could see that only one species is present in solution and that is the information we wanted. The ^{13}C spectrum shows 8 peaks and therefore supports the assignment of one symmetric species in solution.

The ^{1}H and ^{13}C NMR spectra for **19b** produced an interesting result. The ^{1}H spectrum showed several broad, unassignable peaks in the aliphatic region and broad peaks in the aromatic region while the ^{13}C spectrum gave 7 sharp peaks and 1 broad peak when 9 peaks were expected. It was decided that the broadening was due to a dynamic process and VT NMR would be used to further examine the complex and spectra were taken at 25°C, 35°C, 45°C, 56°C and 65°C. As the temperature of the solution was increased, peaks throughout the ^{1}H and ^{13}C spectra sharpened up.

In the ^{1}H spectrum, the aromatic region gained resolution and the splitting of the signals could be seen. In the aliphatic region of the spectrum, the methylenes flanking the amine, which each started out as broad apparent

69

doublets, converged to singlets. Even the central methylene of the ligand began

to show splitting at 65°C (**Figure 3.5**).

As mentioned above, the ^{13}C spectrum was missing a peak and had a

broad signal. With the increase in temperature the broad peak at 50.6 ppm

sharpened up and gained intensity. Also, the missing peak, which was thought

to be underneath the solvent peak, grew out of the baseline at 26.7 ppm at 65°C

(**Figure 3.15**).
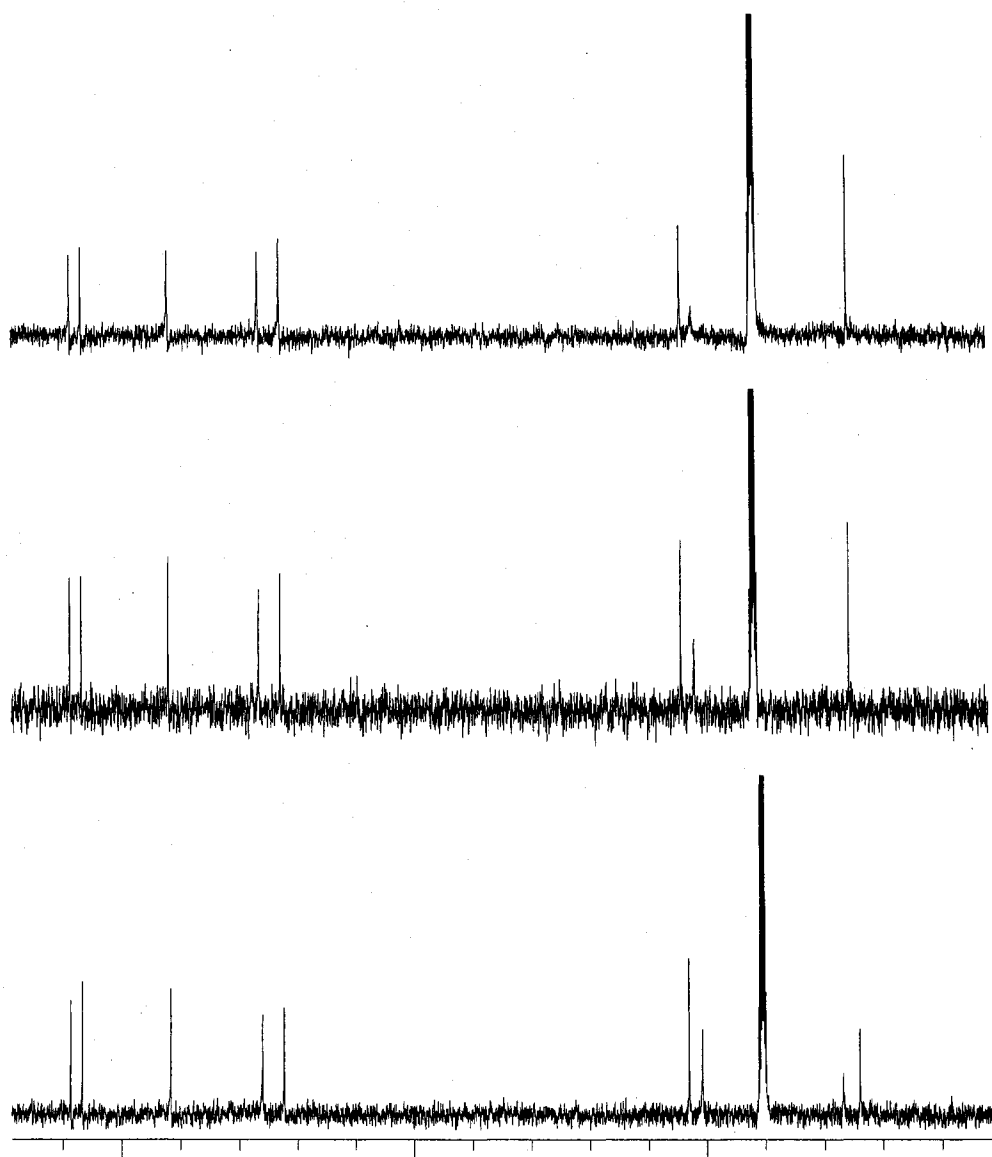
Figure 3.15. ^{13}C NMR spectra of $[Zn(bis6Mepicpn)]^{2+}$ (**19b**) at 25°C, 45°C and 65°C

The spectral changes in **19b** suggest a dynamic process (such as a ring

flip of the 6-membered chelate ring) occurs with greater speed as the

temperature is increased. If the ring was rigid then all of the aliphatic protons

would be inequivalent and produce their own signals. This is what is seen in the

room temperature spectrum. The broad signals at about 4.2 and 2.8 ppm are a

71

result of both sets of methylene protons being inequivalent. The dynamic process occurring is slow enough so we can see individual peaks, but won't allow for any defined splitting. As the temperature is raised the movement in the complex becomes fast on the NMR timescale and the observed spectrum is an average of the movements in the complex.

For **19c**, the same series of solution reactions (ZnX_2 + L^8) were run as were run for **19a** and followed by ^1H and ^{13}C NMR. Again, two types of spectra were observed. For reactions with NO_3^- and Cl^- as the anions one symmetric species was seen in solution while reactions with ClO_4^- and OTf^- as the anions showed two symmetric species in solution. The two reactions that show one species in solution both show evidence of a dynamic process. The NO_3^- product appears to have a slower process relative to the Cl^- product. This can be seen in the multiplicity of the methylene signals around 3 ppm (**Figure 3.16**). The sharper and more defined the peaks are, the faster the movement of the chelator in the complex.
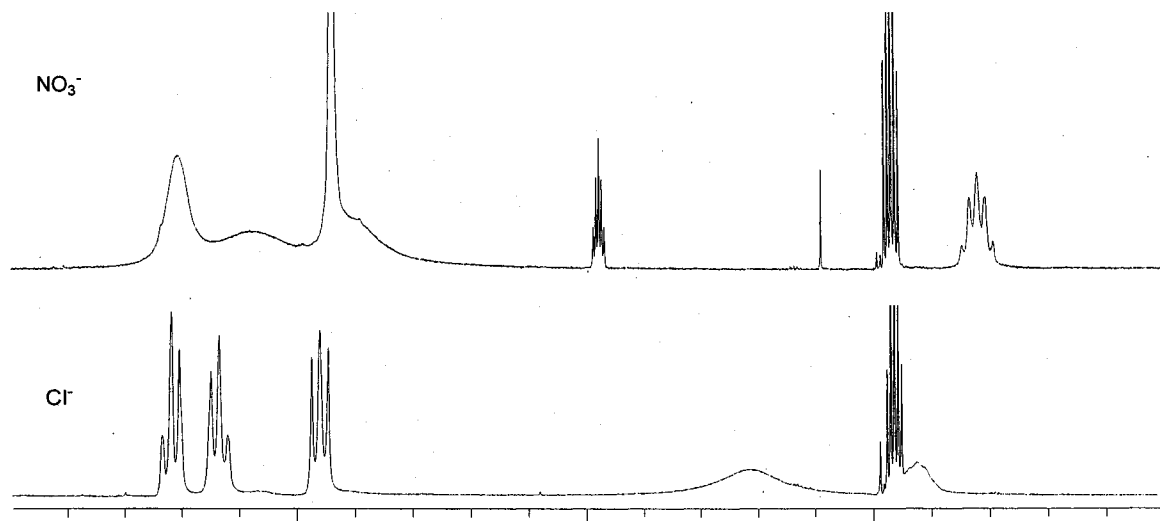
72

Figure 3.16. Aliphatic region of ^1H NMR spectra for **19c** with NO_3^- and Cl^- as anions

The reactions that produced two species in solution gave similar spectra. The presence of multiple peaks with complex splitting patterns in the aliphatic region of the spectra for both the ClO_4^- and OTf^- reactions was a sign of rigid complexes in solution. The aromatic region of these spectra was very similar to those described for **19a** with a set of four large peaks and a set of four small peaks, both with nearly identical splitting patterns. With this data as well as the presence of two sets of peaks present in the ^{13}C spectra it can be stated that two symmetric species are present in solution, but the geometries of those species can only be speculated on without further data.

X-ray Crystallography. For the Zn(II) complexes, **19a – c**, X-ray crystallography was performed to determine their solid state structures. Each complex possesses a distorted octahedral geometry with one nitrate binding in a bidentate manner to occupy the fifth and sixth coordination sites. An amino-N and a pyridyl-N occupy the axial positions while an amino-N, a pyridyl-N and two

73

nitrate oxygens bind at the equatorial sites. All three complexes exist in the cis-β

conformation. This is not surprising, as it has been shown that the pn backbone

in L[6] and its derivatives usually favor the cis-β conformation[90][91].

The six-membered chelate rings, formed upon binding of the two amine

nitrogens of the ligands, exist in a different stereochemistry for each complex.

19a has a chair configuration, **19b** has a twist boat configuration and **19c** has a

distorted boat configuration (**Figure3.17**). This is a good means of comparing

distortion in the complexes since they all have the same, cis-β, conformation.

The complex with the least amount of distortion is **19a**. With the presence of only

one 6-membered chelate ring and no alkylation on the pyridine rings to introduce

steric interactions this is to be expected. The chair conformation of the 6-

membered chelate ring demonstrates the lack of strain in the molecule. Using

the same logic, it can be said that the presence of the more strained twist boat

and distorted boat conformations of **19b** and **19c** respectively show how the

introduction of 6-methyl groups on the pyridine rings or the homologation of the

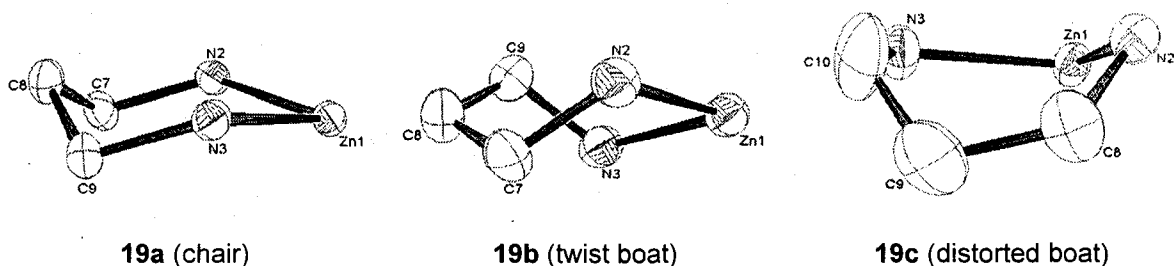ligand lead to a more strained atmosphere around the metal center.

19a (chair)   **19b** (twist boat)   **19c** (distorted boat)

Figure 3.17. 6-membered chelate rings formed from binding of amine nitrogens
in **19a**, **19b** and **19c**

74

Another means of comparing strain in the series of the Zn(II) complexes is by comparing the N_{amine}-Fe-N_{py} axial bond angles of the series. The ideal trans-axial bond angle in an octahedral complex is 180°. The axial bond angles in this series decrease from 176° to 169° in the order **19a** > **19c** > **19b** (**Table 3.6**). Again, **19a** is the least strained complex of the three while **19b** and **19c** show a larger deviation from 180°. However, when comparing the axial bond angles of **19a – c** to other amino/pyridyl complexes with cis-β conformation it is difficult to call these complexes strained. The Ni(II) complex of the N-methyl derivative of L^6 possesses an angle of 170.9°[72] while the Fe(II) complex [Fe(L^6)(NCS)$_2$] has an angle of 164.9°[92]. So, relative to similar complexes with different metal centers the axial bond angles show little strain, but when comparing the three Zn(II) complexes **19a** shows the least amount of distortion in this bond angle.

Table 3.6. Selected angles and conformations of [Zn(bispicpn)(NO$_3$)](NO$_3$) (**19a**), [Zn(bis6Mepicpn)(NO$_3$)](NO$_3$) (**19b**) and [Zn(bpdan)(NO$_3$)](NO$_3$) (**19c**)

	N_{py}-Zn-N_{amine} equatorial angle (°)	N_{py}-Zn-N_{amine} axial angle (°)	O-Zn-O bite angle (°)	Conformation of central chelate ring
[Zn(L^6)(NO$_3$)]$^{+a}$	117.05 (6)	176.63 (6)	57.25 (5)	chair
	115.28 (7)	175.51 (6)	56.94 (5)	
[Zn(L^7)(NO$_3$)]$^+$	117.66 (6)	172.35 (6)	54.29 (5)	twist boat
[Zn(L^8)(NO$_3$)]$^+$	112.65 (8)	169.30 (9)	54.89 (7)	distorted boat

[a]Structure has two independent molecules in the asymmetric unit and both corresponding sets of data are given.

The bond angle between the equatorial amino and pyridyl nitrogens for each complex is closer to that of a trigonal-bipyramidal complex (ideal TBP equatorial angle is 120°) rather than of an octahedral complex (ideal O_h equatorial angle is 90°). For **19a – c**, these angles range from 112 – 117° (**Table 3.6**). For other metal centers bound to L^6 the reported angles are much smaller.

75

The complex [Fe(L^6)Cl$_2$] has a reported N$_{amine}$-Fe-N$_{py}$ equatorial bond angle of 85.9°[90] while the same angle for [Fe(L^6)(NCS)$_2$] is reported as 87.6°[92], both closer to the expected 90° angle for an octahedral complex. The large N$_{py}$-Zn-N$_{amine}$ equatorial bond angle for complexes 19a – c is likely due to a combination of the small O-Zn-O bite angle from the bound nitrate and the lack of ligand field stabilization energy of Zn(II). In the cis-β conformation there are two equatorial sites which are unoccupied by the ligand. Typically, two monodentate ligands will bind in the open sites in a manner such that there is maximum separation between all binding groups. This means they will spread out roughly 90° from each other, resulting in an octahedral environment around the metal center. However, with the chelation of nitrate in a bidentate fashion, the two oxygen atoms are restricted to a smaller angle and this allows for larger angles elsewhere. The small bite angle can't be held solely accountable for the large N$_{py}$-Zn-N$_{amine}$ equatorial bond angle; the metal center also plays a role. The lack of ligand field stabilization energy for Zn(II) means the metal center will not force the chelator to bind in any particular manner and will take on geometries of coordination numbers other than six if necessary. As mentioned above the large equatorial angles are closer to those seen in trigonal-bipyramidal rather than octahedral complexes. Actually, if the bound nitrate in complexes 19a – c is viewed as a large, monodentate ligand, not a bidentate one, the average equatorial bond angles for 19a, 19b and 19c are 119.9°, 119.8° and 119.9°

76

respectively. Thus, **19a – c** are appropriately viewed as pseudo-trigonal-bipyramidal Zinc complexes with a *cis-β(5)* conformation in the solid state.

Conclusion

This work demonstrates that linear, tetradentate amino/pyridyl chelators bind Ni(II), Cu(II) and Zn(II) in aqueous and nonaqueous environments. The effect of 6-substitution of the pyridine rings and homologation of the chelate arms was investigated. In the solid state the effects of substitution and homologation are minimal, as predicted. X-ray structures of the three Zn(II) complexes showed they all took on the same conformation, *cis-β*, with only small differences observed in the structures. In solution, more striking effects of substitution and homologation were seen. Chelators L[7] and L[8] showed a decreased ligand field strength towards both Ni(II) and Cu(II) compared to L[6]. While the Ni(II) complexes **17a – c** all obtained an octahedral geometry in solution, the geometry of the Cu(II) complexes appears to change from tetragonally distorted octahedral for **18a** and **18c** to square-pyramidal for **18b**. While both methylating and homologating L[6] does affect the binding of divalent metals it appears that methylation, with resulting increased steric bulk, provides a greater impact as was seen in their relative affinities for Ni(II) vs Zn(II). L[7] showed the only measurable, and therefore smallest, value of $K_f(Ni^{II})/K_f(Zn^{II})$. Thus, the ligand L[7] emerged from this work as having the largest relative affinity $K_f(Ni^{II})/K_f(Zn^{II})$ (althought still less than one). A reasonable approach to future work is to further

increase the steric bulk on L^7 (i.e., replacement of Me by Et, ^{i}Pr or ^{t}Bu) which may provide even greater affinity for Zn(II) over Ni(II) or Cu(II).

78

CHAPTER IV

EXPERIMENTAL

General Experimental

Instrumentation

^{1}**H and** ^{13}**C NMR** spectra were recorded on a Varian Mercury 400 MHz NMR spectrometer or a Varian INOVA 500 MHz NMR spectrometer with an inverse probe. Spectra were measured in $CDCl_3$, D_2O, MeOD-d_4, MeCN-d_3 or DMSO-d_6 with $(CH_3)_4Si$ as an internal standard. Chemical shifts are reported in parts per million (ppm) relative to the internal standard.

UV/Vis/NIR solution electronic spectra were measured using a Varian Cary 50-Bio UV/Vis spectrometer with 1- or 3-mL quartz cuvettes (1 cm path length). Deconvolutions of electronic absorption spectra were performed using Microcal Origin 6.0 software.

Electrospray ionization (ESI) mass spectra in the positive ion detection mode were obtained with a Finnegan LCQ Classic instrument with dual optical Paul traps and Picoview nanospray source.

IR spectra were recorded on a Thermo Nicolet Avatar 380 FT-IR spectrophotometer.

Elemental analysis was performed by Atlantic Microlabs (Atlanta, Georgia).

79

Solvents

The following solvents were freshly obtained from the automatic still: diethyl ether (Et_2O), dichloromethane (CH_2Cl_2), methanol (MeOH), acetonitrile (MeCN), dimethylformamide (DMF). Et_2O was also used immediately after distillation from Na. E-pure water was obtained from a Barnstead E-pure water purification, module deionization system. All deuterated solvents for NMR analysis were purchased from Cambridge Isotope Laboratories and kept in a dessicator.

Reagents

All reagents were purchased from the following companies: Aldrich, Sigma, Fischer Scientific (Acros), Alfa Aesar or Fluka.

Chapter I Experimental

Work with Fe(II) and Ni(II) involved isolating the complexes while Cu(II) work dealt only with solution reactions. All Fe(II) complexes were prepared under N_2, in a glovebox, unless otherwise stated.

[Fe(tach-3-Mepyr)]Cl$_2$·1.5H$_2$O (1a·1.5H$_2$O) A pale green solution of $FeCl_2·4H_2O$ (0.0070 g, 3.53×10^{-5} mol) in MeOH (1 mL) was added to a pale yellow solution of L1 (0.0155 g, 3.48×10^{-5} mol) in MeOH (1 mL) producing a red-brown solution. Slow diffusion of Et_2O, followed by addition of an aliquot of Et_2O (1 mL) and allowing the solution to sit for 48 hrs at $-10°C$ produced clusters of carmine red needles. Product was isolated and dried under reduced pressure affording deep red needles. ^1H NMR [400 MHz, $(CD_3)_2SO$, 25°C]: δ 7.59, 7.15, 6.91 (d, dd, d, 3H, 3-Me-C$_5\underline{H}_3$N); 5.29 (br t, 1H, N$\underline{H}$-CH$_2$); 4.23, 4.02 [dd, dd, 2H, (NH-C$\underline{H}_2$-py),

diastereotopic]; 2.95 (br s, 1H, cyclohexyl methine $\underline{H}$); 2.37 [s, 3H, (CH_3-py)]; 2.12 (br d, 1H, equatorial cyclohexyl methylene $\underline{H}$); 1.84 (br d, 1H, axial cyclohexyl methylene $\underline{H}$). λ_{max}/cm^{-1} (MeOH) 22700 ($\varepsilon/cm^{-1}M^{-1}$ 7000), 18200 shoulder. (Found: C, 54.17; H, 6.22; N, 13.76. $C_{27}H_{36}Cl_2N_6Fe \cdot 1.5H_2O$ requires: C, 54.25; H, 6.58; N, 14.07%).

[Fe(tach-4-Mepyr)]$Cl_2 \cdot 1.5H_2O$ (1b$\cdot$1.5H_2O) A pale green solution of $FeCl_2 \cdot 4H_2O$ (0.0110 g, 5.53×10^{-5} mol) in MeOH (1 mL) was added to a pale yellow solution of tach-4-Mepyr (0.0244 g, 5.49×10^{-5} mol) in MeOH (1 mL) affording a deep red-brown solution. Slow Et_2O diffusion produced several deep red microcrystals. The supernatant was decanted and the solid was dried under reduced pressure giving deep red microcrystals. ^{1}H NMR [400 MHz, $(CD_3)_2SO$, 25°C]: δ 7.42, 7.17, 6.86 (s, d, d, 3H, 4-Me-$C_5\underline{H}_3$N); 5.45 (br t, 1H, N$\underline{H}$-CH_2); 4.43, 4.19 [dd, dd, 2H, (NH-C$\underline{H}_2$-py), diastereotopic]; 3.21 (br s, 1H, cyclohexyl methine $\underline{H}$); 2.37 [s, 3H, (C$\underline{H}_3$-py)]; 2.02 (br d, 1H, equatorial cyclohexyl methylene $\underline{H}$); 1.79 (br d, 1H, axial cyclohexyl methylene $\underline{H}$). λ_{max}/cm^{-1} (MeOH) 23100 ($\varepsilon/cm^{-1}M^{-1}$ 6600), 17800 shoulder. (Found: C, 54.56; H, 6.16; N, 13.86. $C_{27}H_{36}Cl_2N_6Fe \cdot 1.5H_2O$ requires: C, 54.25; H, 6.58; N, 14.07%).

[Fe(tach-5-Mepyr)]$Cl_2 \cdot H_2O$ (1c$\cdot$$H_2O$) A pale green solution of $FeCl_2 \cdot 4H_2O$ (0.0108 g, 5.43×10^{-5} mol) in MeOH (1 mL) was added to a pale yellow solution of tach-5-Mepyr (0.0235 g, 5.28×10^{-5} mol) in MeOH (1 mL) creating a deep red solution. Slow diffusion of Et_2O followed by an additional aliquot of Et_2O (15 mL) produced a slightly cloudy solution. Allowing the solution to sit for a week

81

generated carmine red needles. The supernatant was decanted and the product was allowed to air dry giving a deep red needles. ^{1}H NMR [400 MHz, $(CD_3)_2SO$, 25°C]: δ7.65, 7.49, 6.78 (d, d, s, 3H, 5-Me-$C_5\underline{H}_3$N); 5.57 (br t, 1H, N$\underline{H}$-CH$_2$); 4.43, 4.12 [dd, dd, 2H, (NH-C$\underline{H}_2$-py)]; 3.13 (br s, 1H, cyclohexyl methine $\underline{H}$); 2.08 (partially obscured) [s, 3H, (C$\underline{H}_3$-py)]; 2.09 (partially obscured) (br d, 1H, equatorial cyclohexyl methylene $\underline{H}$); 1.81 (br d, 1H, axial cyclohexyl methylene $\underline{H}$). λ_{max}/cm^{-1} (MeOH) 22600 (ε/cm^{-1}M^{-1} 4200), 17400 shoulder. (Found: C, 54.73; H, 6.45; N, 13.88. $C_{27}H_{36}Cl_2N_6Fe\cdot H_2O$ requires: C, 55.08; H, 6.51; N, 14.28%).

[Fe(tach-6-Mepyr)](ClO$_4$)$_2$·H$_2$O·MeOH (1d·H$_2$O·MeOH) A yellow solution of Fe(ClO4)•6H$_2$O (0.0160 g, 4.41x10^{-5} mol) in MeOH (1 mL) was added to a pale yellow solution of tach-6-Mepyr (0.0195 g, 4.39x10^{-5} mol) in MeOH (1 mL) producing a dark red solution. During 24 hours at 5°C red needles precipitated from the solution. Removal of the supernatant and air-drying produced bright red needles. μ_{eff} (DMSO, 25°C) = 5.46 B.M. λ_{max}/cm^{-1} (MeCN) 19600 shoulder (ε/cm^{-1}M^{-1} 4.7), 11700 (9.4). (Found C, 45.45; H, 5.31; N, 11.61. $C_{27}H_{38}Cl_2FeN_6O_9$ requires: C, 45.24; H, 5.35; N, 11.73%).

[Fe(tach-6-MeOpyr)]Cl$_2$·1.5H$_2$O (1e·1.5H$_2$O) A pale green solution of FeCl$_2$·4H$_2$O (0.0113 g, 5.68x10^{-5} mol) in MeOH (1 mL) was added to a pale yellow solution of tach-6-MeOpyr (0.0276 g, 5.61x10^{-5} mol) in MeOH (1 mL) producing a yellow solution. Addition of ca. 15 mL of Et$_2$O produced a slightly cloudy solution that deposited yellow prisms upon standing 48 hours. The

82

supernatant was decanted and the product allowed to air-dry resulting in bright yellow prisms. μ_{eff} (DMSO, 25°C) = 5.77 B.M. λ_{max}/cm^{-1} (MeOH) 11100 ($\varepsilon/cm^{-1}M^{-1}$ 4.7). (Found: C, 50.21; H, 6.10; N, 12.84. $C_{27}H_{36}Cl_2N_6FeO_6 \cdot 1.5H_2O$ requires: C, 50.22; H, 6.09; N, 13.02%).

[Ni(tach-3-Mepyr)](ClO$_4$)$_2$ (3a) A pale green solution of Ni(ClO$_4$)$_2$·6H$_2$O (0.0169 g, 4.62x10^{-5} mol) in MeOH (1 mL) was added to a pale yellow solution of L1 (0.0204 g, 4.59x10^{-5} mol) in MeOH (1 mL) affording a pale purple-pink solution. Pink needles formed after 24 hours. The supernatant was decanted and the solid was washed with Et$_2$O and dried, producing pale pink needles (0.0191 g, 59.3%). MS (ESI, MeOH): m/z 501 (M - 2ClO$_4^-$ - H$^+$), 601 (M - ClO$_4^-$). λ_{max}/cm^{-1} (MeCN) 11300 shoulder ($\varepsilon/cm^{-1}M^{-1}$ 10.8), 12900 (15.9), 19500 (11.7). (Found: C, 46.43; H, 5.28; N, 12.06. $C_{27}H_{36}Cl_2N_6NiO_8$ requires: C, 46.20; H, 5.17; N, 11.97%).

[Ni(tach-4-Mepyr)](ClO$_4$)$_2$ (3b) A pale green solution of Ni(ClO$_4$)$_2$·6H$_2$O (0.0159 g, 4.35x10^{-5} mol) in MeOH (1 mL) was added to a pale yellow solution of tach-4-Mepyr (0.0197 g, 4.43x10^{-5} mol) in MeOH (1 mL) producing a pink solution. Small pink needles were produced by Et$_2$O diffusion into the MeOH solution. These crystals were isolated, washed with Et$_2$O, dried under reduced pressure, and taken up in MeOH (1 mL). Et$_2$O diffusion into the MeOH solution yielded pink needle clusters that were isolated and dried affording a pink solid (0.0184 g, 59.2%). MS (ESI, MeOH): m/z 501 (M - 2ClO$_4^-$ - H$^+$), 601 (M - ClO$_4^-$). λ_{max}/cm^{-1} (MeCN) 11300 shoulder ($\varepsilon/cm^{-1}M^{-1}$ 12.7), 12800 (15.9), 19500 (14.2). (Found: C,

83

46.31; H, 5.14; N, 11.94. $C_{27}H_{36}Cl_2N_6NiO_8$ requires: C, 46.20; H, 5.17; N, 11.97%).

[Ni(tach-5-Mepyr)](ClO₄)₂ (3c) A pale green solution of $Ni(ClO_4)_2 \cdot 6H_2O$ (0.0162 g, 4.42x10⁻⁵ mol) in MeOH (1 mL) was added to a pale yellow solution of tach-5-Mepyr (0.0200 g, 4.50x10⁻⁵ mol) in MeOH (1 mL) producing a purple-pink solution. Slow diffusion of Et_2O produced light pink microcrystals. The microcrystals were isolated, washed with Et_2O, dried under reduced pressure, and taken up in MeOH (1 mL). Diffusion of Et_2O into the MeOH solution produced pink needles that were isolated, washed with Et_2O, and dried producing pink needles (0.0221 g, 70.2%). MS (ESI, MeOH): m/z 501 (M - $2ClO_4^-$ - H⁺), 601 (M - ClO_4^-). λ_{max}/cm^{-1} (MeCN) 11200 shoulder ($\varepsilon/cm^{-1}M^{-1}$ 12.7), 12800 (17.0), 19500 (14.2). (Found: C, 46.21; H, 5.13; N, 11.76. $C_{27}H_{36}Cl_2N_6NiO_8$ requires: C, 46.20; H, 5.17; N, 11.97%).

[Ni(tach-6-Mepyr)](ClO₄)₂·H₂O (3d·H₂O) A pale green solution of $Ni(ClO_4)_2 \cdot 6H_2O$ (0.0169 g, 4.62x10⁻⁵ mol) in MeOH (1 mL) was added to a pale yellow solution of tach-6-Mepyr (0.0203 g, 4.57x10⁻⁵ mol) in MeOH (1 mL) affording a dark yellow solution. Small light brown needles along with a yellow-brown oil formed after 24 hours. The supernatant was decanted, the needles and oil were washed with Et_2O, and the needles were isolated and dried under vacuum (0.0046 g, 14%). MS (ESI, MeOH): m/z 501 (M - $2ClO_4^-$ - H⁺), 601 (M - ClO_4^-). λ_{max}/cm^{-1} (MeCN) 10800 ($\varepsilon/cm^{-1}M^{-1}$ 25.4), 12400 shoulder (11.4), 18100

84

(9.3). μ_{eff}: 3.8 B.M. at 25°C. (Found: C, 45.37; H, 5.32; N, 11.63. $C_{27}H_{36}Cl_2N_6NiO_8·H_2O$ requires: C, 45.03; H, 5.32; N, 11.65%).

[Ni(tach-6-MeOpyr)](ClO$_4$)$_2$ (3e) A pale green solution of Ni(ClO$_4$)$_2$·6H$_2$O (0.0167 g, 4.57×10^{-5} mol) in MeOH (1 mL) was added to a pale yellow solution of tach-6-MeOpyr (0.0208 g, 4.23×10^{-5} mol) in MeOH (1 mL) producing a pale violet solution. Violet prisms fell out of solution after 24 hours. The prisms were isolated, washed with Et$_2$O, and dried under vacuum producing violet prisms (0.0150 g, 47.3%). MS (ESI, MeOH): m/z 549 (M - 2ClO$_4^-$ - H$^+$), 649 (M - ClO$_4^-$). λ_{max}/cm^{-1} (MeCN) 10900 (ϵ/cm^{-1}M^{-1} 17.5), 12400 shoulder (11.4), 18100 (7.28). μ_{eff}: 3.1 B.M. at 25°C. (Found: C, 43.09; H, 4.94; N, 11.11. $C_{27}H_{36}Cl_2N_6NiO_{11}$ requires: C, 43.25; H, 4.84; N, 11.21%).

[Cu(tach-3-Mepyr)](ClO$_4$)$_2$ (4a) A blue solution of Cu(ClO$_4$)$_2$·6H$_2$O in MeOH (50 mM, 90 µl) was added to a pale yellow solution of L^1 in MeOH (22.5 mM, 200 µl) producing a fluffy light blue precipitate. After heating at approximately 65°C for 15 sec the solution turned bright blue and was brought to 1 mL. λ_{max}/cm^{-1} (MeOH) 15200 (ϵ/cm^{-1}M^{-1} 86.4).

[Cu(tach-4-Mepyr)](ClO$_4$)$_2$ (4b) A blue solution of Cu(ClO$_4$)$_2$·6H$_2$O in MeOH (50 mM, 97 µl) was added to a pale yellow solution of tach-4-Mepyr in MeOH (24.3 mM, 200 µl) producing a fluffy light blue precipitate. After heating at approximately 65°C for 15 sec the solution turned bright blue and was brought to 1 mL. λ_{max}/cm^{-1} (MeOH) 15200 (ϵ/cm^{-1}M^{-1} 87.9).

[Cu(tach-5-Mepyr)](ClO₄)₂ (4c) A blue solution of Cu(ClO₄)₂·6H₂O in MeOH (50 mM, 63 μl) was added to a pale yellow solution of tach-5-Mepyr in MeOH (25.2 mM, 125 μl) producing a fluffy light blue precipitate. After heating at approximately 65°C for 15 sec the solution turned bright blue and was brought to 1 mL. λ_{max}/cm⁻¹ (MeOH) 15200 (ε/cm⁻¹M⁻¹ 95.9).

[Cu(tach-6-Mepyr)](ClO₄)₂ (4d) A blue solution of Cu(ClO₄)₂·6H₂O in MeOH (50 mM, 92 μl) was added to a pale yellow solution of tach-6-Mepyr in MeOH (22.9 mM, 200 μl) producing a bright green solution. The solution was brought to 1 mL. λ_{max}/cm⁻¹ (MeOH) 14600 (ε/cm⁻¹M⁻¹ 168.2), 11100 shoulder (ε/cm⁻¹M⁻¹ 87.7).

[Cu(tach-6-MeOpyr)](ClO₄)₂ (4e) A blue solution of Cu(ClO₄)₂·6H₂O in MeOH (50 mM, 81 μl) was added to a pale yellow solution of tach-6-MeOpyr in MeOH (20.3 mM, 200 μl) producing a fluffy light blue precipitate. After heating at approximately 65°C for 15 sec the solution turned bright blue and was brought to 1 mL. λ_{max}/cm⁻¹ (MeOH) 14900 (ε/cm⁻¹M⁻¹ 169.0), 10300 shoulder (ε/cm⁻¹M⁻¹ 105.7).

<div align="center">

Chapter II Experimental

</div>

[Fe(tach-3-Mepyr-ox-4)](PF₆)₂ (9) A pale green solution of FeCl₂•4H₂O (0.0038 g, 1.91 x 10⁻⁵ mol) in MeOD-d_4 (0.4 mL) was added to a pale yellow solution of tach-3-Mepyr (0.0083 g, 1.87 x 10⁻⁵ mol) in MeOD-d_4 (0.4 mL) producing a brown-yellow solution that immediately turned green-blue. After sitting for 60 hours the solution was a deep blue color. ¹H NMR confirmed the presence of solely the bisimine complex. NH₄PF₆ (0.0128 g, 7.85 x 10⁻⁵ mol) was added to

the solution immediately producing dark blue microcrystals. Slow diffusion of

Et$_2$O (2 mL) into the solution afforded more microcrystals. The dark blue

microcrystals were isolated by decanting the supernatant and washed with cold

methanol then dried under reduced pressure. The microcrystals were dissolved

in MeCN/EtOH (1:1, 0.4 mL). Slow diffusion of Et$_2$O (2 mL) at 4°C produced dark

blue plates that were isolated by decantation of the supernatant, and dried under

reduced pressure resulting in a 60.3 % yield (0.0076 g, 1.13 x 10^{-5} mol). ^{1}H

NMR (400 MHz, DMSO-d_6, 25 °C): δ 9.38, 9.32 (s, s, 2 H, N=C$\underline{H}$-C$_5$H$_3$NCH$_3$); 9

peaks from δ 8.03 to δ 5.89 (9 aromatic H, C$_5\underline{H}_3$NCH$_3$); numerous peaks from δ

4.93 to δ 3.12 for (cyclohexyl methine H and NH-C$\underline{H}_2$-py); numerous peaks from

δ 2.76 to δ 1.58 for (methyl H's and cyclohexyl methylene H's). UV/Vis (MeCN):

26600 cm^{-1} (ε = 4280 cm^{-1} M^{-1}), 19400 sh (ε = 3580 cm^{-1} M^{-1}), 16200 (ε = 8560

cm^{-1} M^{-1}). UV/Vis (0.1 M MOPS, pH 7.4): 26800 cm^{-1} (ε = 4120 cm^{-1} M^{-1}), 19300

sh (ε = 3820 cm^{-1} M^{-1}), 16300 (ε = 8240 cm^{-1} M^{-1}). MS (ESI, MeOH): 495.3 (M −

2PF6$^-$ − H$^+$); 248.3 (M − 2PF$_6^-$). Anal. Calcd for C$_{27}$H$_{32}$F$_{12}$FeN$_6$P$_2$: C, 41.24; H,

4.10; N, 10.69. Found: C, 41.15; H, 4.27; N, 10.77.

[Fe(tach-3-Mepyr-ox-6)](ClO4))$_2$•3.5H$_2$O (13•3.5H$_2$O) A yellow solution of

Fe(ClO$_4$)$_2$•6H$_2$O (0.0127 g, 3.50 x 10^{-5} mol) in MeOH (0.5 mL) was added to a

pale yellow solution of tach-3-Mepyr-trisimine (0.0143 g, 3.26 x 10^{-5} mol) in

MeOH (0.5 mL) producing a violet solution followed by immediate precipitation of

violet microcrystals. Slow diffusion of Et$_2$O (2 mL) afforded more microcrystals.

The crystals were isolated, washed with Et$_2$O and dried under reduced pressure

affording the product as a violet solid in 86.3% yield (0.0195 g, 2.81×10^{-5} mol).

^{1}H NMR (400 MHz, DMSO-d_6, 25 °C): δ 9.44 (s, 1H, N-C$\underline{H}$-py); 8.03, 7.52, 6.41

(d, dd, d, 3H, C$_5\underline{H}_3$N(CH$_3$)); 4.87 (br s, 1H, cyclohexyl methine H); 2.68 (s, 3H,

C$_5$H$_3$N(C$\underline{H}_3$)); 2.66 (obscured d, 1H, equatorial cyclohexyl methylene H); 1.86 (br

d, 1H, axial cyclohexyl methylene H). UV/Vis (CH$_3$CN): 27600 cm^{-1} (ε = 3540

cm^{-1} M^{-1}), 18700 sh (ε = 5960 cm^{-1} M^{-1}), 17100 (ε = 8540 cm^{-1} M^{-1}). UV/Vis (0.1

M MOPS, pH 7.4): 27800 cm^{-1} (ε = 2160 cm^{-1} M^{-1}), 18900 sh (ε = 3930 cm^{-1} M^{-1}),

17100 (ε = 5940 cm^{-1} M^{-1}). Anal. Calcd for C$_{27}$H$_{37}$Cl$_2$FeN$_6$O$_{11.5}$: C, 42.87; H,

4.93; N, 11.11. Found: C, 42.41; H, 4.75; N, 11.10.

Disproportionation Reaction A mixture of [Fe(tach-4-Mepyr)]$^{2+}$ and [Fe(tach-4-

Mepyr-ox-2)]$^{2+}$ (ca. 1:1) was prepared by reaction of FeCl$_3$•6H$_2$O (.0040 g, 1.48 x

10^{-5} mol) in MeOD-d_4 (0.5 mL) and tach-4-Mepyr (0.0064 g, 1.44 x 10^{-5} mol) in

MeOD-d_4 (0.5 mL) under N$_2$. The solution immediately turned green/blue. The

composition was confirmed by ^{1}H NMR spectroscopy. UV/Vis (MeOH): 16530

cm^{-1} (ε = 2650 cm^{-1} M^{-1}), 24570 (ε = 4900 cm^{-1} M^{-1}).

Competition Reactions To a mixture of [Fe(tach-4-Mepyr)]$^{2+}$ and [Fe(tach-4-

Mepyr-ox-2)]$^{2+}$ (ca. 1:1), prepared as described above, was added 1.5

equivalents of either 1,10-phenanthroline (phen) or 2,2'-bipyridine (bipy) under

N$_2$. With the addition of either reagent the solution respective solution

immediately took on a deep red color. The compositions of the resulting

solutions were analyzed by ^{1}H NMR spectroscopy.

Inertness of Fe(II)-bisimine and Fe(II)-trisimine complexes in aqueous pH 7.4 medium Solutions of the complexes **9** and **13** (5×10^{-5} M in 0.1 M MOPS, pH = 7.4) were heated to 65°C in air while monitoring UV-vis spectra. After 24 h, the solution of **9** was unchanged while the UV-vis spectrum of **13** showed a decrease in intensity accompanied by formation of a pale-brown flocculent precipitate.

Chapter III Experimental

1,7-bis(2-pyridyl)-2,6-diazaheptane (bispicpn) (L^6) Under a nitrogen atmosphere a solution of freshly distilled 2-pyridinecarboxaldehyde (0.256 g, 2.40×10^{-3} mol) in EtOH (2 mL) was added to a stirred solution of 1,3-diaminopropane (0.0886 g, 1.2×10^{-3} mol) in EtOH (10 mL). The solution was refluxed for 1.5 hours. After cooling to room temperature the solution was diluted with EtOH (5 mL). Excess $NaBH_4$ (0.130 g, 3.40×10^{-3} mol) was slowly added to the solution with stirring. The mixture was refluxed for 18 hours, allowed to cool to room temperature, and concentrated. 4 M HCl (15 mL) was carefully added and the resulting solution was washed with $CHCl_3$ (3 x 10 mL). The pH was raised to 12 with NaOH. The ligand was extracted with $CHCl_3$ (3 x 10 mL). The organic phase was dried over $MgSO_4$, concentrated, and dried under reduced pressure affording the free ligand as a yellow oil (0.259 g, 1.00×10^{-3} mol, 85.0%). ^{1}H-NMR (400 MHz, CDCl3, 25°C): δ = 8.53, 7.64, 7.32, 7.16 (m, t, d, m, 4 H, C_5H_4N), 3.94 (s, 2 H, pyrCH_2N), 2.80 (t, 2 H, NCH_2CH$_2$), 2.15 (br s, NH), 1.82 (p, 1 H, CH$_2$CH_2CH$_2$).

89

1,7-bis(6-methyl-2-pyridyl)-2,6-diazaheptane (bis6Mepicpn) (L^7) Under a

nitrogen atmosphere a solution of 6-methylpyridine-2-aldehyde (0.437 g,

3.60×10^{-3} mol) in EtOH (6 mL) was added to a stirred solution of 1,3-

diaminnpropane (0.133 g, 1.8×10^{-3} mol) in EtOH (6 mL). The solution was

refluxed for one hour. After cooling to room temperature EtOH (6 mL) was added

to the solution. Excess $NaBH_4$ (0.204 g, 5.40×10^{-3} mol) was slowly added to the

solution with stirring. The mixture was refluxed for 20 hours, allowed to cool to

room temperature, and concentrated. 4 M HCl (10 mL) was carefully added.

The solution was washed with $CHCl_3$ (3 x 5 mL). The pH was adjusted to 12 with

NaOH. The ligand was extracted with CH_2Cl_2 (3 x 10 mL). The organic phase

was dried over $MgSO_4$, concentrated, and dried under reduced pressure

producing the free ligand as a yellow oil (0.488 g, 1.70×10^{-3} mol, 96.6%). ^{1}H-

NMR (400 MHz, $CDCl_3$, 25°C): $\delta = 7.51, 7.10, 7.01$ (t, d, d, 3 H, 6-MeC$_5$$H_3$N),

3.87 (s, 2 H, pyCH_2N), 2.76 (t, 2 H, NCH_2CH$_2$), 2.52 (s, 3 H, CH_3C$_5$H$_3$N), 2.30 (br

s, NH), 1.79 (p, 1 H, CH$_2$CH_2CH$_2$).

N-(2-(2-pyridyl)ethyl)-4-toluenesulfonamide A solution of p-toluenesulfonyl

chloride (0.800 g, 4.20×10^{-3} mol) in Et_2O (25 mL) was added to a stirred solution

of 2-(2-aminoethyl)pyridine (0.511 g, 4.18×10^{-3} mol) and NaOH (0.261 g,

6.53×10^{-3} mol) in water (5 mL). The biphasic system was stirred at room

temperature for 18 hours. The Et_2O was removed by rotary evaporation and the

pH of the aqueous phase adjusted to 7 with 1 M HCl. The resulting white

precipitate was collected on a glass frit (10 – 15 M), washed with cold water, and

recrystallized from hot EtOH to produce white cubes. The solid was dried under vacuum to afford white cubes (1.0297 g, 89.2%). ^{1}H NMR (400 MHz, CDCl$_3$, 25°C): δ = 8.47, 7.58, 7.14, 7.07 (d, td, dd, d, 4 H, C$_5$$H_4$N), 7.73, 7.27 (d, d, 4 H, CH$_3$C$_6$$H_4$), 6.09 (br. t, 1 H, CH$_2$-N$H$), 3.36 (q, 2 H, pyCH$_2CH_2$NH), 2.93 (t, 2 H, pyC$H_2CH_2$), 2.41 (s, 3 H, C$H_3C_6H_4$). IR (KBr pellet): ν/cm^{-1} = 1595.2, 1570.3 (py ring deformations), 1324.7, 1154.8 (S=O symmetric and asymmetric stretches).

N-(2-(2-pyridyl)ethyl)-4-toluenesulfonamide sodium salt Under a nitrogen atmosphere NaH (0.156 g, 6.50x10^{-3} mol) in a minimal amount of hexanes was added to a stirred solution of N-(2-(2-Pyridyl)ethyl)-4-toluenesulfonamide (0.901 g, 3.26x10^{-3} mol) in MeCN (75 mL). The solution was slowly brought to a reflux over a 45 minute period. As solution stirred a fluffy white solid appeared. The reaction mixture was run through a glass frit (10 – 15 M) to isolate white solid. The solid was dried under vacuum to produce a white, granular solid (0.9953 g, approx. quantitative). IR (KBr pellet): ν/cm^{-1} = 1594.7, 1567.8 (py ring deformations), 1199.5, 1116.5 (S=O symmetric and asymmetric stretches).

1,3-bis(4-toluenesulfonyloxy)propane A solution of 1,3-propanediol (0.300 g, 3.94x10^{-3} mol) in pyridine (0.7 mL) was slowly added to a cooled (0°C) solution of p-toluenesulfonyl chloride (1.807 g, 9.48x10^{-3} mol) in pyridine (3 mL) with stirring. The solution was allowed to stir for 4 hours while keeping the temperature between 0 – 10°C. Water (6 mL) was added to quench the reaction. The resulting white solid was collected on a glass frit (10 – 15 M), washed with cold water, and recrystallized from hot EtOH to produce white sheets. The solid was

dried under vacuum to afford white flakes (1.055 g, 69.6%). ^{1}H NMR (400 MHz, CDCl$_3$, 25°C): δ = 7.75, 7.35 (d, d, 4 H, CH$_3$C$_6$H$_4$), 4.07 (t, 2 H, NHCH$_2$CH$_2$), 2.46 (s, 3 H, CH$_3$C$_6$H$_4$), 2.00 (p, 1 H, CH$_2$CH$_2$CH$_2$).

1,9-bis(2-pyridyl)-3,7-bis(4-methylsulfonyl)-3,7-diazanonane Under a nitrogen atmosphere N-(2-(2-Pyridyl)ethyl)-4-toluenesulfonamide sodium salt (0.973 g, 3.26x10^{-3} mol) was suspended in MeCN (50 mL). The mixture was brought to reflux and a solution of 1,3-bis(4-toluenesulfonyloxy)propane (0.493 g, 1.28x10^{-3} mol) in MeCN (20 mL) was added over the period of an hour. The solution was allowed to reflux 18 hours. After the mixture cooled, it was filtered through a glass frit (10 – 15 M) and the MeCN removed under reduced pressure to afford an orange oil. Flash column chromatography was performed (EtOAc/CHCl$_3$/MeOH (10:9:1)) to obtain desired product as an orange oil (0.1608 g, 21.2%). ^{1}H NMR (400 MHz, CDCl$_3$, 25°C): δ = 8.49 – 8.47, 7.57, 7.16, 7.12 – 7.09 (m, td, d, m, 4 H, C$_5$H$_4$N), 7.68, 7.27 (d, d, 4 H, CH$_3$C$_5$H$_4$), 3.50 (t, 2 H, pyCH$_2$CH$_2$), 3.14 (t, 2 H, NCH$_2$CH$_2$), 3.03 (t, 2 H, pyCH$_2$CH$_2$), 2.39 (s, 3 H, CH$_3$C$_6$H$_4$), 1.75 (p, 1 H, CH$_2$CH$_2$CH$_2$).

1,9-bis(2-pyridyl)-3,7-diazanonane (bpdan) (L^8) Under a nitrogen atmosphere a solution of 1,9-bis(2-pyridyl)-3,7-bis(4-methylsulfonyl)-3,7-diazanonane (0.130 g, 2.19x10^{-3} mol) in concentrated sulfuric acid (10 mL) was refluxed for 20 hours. After the solution cooled to room temperature, it was filtered through a glass frit (10 –15 M). The filtrate was carefully added to cold EtOH (80 mL) affording a fine white precipitate. The precipitate was isolated on a glass frit (10 – 15 M) and

92

dried under vacuum. The solid was dissolved in water (15 mL) and the pH adjusted to 12 by slow addition of 6 M NaOH. The amine was extracted with CH_2Cl_2 (3 x 10 mL). The solvent was removed under reduced pressure affording the desired product as a yellow oil (0.0205 g, 32.9%). ^1H NMR (400 MHz, $CDCl_3$, 25°C): δ = 8.50 – 8.49, 7.56, 7.14, 7.08 (m, td, d, dd, 4 H, C_5H_4N), 3.00 – 2.91 (m, 4 H, pyCH_2CH_2), 2.68 (t, 2 H, NHCH_2CH_2$), 2.12 (br. s, CH_2$NHCH_2), 1.66 (p, 1 H, CH_2CH_2CH_2$).

[Ni(bispicpn)](ClO$_4$)$_2$ (17a) A pale green solution of Ni(ClO$_4$)$_2$•6H$_2$O (0.0156 g, 4.27x10^{-5} mol) in MeOH (350 µL) was added to a pale yellow solution of bispicpn (0.0110 g, 4.29^{-5} mol) in MeOH (350 µL) producing a violet solution. Diffusion of Et$_2$O overnight afforded a violet oil. Trituration of the oil produced violet powder. The powder was isolated and dried under vacuum affording a very fine lavender powder (0.0172 g, 3.35x10^{-5} mol, 78.2%). UV/Vis/NIR (MeCN): λ_{max}/cm^{-1} (ε/cm^{-1}M^{-1}) = 18900 (9.7), 12800 (sh) (5.4) 11900 (6.7).

[Ni(bis6Mepicpn)](ClO$_4$)$_2$ (17b) A pale green solution of Ni(ClO$_4$)$_2$•6H$_2$O (0.0322 g, 8.81x10^{-5} mol) in MeOH (500 µL) was added to a pale yellow solution of bis6Mepicpn (0.0242 g, 8.58x10^{-5} mol) in MeOH (500 µL) producing a light blue suspension that quickly went back into solution. A bright blue solution resulted. Diffusion of Et$_2$O overnight afforded pale lavender clusters along with a violet/blue oil. The crystals were manually separate from the oil. The oil was redissolved in MeOH/MeCN (4:1) producing a violet solution. Slow diffusion of Et$_2$O overnight produced more lavender crystals. The crystals were combined,

93

washed with Et_2O, and dried under vacuum (0.0316 g, 68.0%). UV/Vis/NIR (MeCN): λ_{max}/cm^{-1} ($\varepsilon/cm^{-1}M^{-1}$) = 10900 (9.5), 12800 (sh) (5.4), 17900 (8.3), 28900 (13.1).

[Ni(bpdan)](ClO$_4$)$_2$ (17c) A pale green solution of $Ni(ClO_4)_2 \bullet 6H_2O$ (0.0093 g, 2.54×10^{-5} mol) in MeOH (400 µL) was added to a pale yellow solution of bpdan (0.0069 g, 2.43×10^{-5} mol) in MeOH (400 µL) resulting in a blue solution. Diffusion of Et_2O overnight produced clusters of violet needles. The needles were isolated, washed with Et_2O, and dried under vacuum affording violet microcrystals (.0109 g, 2.01×10^{-5} mol, 83.8%). UV/Vis/NIR (H_2O): λ_{max}/cm^{-1} ($\varepsilon/cm^{-1}M^{-1}$) = 10700 (7.3), 12900 (sh) (2.1), 17100 (10.6), 27500 (16.6).

[Cu(bispicpn)](ClO$_4$)$_2$ (18a) A pale blue solution of $Cu(ClO_4)_2 \bullet 6H_2O$ (0.0418 g, 1.13×10^{-4} mol) in MeOH (500 µL) was added to a pale yellow solution of bispicpn (0.0285 g, 1.12×10^{-4} mol) in MeOH (500 µL) producing a deep violet solution. After standing for approximately one minute violet microcrystals began to fall out of solution. Slow diffusion of Et_2O overnight afforded more violet microcrystals. The crystals were isolated, washed with Et_2O, and dried under vacuum producing violet microcrystals (0.0466 g, 80.2%). UV/Vis/NIR (H_2O): λ_{max}/cm^{-1} ($\varepsilon/cm^{-1}M^{-1}$) =16500 (134.7).

[Cu(bis6Mepicpn)](ClO$_4$)$_2$ (18b) A pale blue solution of $Cu(ClO_4)_2 \bullet 6H_2O$ (0.0306 g, 8.26×10^{-5} mol) in MeOH (500 µL) was added to a pale yellow solution of bis6Mepicpn (0.0228 g, 8.08×10^{-5} mol) in MeOH (500 µL) producing a royal

94

blue solution. Slow diffusion of Et_2O in to the solution produces deep blue clusters of microcrystals within 5 minutes. The crystals were isolated, washed with Et_2O, and dried under vacuum affording blue microcrystals (0.0353 g, 79.8%). UV/Vis/NIR (H_2O): λ_{max}/cm^{-1} ($\varepsilon/cm^{-1}M^{-1}$) = 14000 (139).

[Cu(bpdan)](NO$_3$)$_2$ (18c) A pale blue solution of $Cu(ClO_4)_2 \bullet 6H_2O$ (0.0123 g, 3.32×10^{-5} mol) in MeOH (500 μL) was added to a pale yellow solution of bpdan (0.0076 g, 2.67×10^{-5} mol) in MeOH (500 μL) producing a bright blue solution. Diffusion of Et_2O overnight produced clusters of bright blue sheets. The sheets were isolated, washed with Et_2O, and dried under vacuum affording blue sheets (0.0133 g, 2.43×10^{-5} mol, 91.0%). UV/Vis/NIR (H_2O): λ_{max}/cm^{-1} ($\varepsilon/cm^{-1}M^{-1}$) = 14900 (159.3).

[Zn(bispicpn)](NO$_3$)$_2$ (19a) A colorless solution of $Zn(NO_3)_2 \bullet 6H_2O$ (0.0255 g, 8.57×10^{-5} mol) in MeOH (400 μL) was added to a pale yellow solution of bispicpn (0.0220 g, 8.58×10^{-5} mol) in MeOH (400 μL). Upon addition of the metal solution a suspension formed and redissolved in less than thirty seconds. Slow diffusion of Et_2O into the solution resulted in a mixture of small off-white crystals and a pale yellow oil. Triturating the mixture with Et_2O produced an off-white powder. The powder was isolated by decanting the supernatant and dried under reduced pressure. Suspending the powder in MeCN (750 μL) and adding DMSO dropwise until all the powder dissolved produced a colorless solution. Slow diffusion of Et_2O into the solution overnight produced colorless cubes. The product was isolated, washed with MeOH, and dried under reduced pressure

95

affording white cubes (0.0254 g, 5.70×10^{-5} mol, 66.4%). MS (ESI, MeOH): m/z = 319 [M − 2 NO_3^- - H^+], 382 [M − NO_3^-]. $C_{15}H_{20}N_6O_6Zn$ (445.7): calcd. C 40.42, H 4.52, N 18.85; found C 40.41, H 4.55, N 18.84.

[Zn(bis6Mepicpn)](NO_3)$_2$•0.75H$_2$O (19b) A colorless solution of Zn(NO_3)$_2$•6H$_2$O (0.0293 g, 9.85×10^{-5} mol) in MeOH (500 µL) was added to a pale yellow solution of bis6Mepicpn (0.0264 g, 9.36×10^{-5} mol) in MeOH (500 µL). Slow diffusion of Et$_2$O into the solution over an 18 hour period resulted in a colorless oil. Trituration of the oil with Et$_2$O produced a white powder. After isolation of the powder under reduced pressure it was suspended in MeCN. DMSO was added dropwise until the powder dissolved. Slow diffusion of Et$_2$O overnight produced colorless prisms. Decanting the supernatant and drying under reduced pressure affords white prisms (0.0340 g, 7.18×10^{-5} mol, 76.7%). ^{1}H NMR (400 MHz, [D$_6$]DMSO, 65°C): δ = 8.02, 7.49 (t, t, 3H, 6-MeC$_5$H$_3$N), 5.08 (br s, 1 H, NHCH$_2$), 4.16 (br s, 2 H, MepyrCH$_2$N), 2.84 (br s, 2 H NCH$_2$CH$_2$), 2.34 (s, 3 H CH$_3$pyr), 1.74 (br t, 1 H, CH$_2$CH$_2$CH$_2$). ^{13}C NMR (400 MHz, [D$_6$]DMSO, 65°C): δ = 158.6, 156.7, 141.6, 126.1, 122.4, 53.1, 50.1, 26.8, 24.0. MS (ESI, MeOH): m/z = 347 [M - 2 NO_3^- - H^+], 410 [M - NO_3^-]. $C_{17}H_{25.5}N_6O_{6.75}Zn$ (487.31): calcd. C 41.90, H 5.27, N 17.25; found C 42.05, H 5.28, N 17.24.

[Zn(bpdan)(NO_3)]NO_3 (19c) A colorless solution of Zn(NO_3)$_2$•6H$_2$O (0.0067 g, 2.25×10^{-5} mol) in MeOH (400 µL) was added to a pale yellow solution of bpdan (0.0061 g, 2.14×10^{-5} mol) in MeOH (400 µL). Slow diffusion of Et$_2$O into the solution over an 18 hour period resulted in a colorless oil. Trituration of the oil

96

with Et_2O produced a white powder. After isolation of the powder under reduced pressure it was suspended in MeCN. DMSO was added dropwise until the powder dissolved. Slow diffusion of Et_2O overnight produced colorless prisms of X-ray quality. For analysis the solid was washed with Et_2O and dried under vacuum affording white cubes (0.0092 g, 1.95×10^{-5} mol, 91.0%). ^1H NMR (400 MHz, $[D_3]MeCN/[D_6]DMSO$, 25°C): $\delta = 8.08, 7.98, 7.53, 7.36$ (dd, td, d, td, 4 H, C_5H_4N), 3.30 – 2.70 (multiple broad peaks and a large singlet, $CH_2NHCH_2CH_2py$), 1.82 (p, 1 H, $CH_2CH_2CH_2$). $C_{17}H_{24}N_6O_6Zn$ (473.87): calcd. C 43.10, H 5.10, N 17.74; found C 43.14, H 5.15, N 17.71.

LIST OF REFERENCES

(1)   Busch, D. H. *Chem. Rev. (Washington, DC, U. S.)* **1993**, *93*, 847-60.

(2)   Hancock, R. D.; Martell, A. E. *Chem. Rev. (Washington, DC, U. S.)* **1989**, *89*, 1875-914.

(3)   Hou, Z.; Stack, T. D. P.; Sunderland, C. J.; Raymond, K. N. *Inorg. Chim. Acta* **1997**, *263*, 341-355.

(4)   de Angelis, S.; Batsanov, A.; Norman, T. J.; Parker, D.; Senanayake, K.; Vepsalainen, J. *J. Chem. Soc., Chem. Commun.* **1995**, 2361-3.

(5)   Park, G.; Przyborowska, A. M.; Ye, N.; Tsoupas, N. M.; Bauer, C. B.; Broker, G. A.; Rogers, R. D.; Brechbiel, M. W.; Planalp, R. P. *Dalton Trans.* **2003**, 318-324.

(6)   Park, G.; Lu, F. H.; Ye, N.; Brechbiel, M. W.; Torti, S. V.; Torti, F. M.; Planalp, R. P. *JBIC, J. Biol. Inorg. Chem.* **1998**, *3*, 449-457.

(7)   Park, G.; Dadachova, E.; Przyborowska, A.; Lai, S.-j.; Ma, D.; Broker, G.; Rogers, R. D.; Planalp, R. P.; Brechbiel, M. W. *Polyhedron* **2001**, *20*, 3155-3163.

(8)   Park, G.; Ye, N.; Rogers, R. D.; Brechbiel, M. W.; Planalp, R. P. *Polyhedron* **2000**, *19*, 1155-1161.

(9)   Shannon, R. D.; Prewitt, C. T. *Acta Crystallographica, Section B: Structural Crystallography and Crystal Chemistry* **1969**, *25*, 925-46.

(10)   Shannon, R. D. *Acta Crystallographica, Section A: Crystal Physics, Diffraction, Theoretical and General Crystallography* **1976**, *A32*, 751-67.

(11)   Bowen, T.; Planalp, R. P.; Brechbiel, M. W. *Bioorg. Med. Chem. Lett.* **1996**, *6*, 807-10.

(12)   Hilfiker, K. A.; Brechbiel, M. W.; Rogers, R. D.; Planalp, R. P. *Inorg. Chem.* **1997**, *36*, 4600-4603.

(13)   Torti, S. V.; Planalp, R. P.; Brechbiel, M. W.; Park, G.; Torti, F. M. *Molecular Biology of Hematopoiesis 6, [Proceedings of the Symposium on the Molecular Biology of Hematopoiesis], 11th, Bormio, Italy, June 25-29, 1998* **1999**, 381-389.

(14)   Le, N. T. V.; Richardson, D. R. *Biochimica et Biophysica Acta, Reviews on Cancer* **2002**, *1603*, 31-46.

(15)   Easmon, J. *Expert Opin. Ther. Pat.* **2002**, *12*, 789-818.

(16)   Zhao, R.; Planalp, R. P.; Ma, R.; Greene, B. T.; Jones, B. T.; Brechbiel, M. W.; Torti, F. M.; Torti, S. V. *Biochem. Pharmacol.* **2004**, *67*, 1677-1688.

(17)   Chum, H. L.; Vanin, J. A.; Holanda, M. I. D. *Inorg. Chem.* **1982**, *21*, 1146-52.

(18)   Toftlund, H.; Yde-Andersen, S. *Acta Chemica Scandinavica, Series A: Physical and Inorganic Chemistry* **1981**, *A35*, 575-85.

(19)   Wieghardt, K.; Schoeffmann, E.; Nuber, B.; Weiss, J. *Inorg. Chem.* **1986**, *25*, 4877-83.

(20)   Wilson, L. J.; Georges, D.; Hoselton, M. A. *Inorg. Chem.* **1975**, *14*, 2968-75.

(21) Hancock, R. D.; McDougall, G. J. *Journal of the Chemical Society, Dalton Transactions: Inorganic Chemistry (1972-1999)* **1977**, 67-70.

(22) Zhang, D.; Busch, D. H. *Inorg. Chem.* **1994**, *33*, 5138-43.

(23) Banci, L.; Bencini, A.; Benelli, C.; Gatteschi, D.; Zanchini, C. *Structure and Bonding (Berlin, Germany)* **1982**, *52*, 37-86.

(24) Sacconi, L.; Mani, F.; Bencini, A. *Nickel*; Pergamon: New York, 1987.

(25) Hathaway, B. J. *Copper*; Pergamon: New York, 1987.

(26) Karlin, K. D.; Hayes, J. C.; Juen, S.; Hutchinson, J. P.; Zubieta, J. *Inorg. Chem.* **1982**, *21*, 4106-4108.

(27) Duggan, M.; Hathaway, B. J.; Mullane, J. *Journal of the Chemical Society, Dalton Transactions: Inorganic Chemistry (1972-1999)* **1980**, 690-8.

(28) Park, G.; Shao, J.; Lu, F. H.; Rogers, R. D.; Chasteen, N. D.; Brechbiel, M. W.; Planalp, R. P. *Inorg. Chem.* **2001**, *40*, 4167-4175.

(29) Duggan, M.; Ray, N.; Hathaway, B.; Tomlinson, G.; Brint, P.; Pelin, K. *Journal of the Chemical Society, Dalton Transactions: Inorganic Chemistry (1972-1999)* **1980**, 1342-8.

(30) Christiansen, L.; Hendrickson, D. N.; Toftlund, H.; Wilson, S. R.; Xie, C. L. *Inorg. Chem.* **1986**, *25*, 2813-18.

(31) Greenaway, A. M.; Sinn, E. *J. Am. Chem. Soc.* **1978**, *100*, 8080-4.

(32) Alcock, N. W.; Zhang, D.; Busch, D. H. *Acta Crystallogr., Sect. C: Cryst. Struct. Commun.* **1999**, *C55*, 886-889.

(33) Childers, M. L.; Su, F.; Przyborowska, A. M.; Bishwokarma, B.; Park, G.; Brechbiel, M. W.; Torti, S. V.; Torti, F. M.; Broker, G.; Alexander, J. S.; Rogers, R. D.; Ruhlandt-Senge, K.; Planalp, R. P. *Eur. J. Inorg. Chem.* **2005**, 3971-3982.

(34) Bernal, I.; Jensen, I. M.; Jensen, K. B.; McKenzie, C. J.; Toftlund, H.; Tuchagues, J.-P. *J. Chem. Soc., Dalton Trans.* **1995**, 3667-75.

(35) Koikawa, M.; Jensen, K. B.; Matsushima, H.; Tokii, T.; Toftlund, H. *J. Chem. Soc., Dalton Trans.* **1998**, 1085-1086.

(36) Tomlinson, A. A. G.; Hathaway, B. J. *Journal of the Chemical Society [Section] A: Inorganic, Physical, Theoretical* **1968**, 1685-8.

(37) Butcher, R. J.; Addison, A. W. *Inorg. Chim. Acta* **1989**, *158*, 211-15.

(38) Planalp, R. P.; Przyborowska, A. M.; Park, G.; Ye, N.; Lu, F. H.; Rogers, R. D.; Broker, G. A.; Torti, S. V.; Brechbiel, M. W. *Biochem. Soc. Trans.* **2002**, *30*, 758-762.

(39) Goedken, V. L.; Busch, D. H. *J. Am. Chem. Soc.* **1972**, *94*, 7355.

(40) Toma, H.; Ferreira, A.; Iha, N. *New J. Chem.* **1985**, *9*, 473 - 478.

(41) Goto, M.; Koga, N.; Ohse, Y.; Kurosaki, H.; Komatsu, T.; Kuroda, Y. *J. Chem. Soc., Chem. Commun.* **1994**, 2015 - 2016.

(42) Kuroda, Y.; Tanaka, N.; Goto, M.; Sakai, T. *Inorg. Chem.* **1989**, *28*, 2163 - 2169.

(43) Morgenstern-Badarau, I.; Lambert, F.; Philippe Renault, J.; Cesario, M.; Marechal, J. D.; Maseras, F. *Inorg. Chim. Acta* **2000**, *297*, 338 - 350.

(44) Krumholz, P. *Struct. Bonding (Berlin)* **1971**, *9*, 139 - 174.

(45) Torti, S. V.; Torti, F. M.; Whitman, S. P.; Brechbiel, M. W.; Park, G.; Planalp, R. P. *Blood* **1998**, *92*, 1384-1389.

(46) Lions, F.; Martin, K. V. *J. Am. Chem. Soc.* **1957**, *79*, 1572 - 1575.

(47) Gillum, W. O.; Wentworth, R. A. D.; Childers, R. F. *Inorg. Chem.* **1970**, *9*, 1825 - 1832.

(48) Krumholz, P.; Serra, O. A.; De Paoli, M. A. *Inorg. Chim. Acta* **1975**, *15*, 25 - 32.

(49) Park, G. Doctoral Dissertation, University of New Hampshire, 2000.

(50) Wentworth, R. A. D. *Coord. Chem. Rev.* **1972/73**, *9*, 171 - 187.

(51) Childers, R. F.; Wentworth, R. A. D. *Inorg. Chem.* **1973**, *12*, 2778 - 2782.

(52) Boubedeur, K.; Deroche, A.; Lambert, F.; Morgenstern-Badarau, I. *Acta Crystallogr., Sect. C: Cryst. Struct. Commun.* **1995**, *C51*, 2244 - 2246.

(53) Wentworth, R. A. D.; Dahl, P. S.; Huffman, C. J.; Gillum, W. O.; Streib, W. E.; Huffman, J. C. *Inorg. Chem.* **1982**, *21*, 3060 - 3063.

(54) Fahrni, C. J.; O'Halloran, T. V. *J. Am. Chem. Soc.* **1999**, *121*, 11448-11458.

(55) Reany, O.; Gunnlaugsson, T.; Parker, D. *Perkin 2* **2000**, 1819-1831.

(56) Walkup, G. K.; Burdette, S. C.; Lippard, S. J.; Tsien, R. Y. *J. Am. Chem. Soc.* **2000**, *122*, 5644-5645.

(57) Farkas, E.; Katz, Y.; Bhusare, S.; Reich, R.; Roeschenthaler, G.-V.; Koenigsmann, M.; Breuer, E. *JBIC, J. Biol. Inorg. Chem.* **2004**, *9*, 307-315.

(58) Bates, G. B.; Parker, D.; Tasker, P. A. *J. Chem. Soc., Perkin Trans. 2* **1996**, 1117-1125.

(59) Edlin, C. D.; Parker, D.; Perry, J. J. B.; Chartroux, C.; Gloe, K. *New J. Chem.* **1999**, *23*, 819-826.

(60) Congreve, A.; Kataky, R.; Knell, M.; Parker, D.; Puschmann, H.; Senanayake, K.; Wylie, L. *New J. Chem.* **2003**, *27*, 98-106.

(61) Irving, H.; Williams, R. J. P. *Nature (London, U. K.)* **1948**, *162*, 746-7.

(62) Irving, H. M.; Williams, R. J. P. *J. Chem. Soc.* **1953**, 3192-3210.

(63) Miessler, G. L.; Tarr, D. A. *Inorganic Chemistry*; Prentice Hall: Upper Saddle River, New Jersey, 2000.

(64) Bates, G. B.; Parker, D. *J. Chem. Soc., Perkin Trans. 2* **1996**, 1109-1115.

(65) Bates, G. B.; Parker, D. *Tetrahedron Lett.* **1996**, *37*, 267-70.

(66) Koike, T.; Kimura, E.; Nakamura, I.; Hashimoto, Y.; Shiro, M. *J. Am. Chem. Soc.* **1992**, *114*, 7338-45.

(67) Alcock, N. W.; Benniston, A. C.; Moore, P.; Pike, G. A.; Rawle, S. C. *J. Chem. Soc., Chem. Commun.* **1991**, 706-8.

(68) Rawle, S. C.; Clarke, A. J.; Moore, P.; Alcock, N. W. *Journal of the Chemical Society, Dalton Transactions: Inorganic Chemistry (1972-1999)* **1992**, 2755-7.

(69) Xu, X.; Allen, C. S.; Chuang, C.-L.; Canary, J. W. *Acta Crystallogr., Sect. C: Cryst. Struct. Commun.* **1998**, *C54*, 600-601.

(70) Yu, Y.; Smith, J. M.; Flaschenriem, C. J.; Holland, P. L. *Inorg. Chem.* **2006**, *45*, 5742-5751.

(71) Gan, W.; Jones, S. B.; Reibenspies, J. H.; Hancock, R. D. *Inorg. Chim. Acta* **2005**, *358*, 3958-3966.

(72) Hernandez, H. J. G.; Pandiyan, T.; Bernes, S. *Inorg. Chim. Acta* **2006**, *359*, 1-12.

(73) McKenzie, E. D.; Stephens, F. S. *Inorg. Chim. Acta* **1980**, *42*, 1-10.

(74) Newkome, G. R.; Frere, Y. A.; Fronczek, F. R.; Gupta, V. K. *Inorg. Chem.* **1985**, *24*, 1001-6.

(75) Pandiyan, T.; Consuelo-Estrada, V. M.; Moreno-Esparza, R.; Ruiz-Ramirez, L. *Inorg. Chim. Acta* **2003**, *343*, 79-89.

(76) Phillip, A. T.; Casey, A. T.; Thompson, C. R. *Aust. J. Chem.* **1970**, *23*, 491-9.

(77) Nikles, D. E.; Powers, M. J.; Urbach, F. L. *Inorg. Chim. Acta* **1979**, *37*, L499-L501.

(78) Rybak-Akimova, E. V.; Nazarenko, A. Y.; Chen, L.; Krieger, P. W.; Herrera, A. M.; Tarasov, V. V.; Robinson, P. D. *Inorg. Chim. Acta* **2001**, *324*, 1-15.

(79) Nikles, D. E.; Powers, M. J.; Urbach, F. L. *Inorg. Chem.* **1983**, *22*, 3210-17.

(80) McKenzie, E. D.; Gibson, J. G. *Journal of the Chemical Society [Section] A: Inorganic, Physical, Theoretical* **1971**, 1666-83.

(81) Hancock, R. D. *J. Chem. Educ.* **1992**, *69*, 615-621.

(82) Cukrowski, I.; Cukrowska, E.; Hancock, R. D.; Anderegg, G. *Anal. Chim. Acta* **1995**, *312*, 307-321.

(83) Hathaway, B. J. *Struct. Bonding (Berlin)* **1984**, *57*, 55-118.

(84) Hathaway, B. J.; Billing, D. E. *Coord. Chem. Rev.* **1970**, *5*, 143-207.

(85) Hartman, J. A. R.; Kammier, A. L.; Spracklin, R. J.; Pearson, W. H.; Combariza, M. Y.; Vachet, R. W. *Inorg. Chim. Acta* **2004**, *357*, 1141-1151.

(86) McLachlan, G. A.; Fallon, G. D.; Martin, R. L.; Spiccia, L. *Inorg. Chem.* **1995**, *34*, 254-261.

(87) Anderegg, G.; Podder, N. G.; Blaeuenstein, P.; Hangartner, M.; Stuenzi, H. *J. Coord. Chem.* **1975**, *4*, 267-75.

(88) Brown, H. C. *J. Chem. Soc.* **1956**, 1248-68.

(89) Beck, M. T.; Nagypal, I. *Chemistry of Complex Equilibria*; Ellis Horwood Limited: New York, 1990.

(90) Alcock, N. W.; Rybak-Akimova, E. V.; Busch, D. H. *Acta Crystallogr., Sect. C: Cryst. Struct. Commun.* **1997**, *C53*, 1385-1387.

(91) Arulsamy, N.; Goodson, P. A.; Hodgson, D. J. *Inorg. Chim. Acta* **1994**, *216*, 21-29.

(92) Yu, Z. Doctoral Dissertation, University of Mainz Institut fur Anorganische Chemie und Analytische Chemie, 1994.

101

APPENDICES

APPENDIX A: Electronic Absorption Spectra

103

Electronic Absorption Spectra of [(Fe(tach-x-Mepyr)]$^{2+}$ (x = 3, 4, or 5)

104
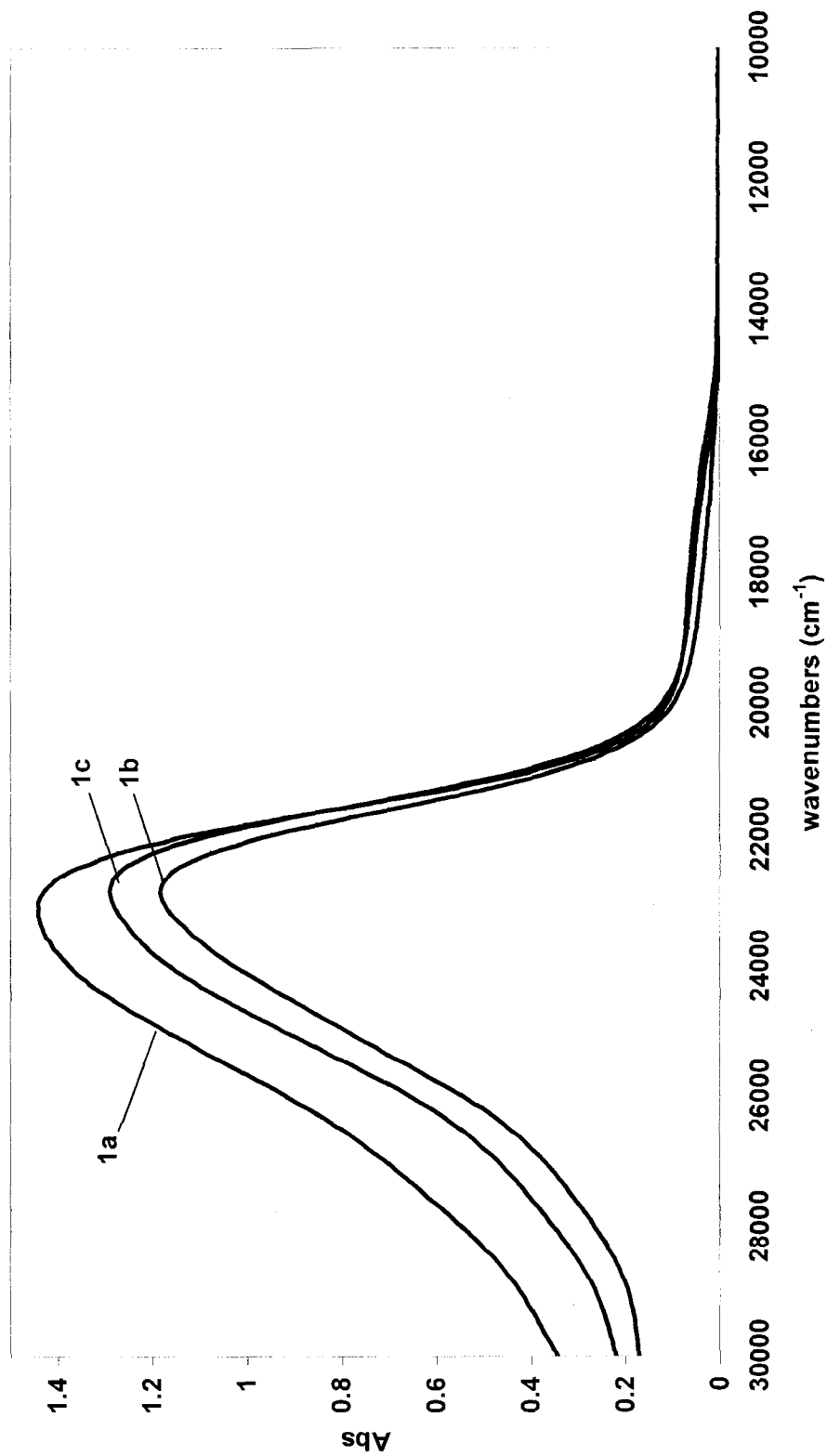
Electronic Absorption Spectra of [Fe(tach-6-Rpyr)]²⁺ (R = Me or MeO)

105
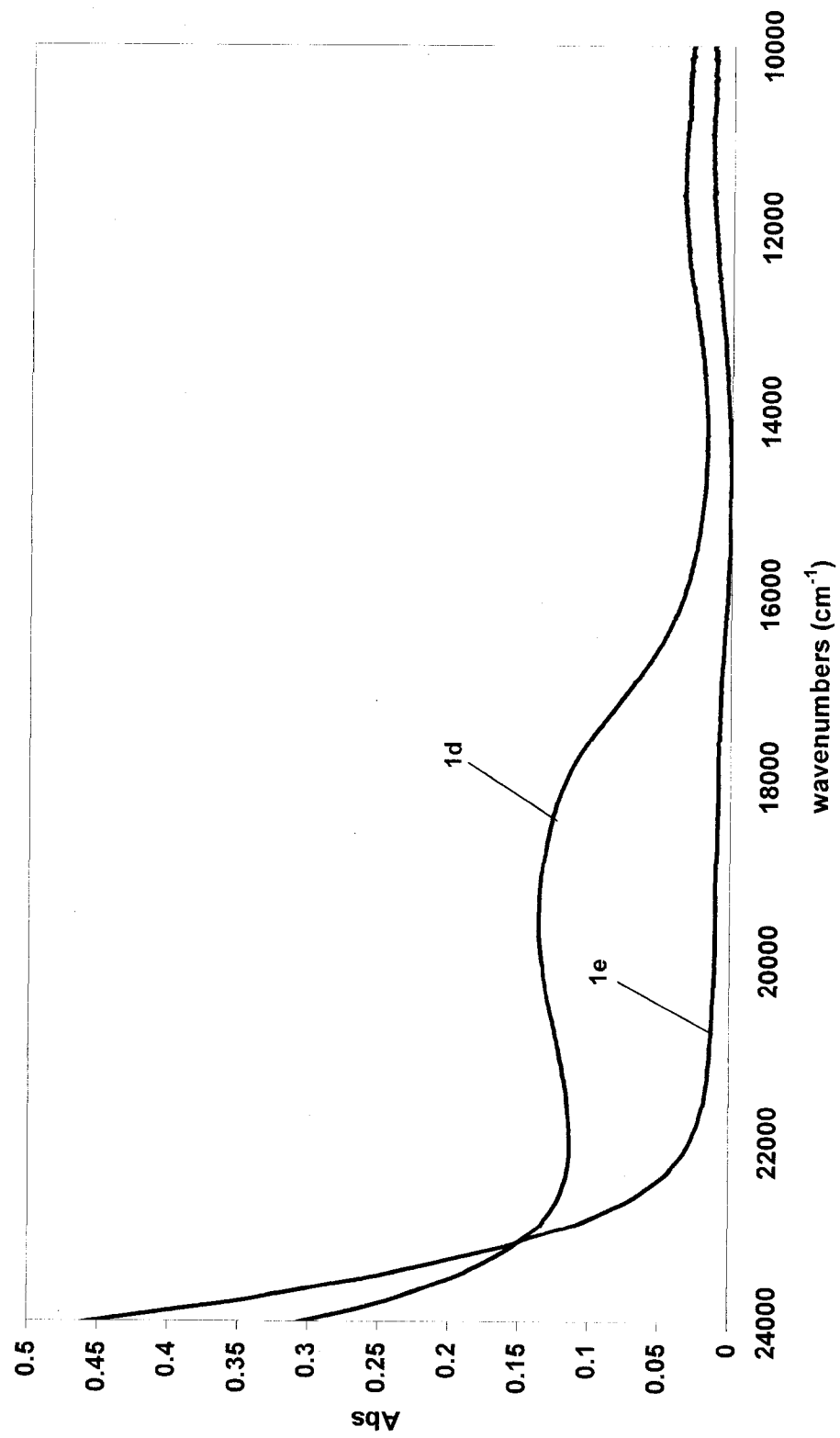
Electronic Absorption Spectra of [Co(tach-x-Mepyr)]$^{2+}$ in MeOH (x = 3, 4 or 5)

106
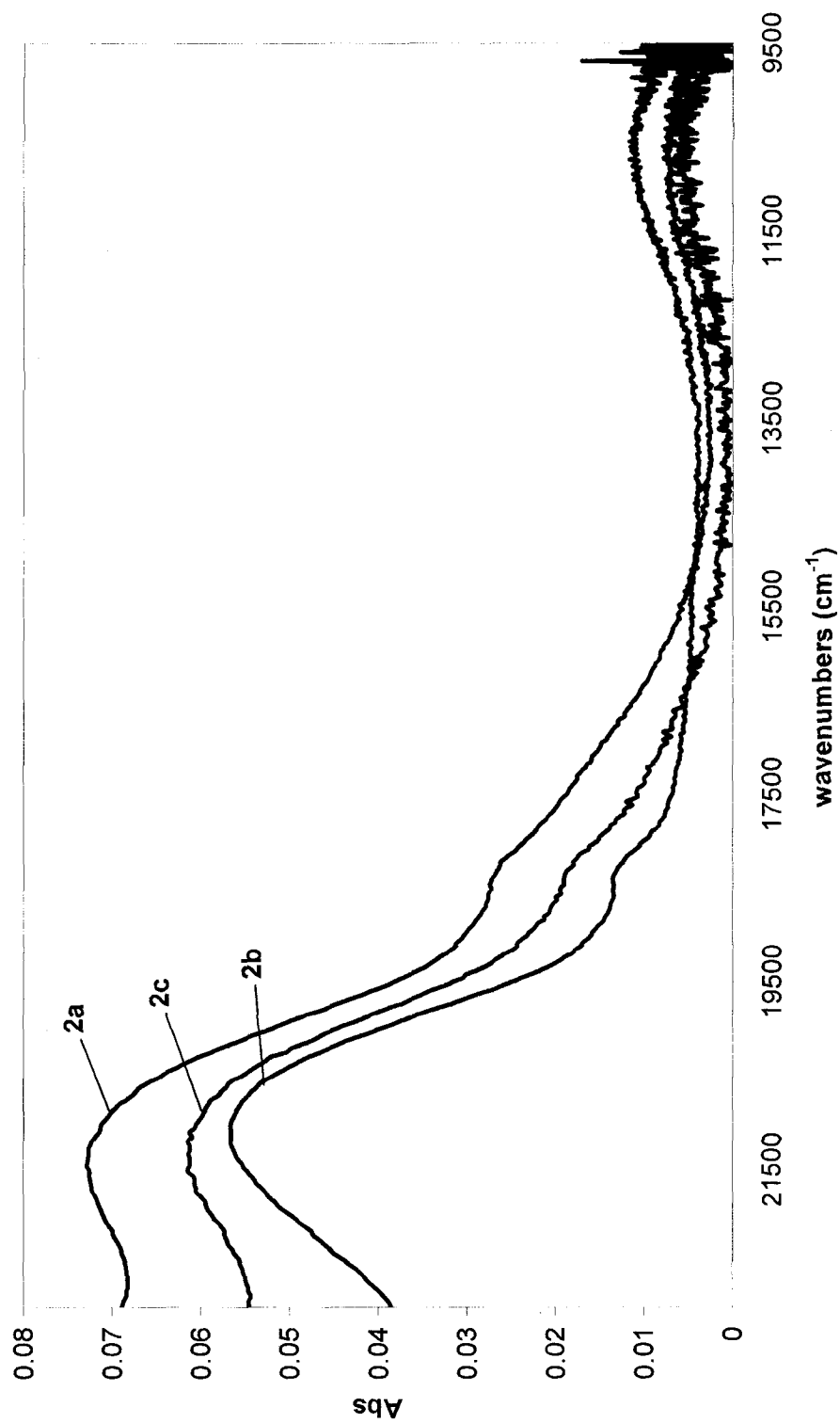
Electronic Absorption Spectra of [Ni(tach-x-Mepyr)]]$^{2+}$ in MeCN (x = 3, 4 or 5)

107
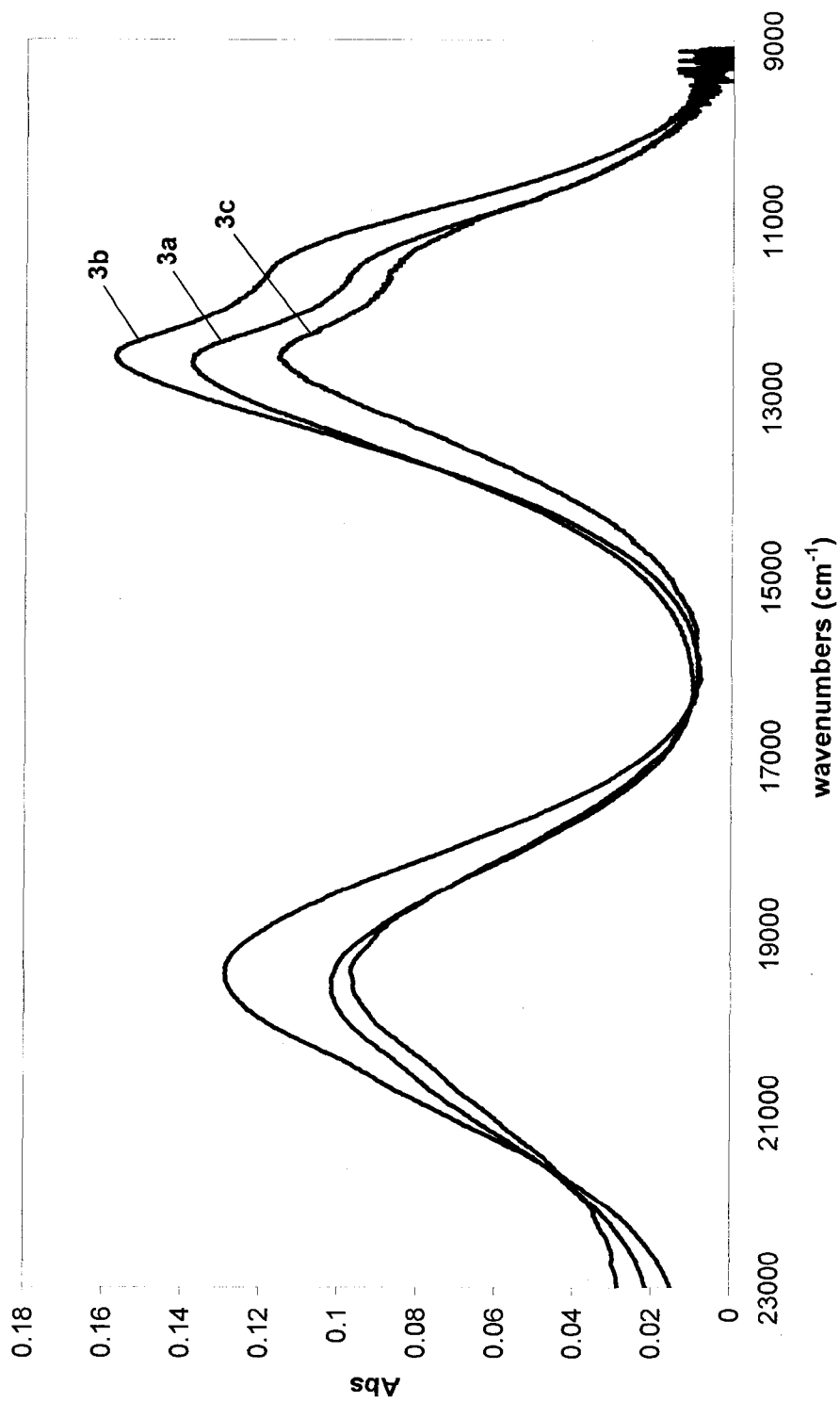
Electronic Absorption Spectra of [Ni(tach-6-Rpyr)]$^{2+}$ in MeCN (R = Me or MeO)

108
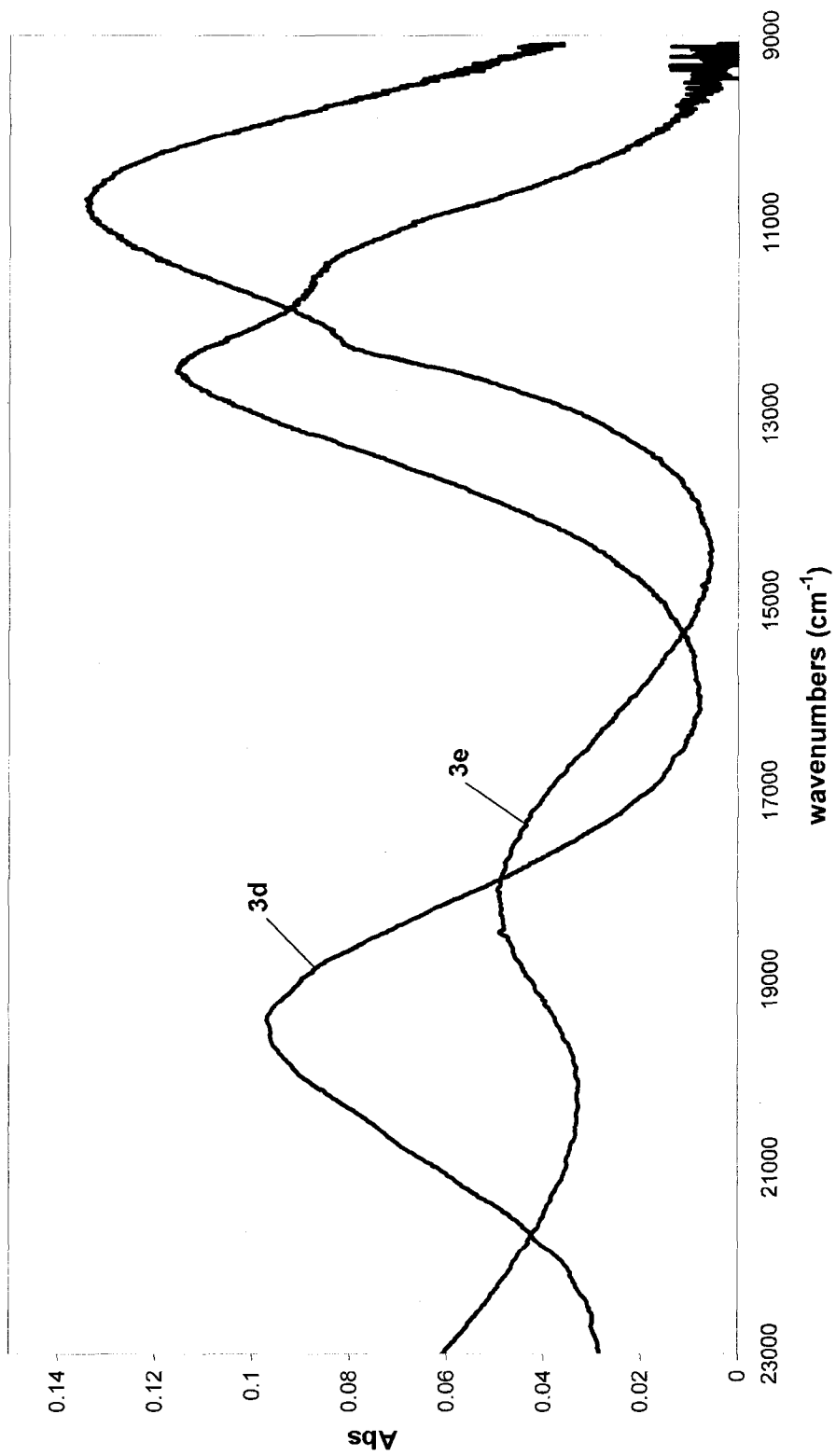
Electronic Absorption Spectra of [Cu(tach-x-Mepyr)]$^{2+}$
in MeOH (x = 3, 4 or 5)

4b

4a

4c

wavenumbers (cm^{-1})

Abs

109
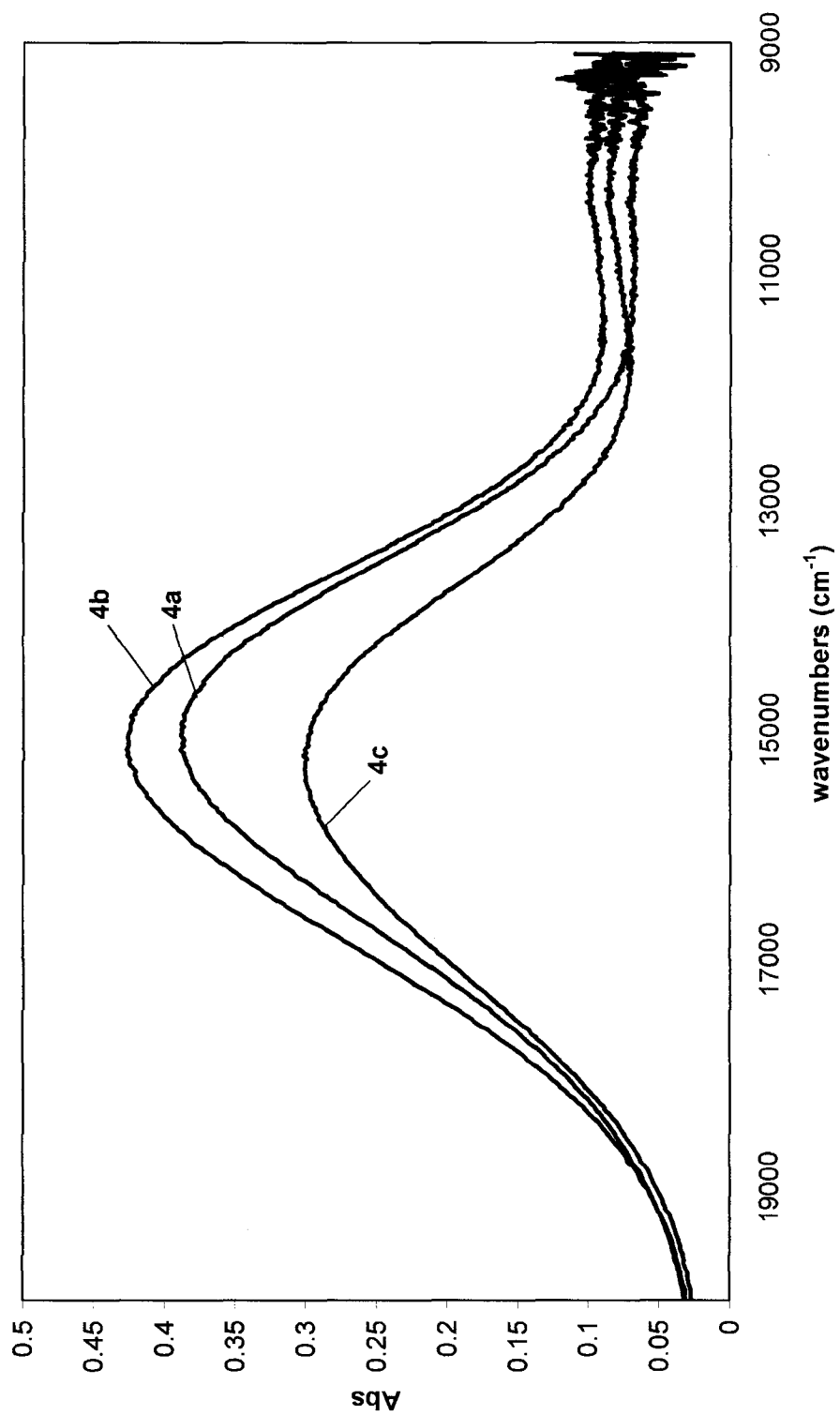
Electronic Absorption Spectra of [Cu(tach-6-Rpyr)]$^{2+}$ in MeOH (R = Me or MeO)

110

111
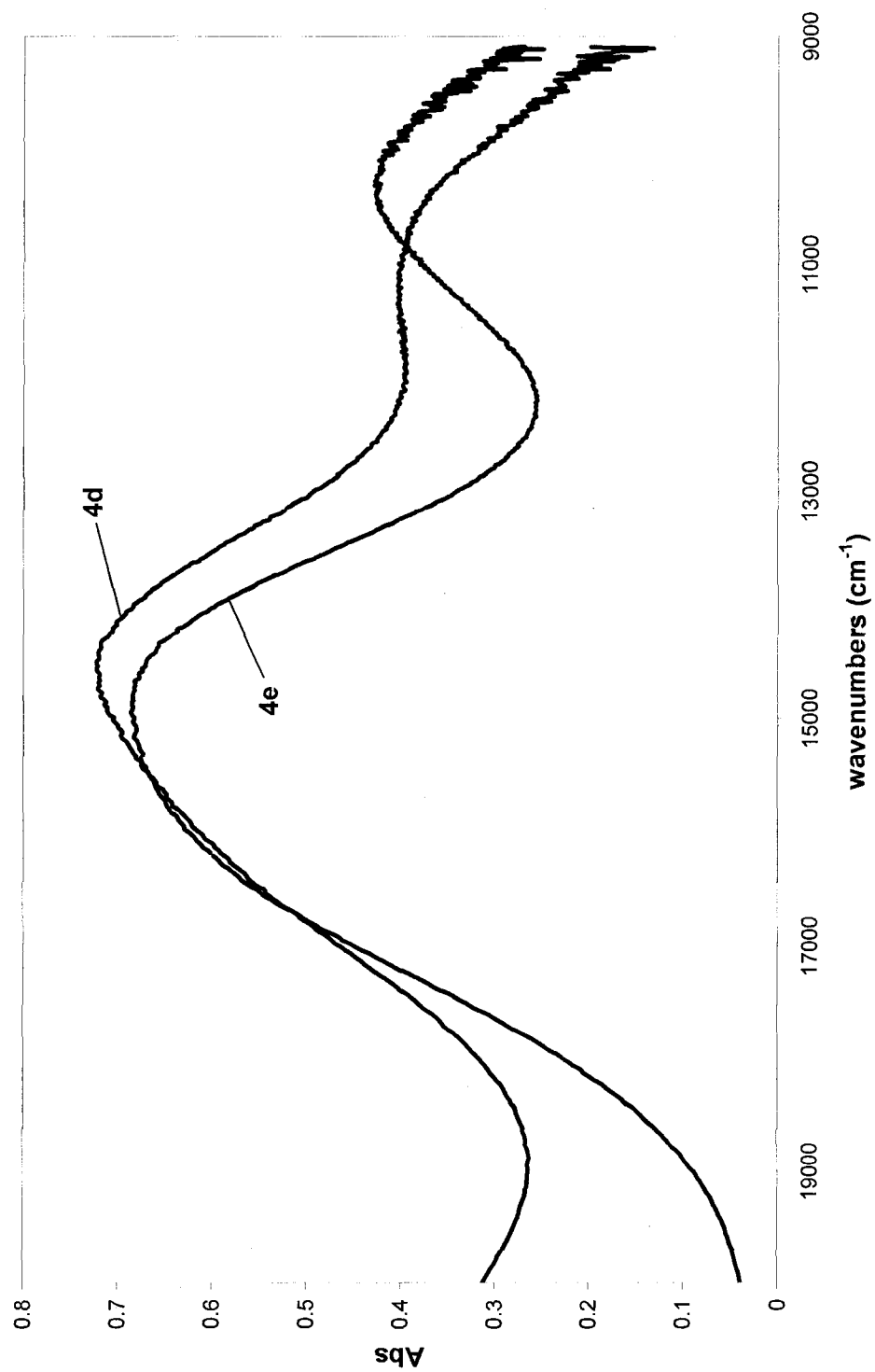
Deconvolution of [Cu(tach-6-Mepyr)]$^{2+}$ Electronic Absorption Spectrum; red dashed line is the sum of the calculated peaks
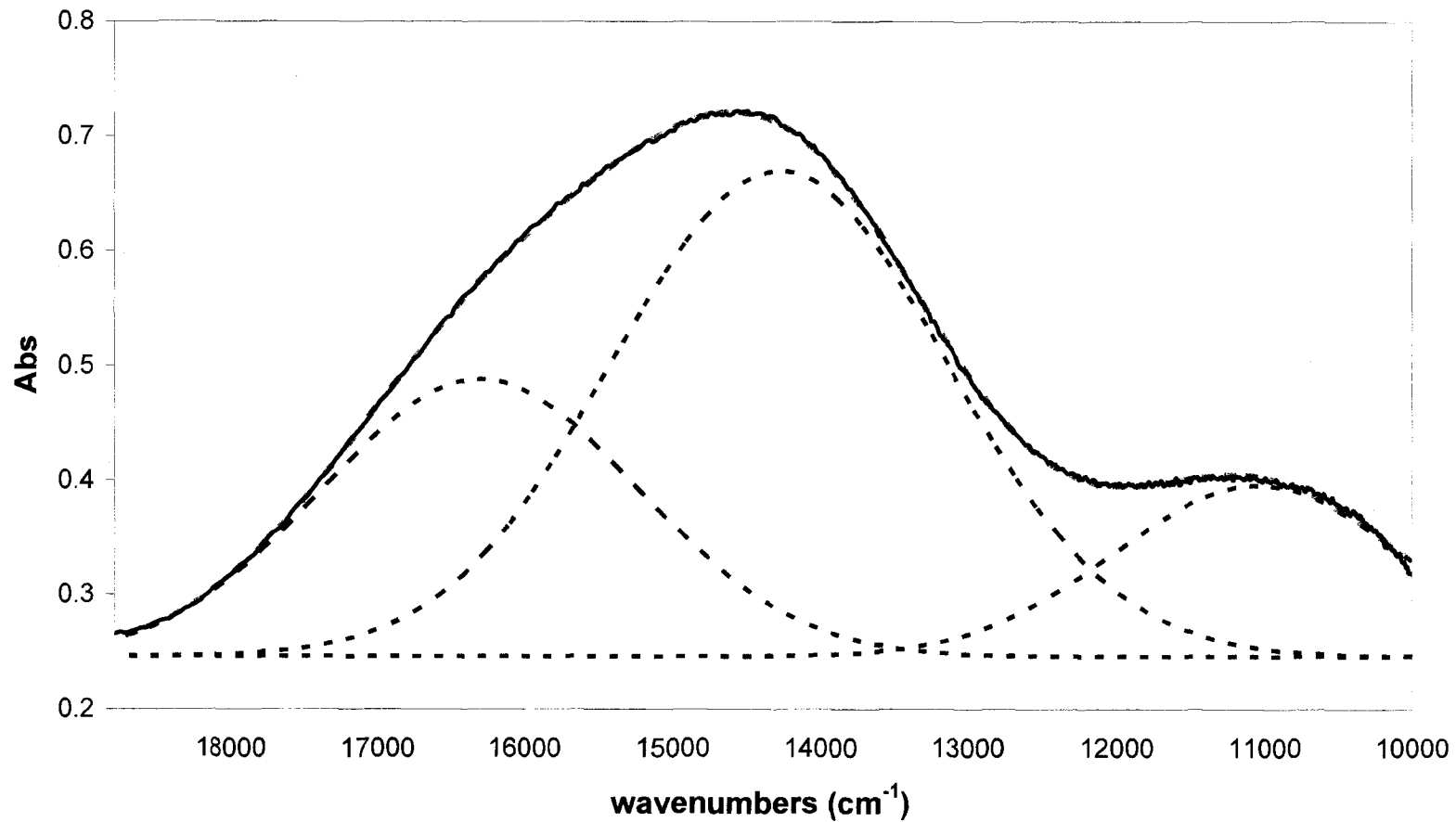
Deconvolution of [Cu(tach-6-MeOpyr)]$^{2+}$ Electronic Absorption Spectrum; red dashed line is the sum of the calculated peaks

112
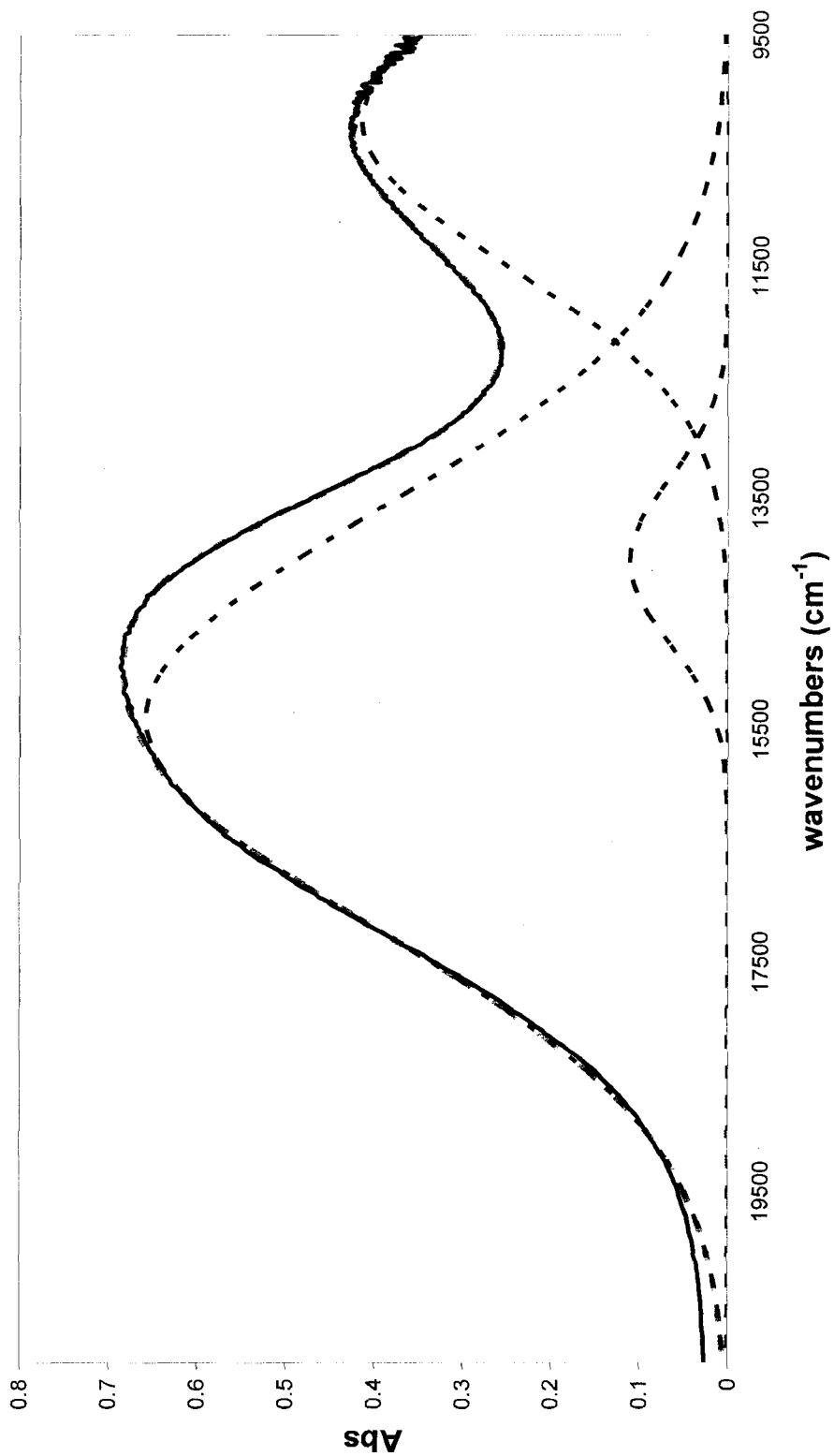
Disproportionation Reaction: Fe(III) + tach-4-Mepyr in MeOH (approx. 1:1, [Fe(tach-4-Mepyr)]$^{2+}$: [Fe(tach-4-Mepyr-ox-2)]$^{2+}$)

113
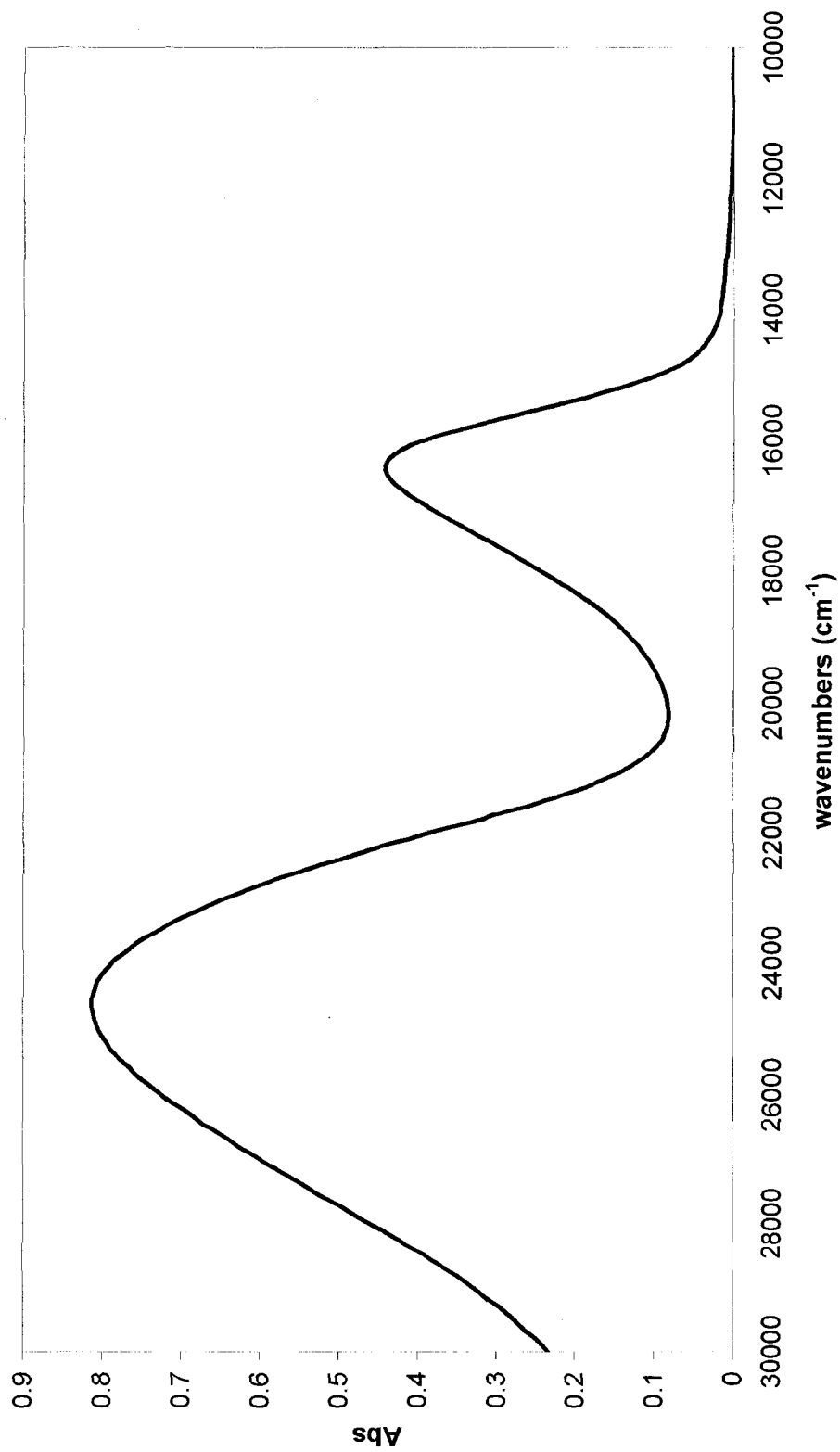
Electronic Absorption Spectrum of [Fe(tach-3-Mepyr-ox-4)]²⁺ (9) in MeCN

114
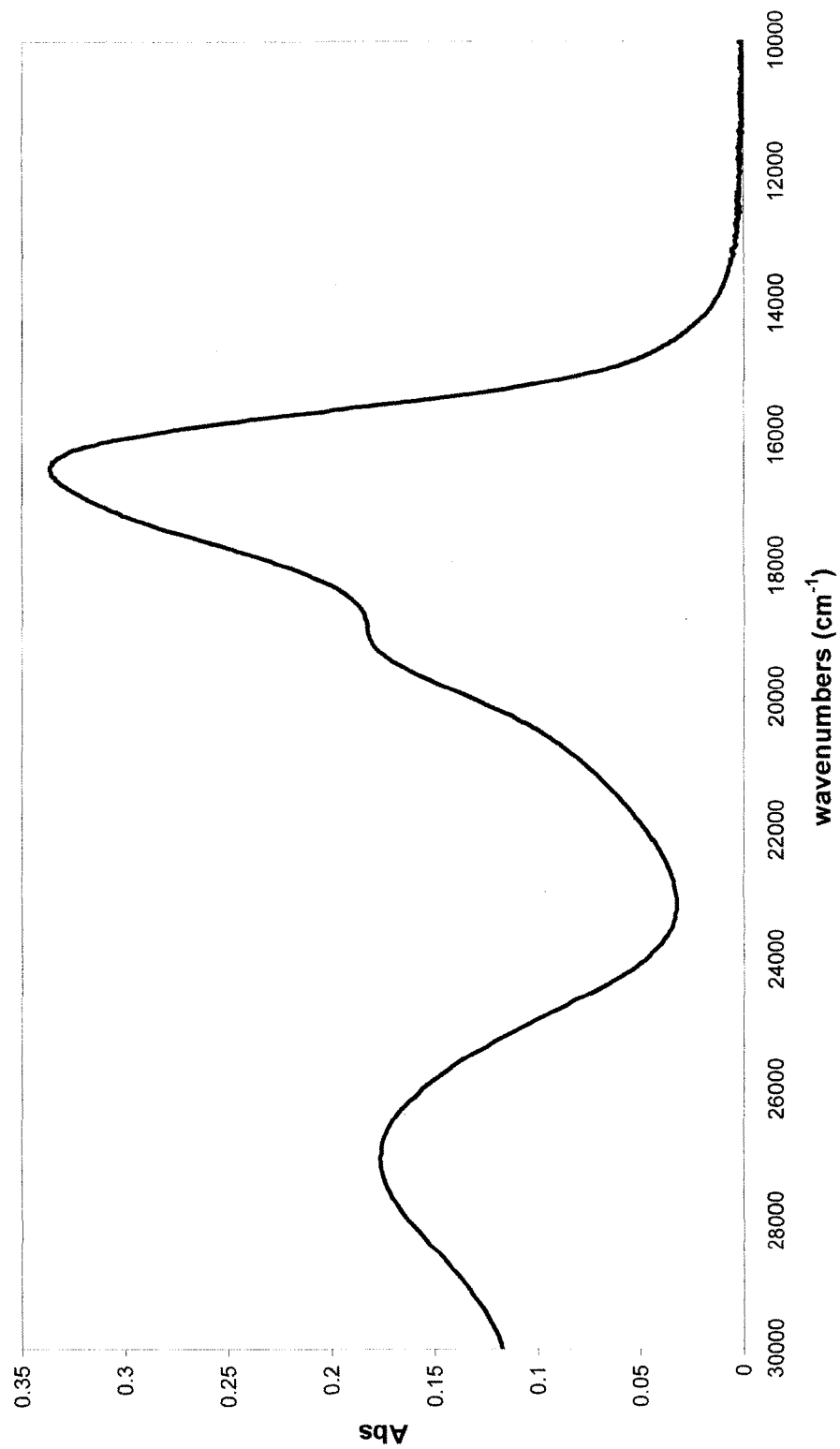
Electronic Absorption Spectrum of [Fe(tach-3-Mepyr-ox-6)]²⁺ (13) in MeCN

115

116
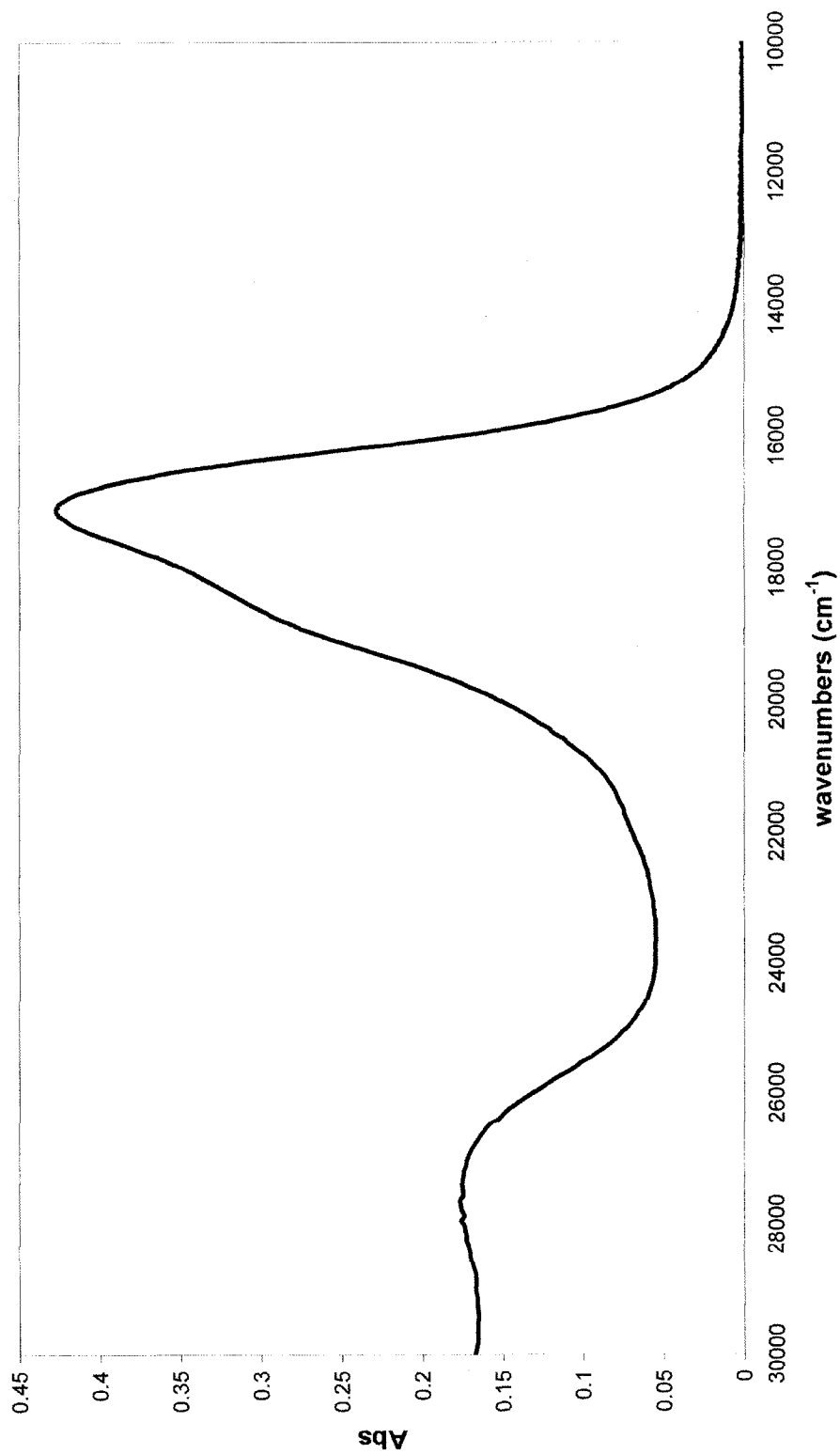
Electronic Absorption Spectra of [Ni(bispicpn)]$^{2+}$, [Ni(bis6Mepicpn)]$^{2+}$ and [Ni(bpdan)]$^{2+}$ in H$_2$O
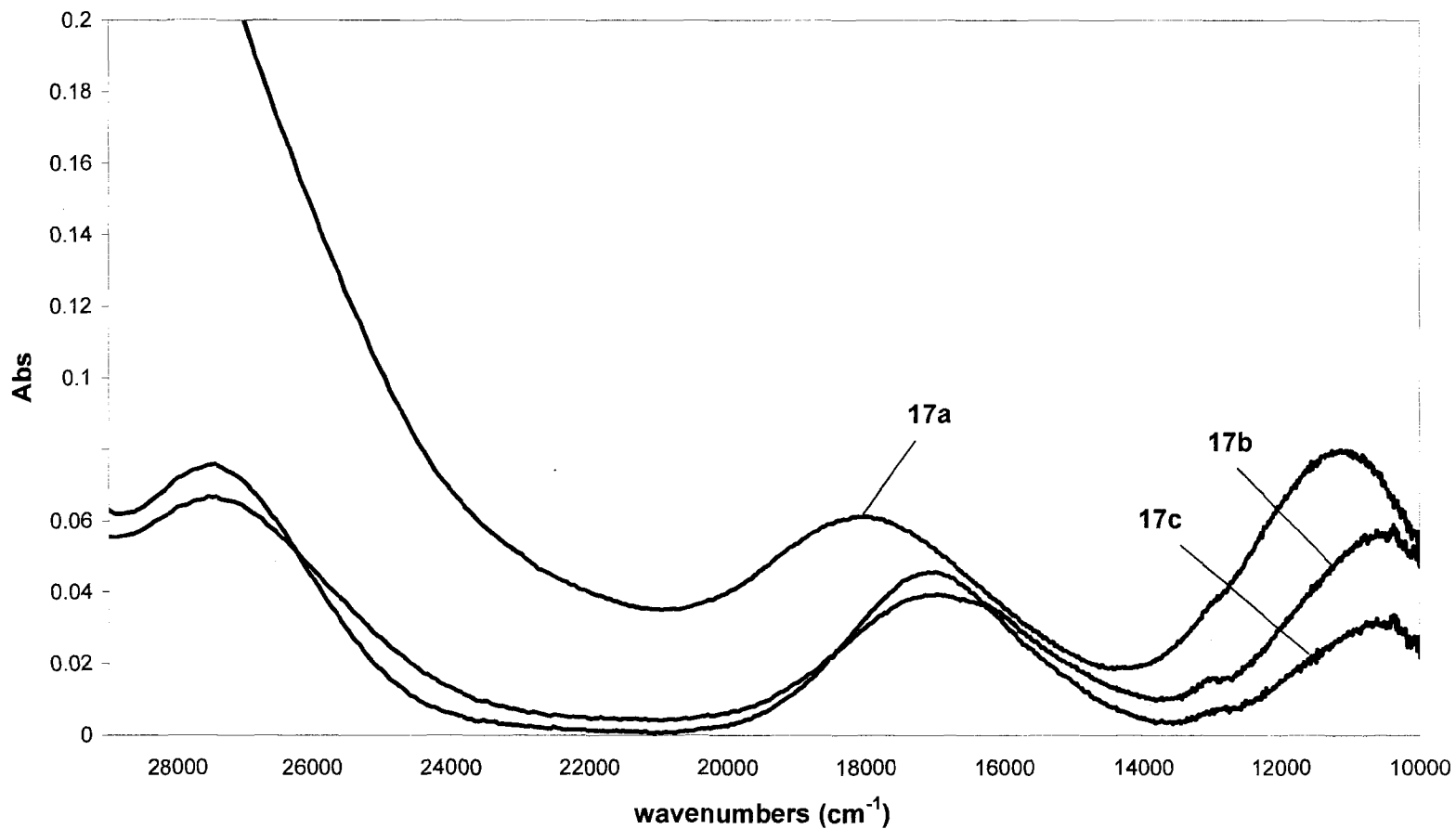
Electronic Absorption Spectra of [Ni(bispicpn)]$^{2+}$, [Ni(bis6Mepicpn)]$^{2+}$ and [Ni(bpdan)]$^{2+}$ in MeCN

117
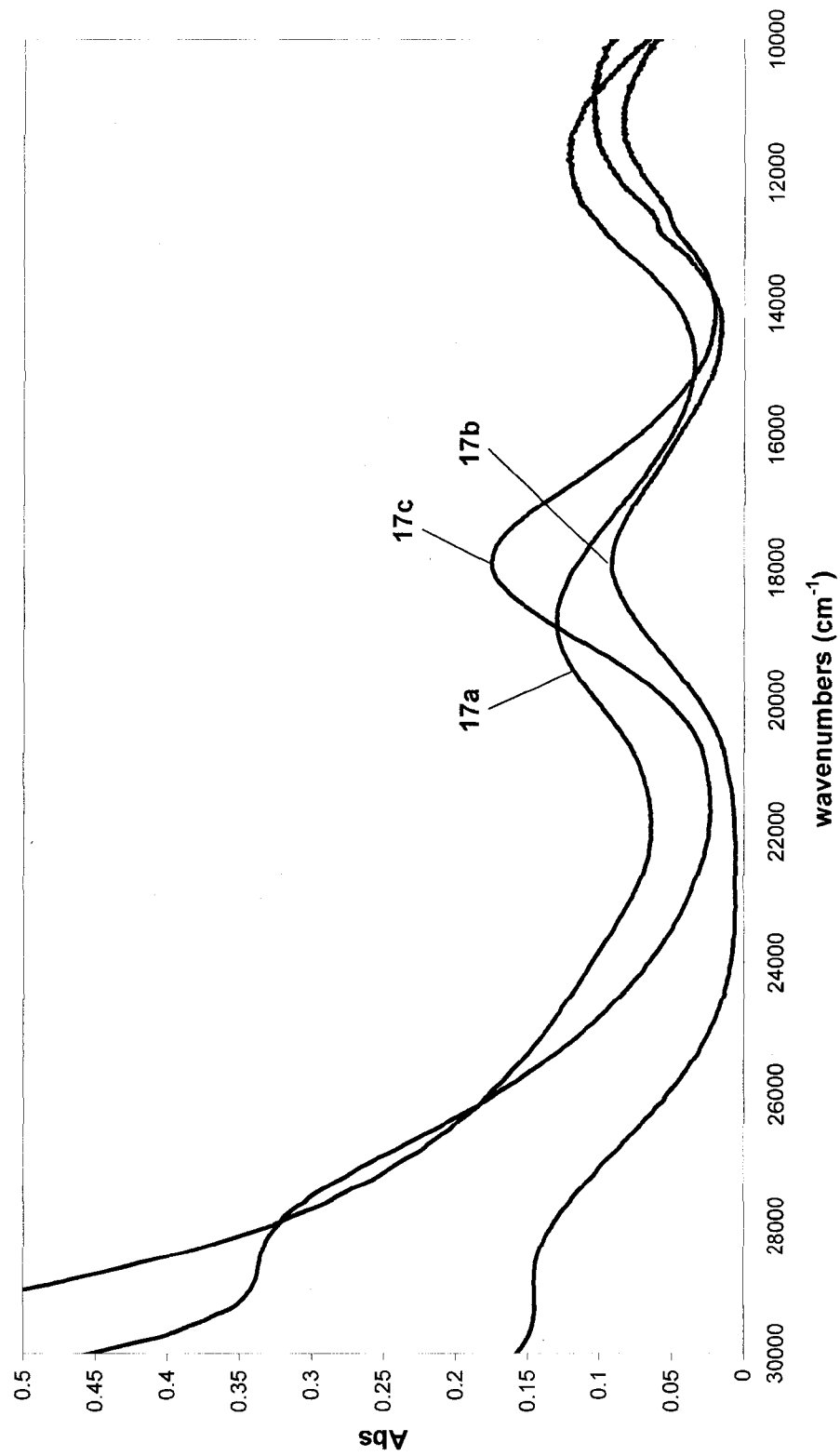
Electronic Absorption Spectra of [Cu(bispicpn)]$^{2+}$, [Cu(bis6Mepicpn)]$^{2+}$ and [Cu(bpdan)]$^{2+}$ in H$_2$O

118
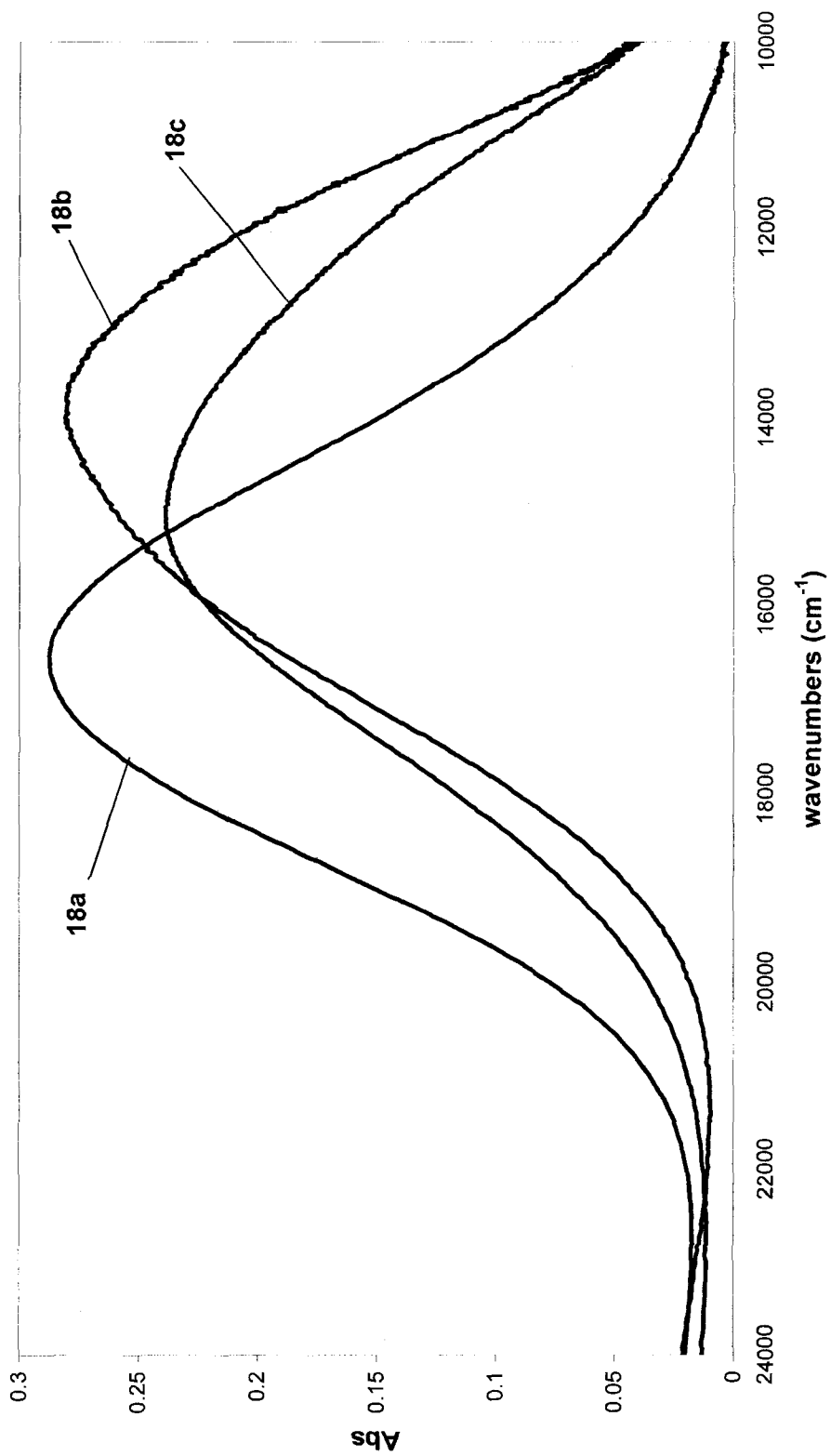
Electronic Absorption Spectra of [Cu(bispicpn)]$^{2+}$, [Cu(bis6Mepicpn)]$^{2+}$ and [Cu(bpdan)]$^{2+}$ in MeCN

119

120
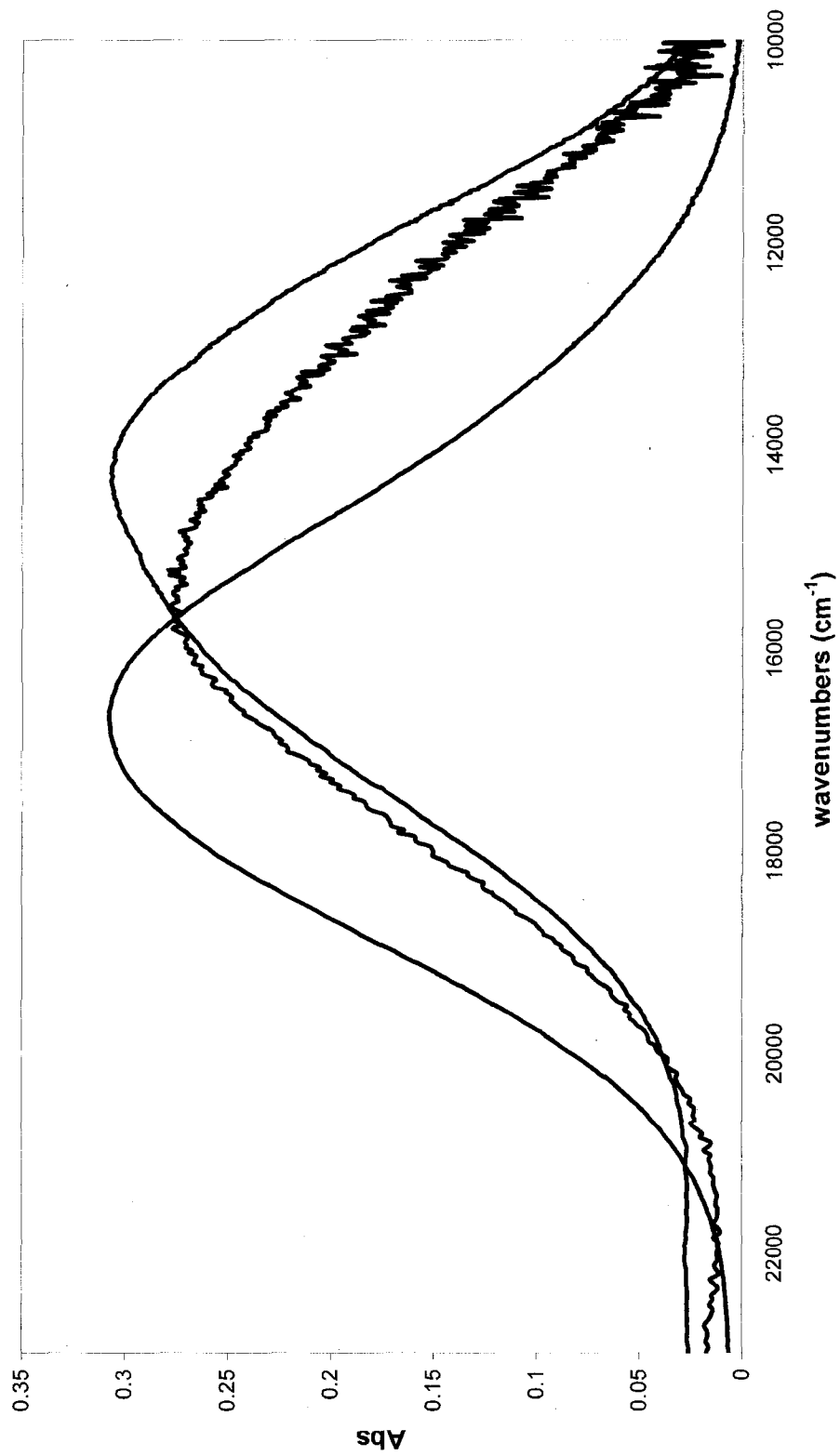
Deconvolution of [Cu(bis6Mepicpn)]$^{2+}$ Electronic Absorption Spectrum; red dashed line is sum of calculated peaks

wavenumbers (cm^{-1})

121
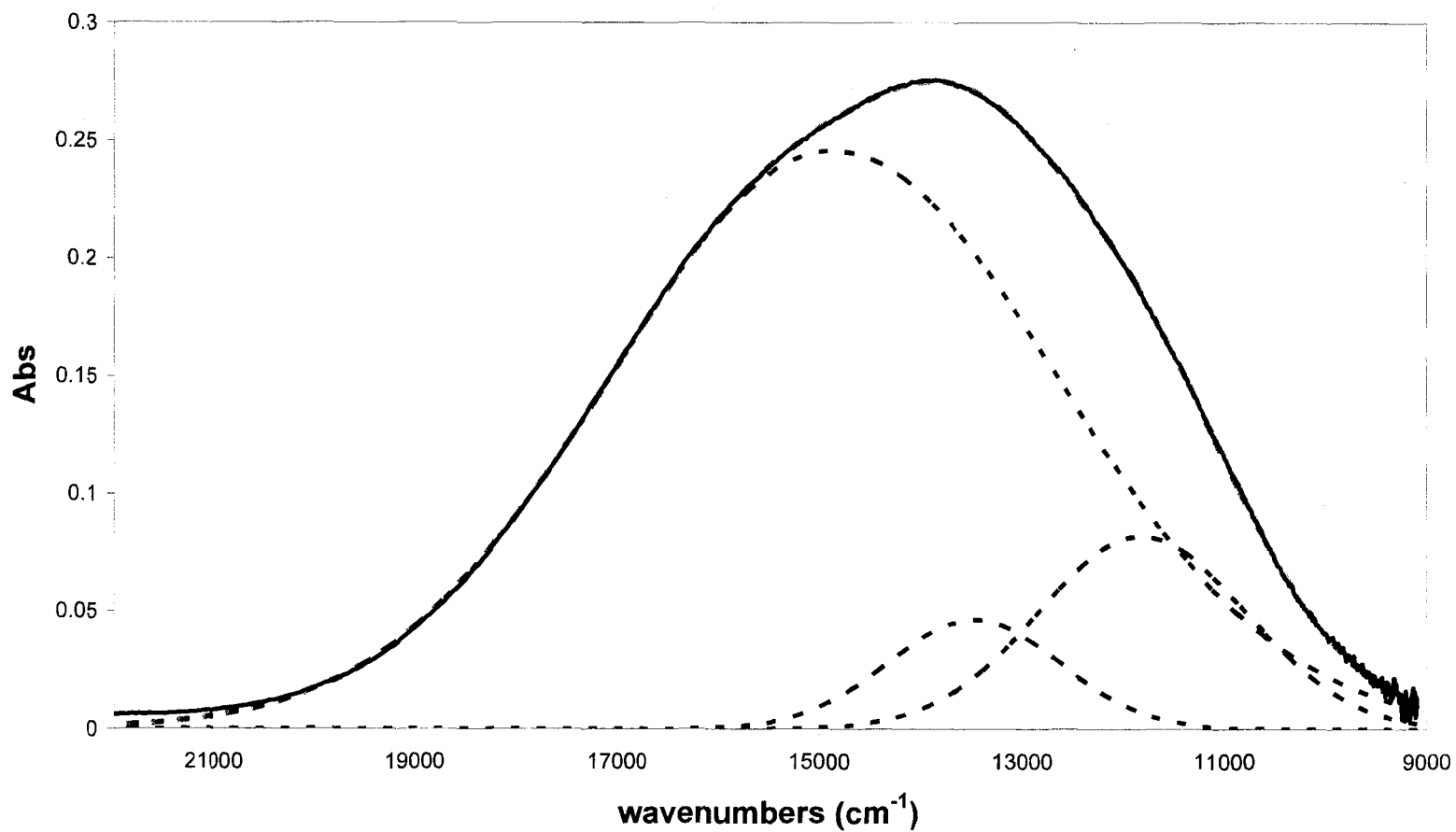
Deconvolution of [Cu(bpdan)]$^{2+}$ Electronic Absorption Spectrum; red dashed line is the sum of the calculated peaks
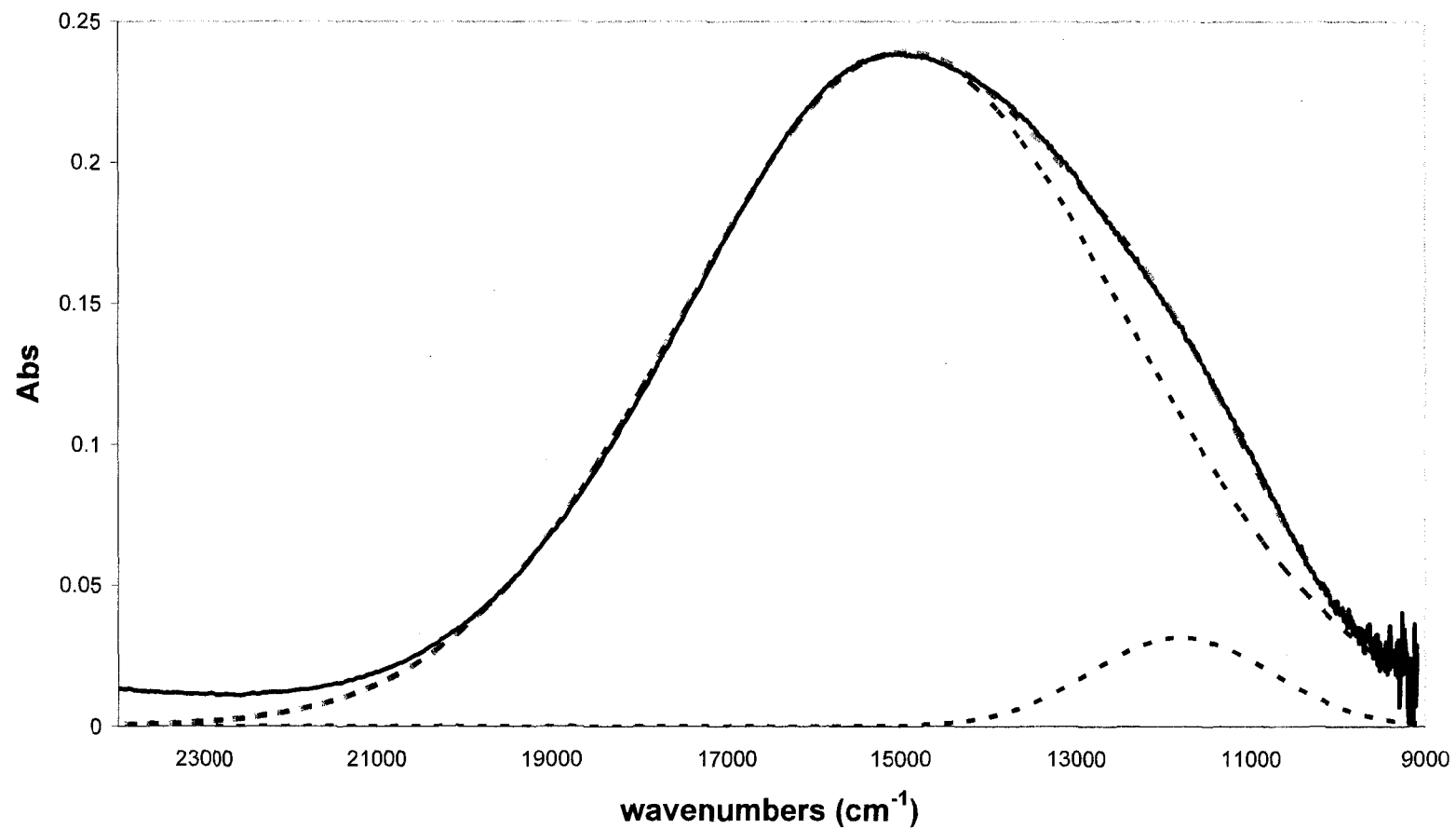
Displacement of Ni(II) from [Ni(bis6Mepicpn)]²⁺ by Zn(II)

122
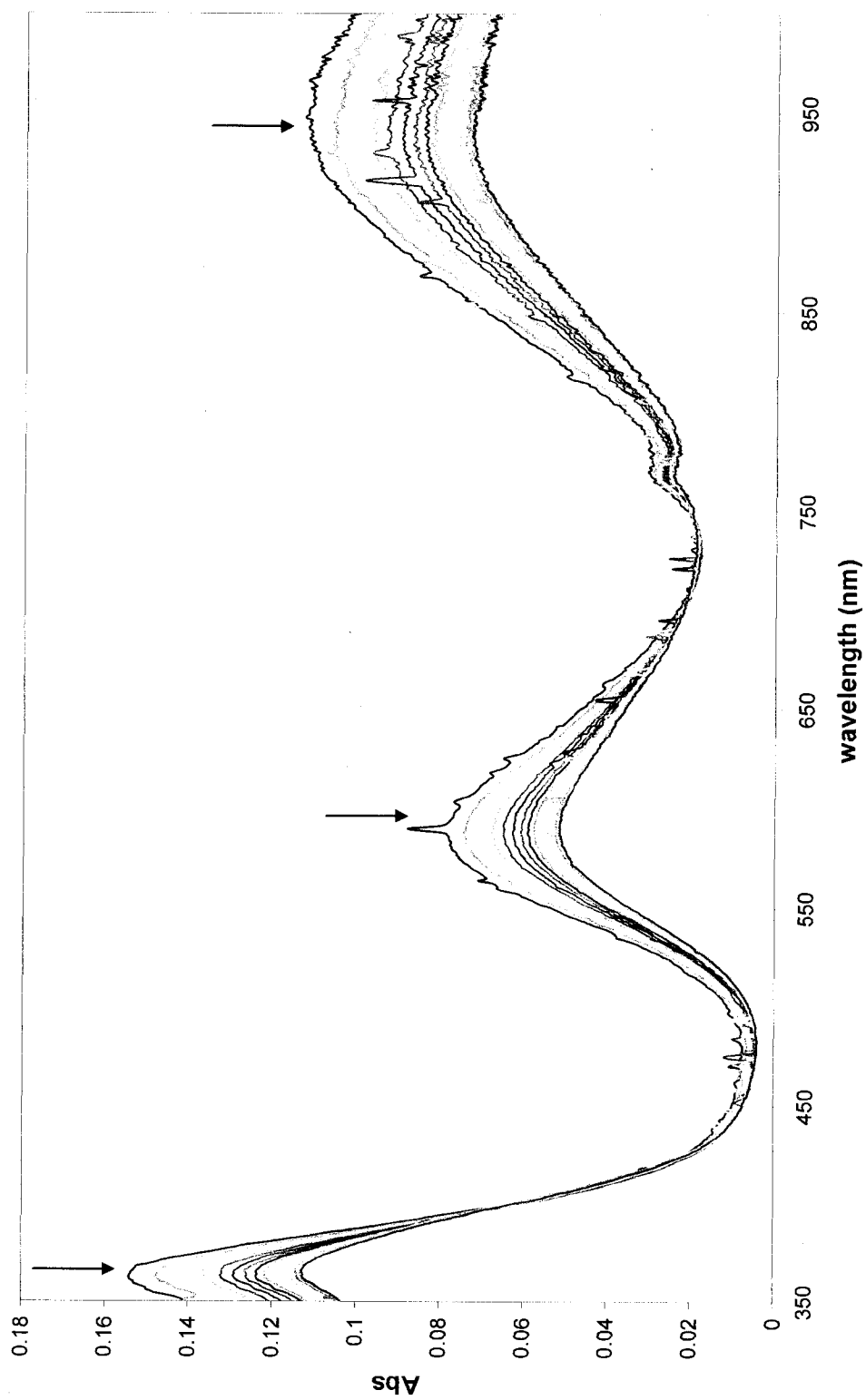
APPENDIX B: NMR Spectra

[Fe(tach-3-Mepyr)]$^{2+}$ (1a)

124

[Fe(tach-4-Mepyr)]²⁺ (1b)

125

[Fe(tach-5-Mepyr)]²⁺ (1c)

126

127
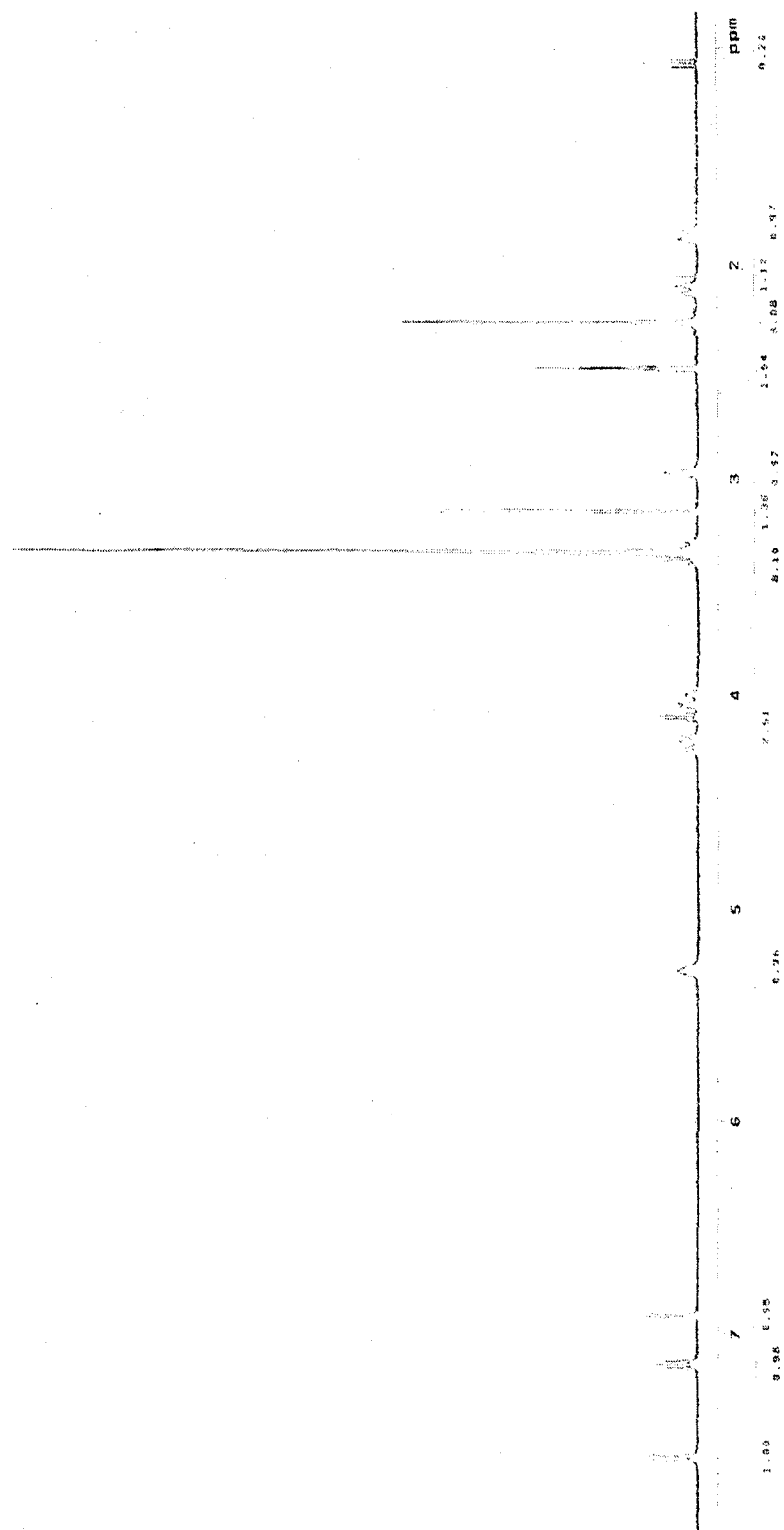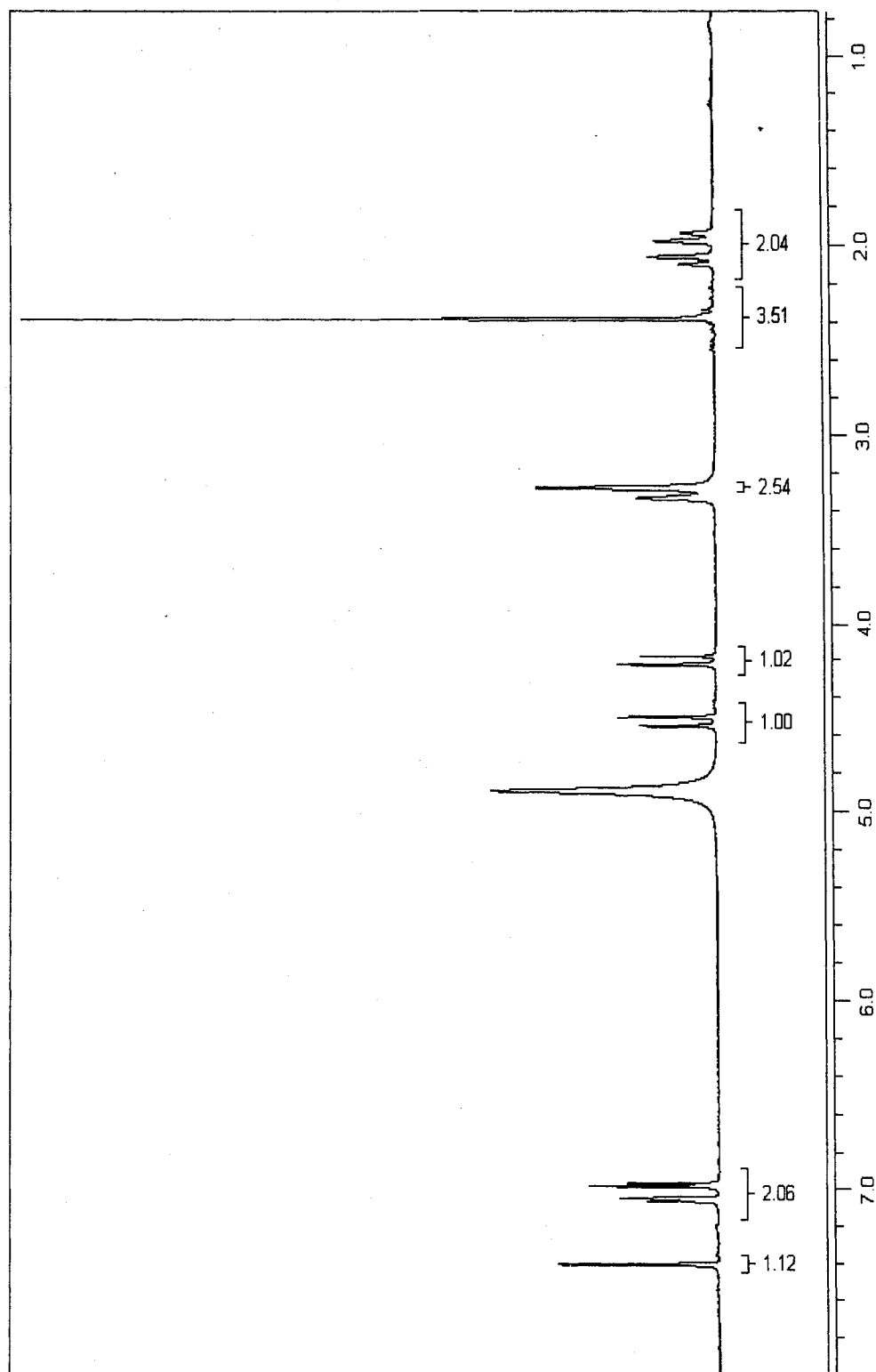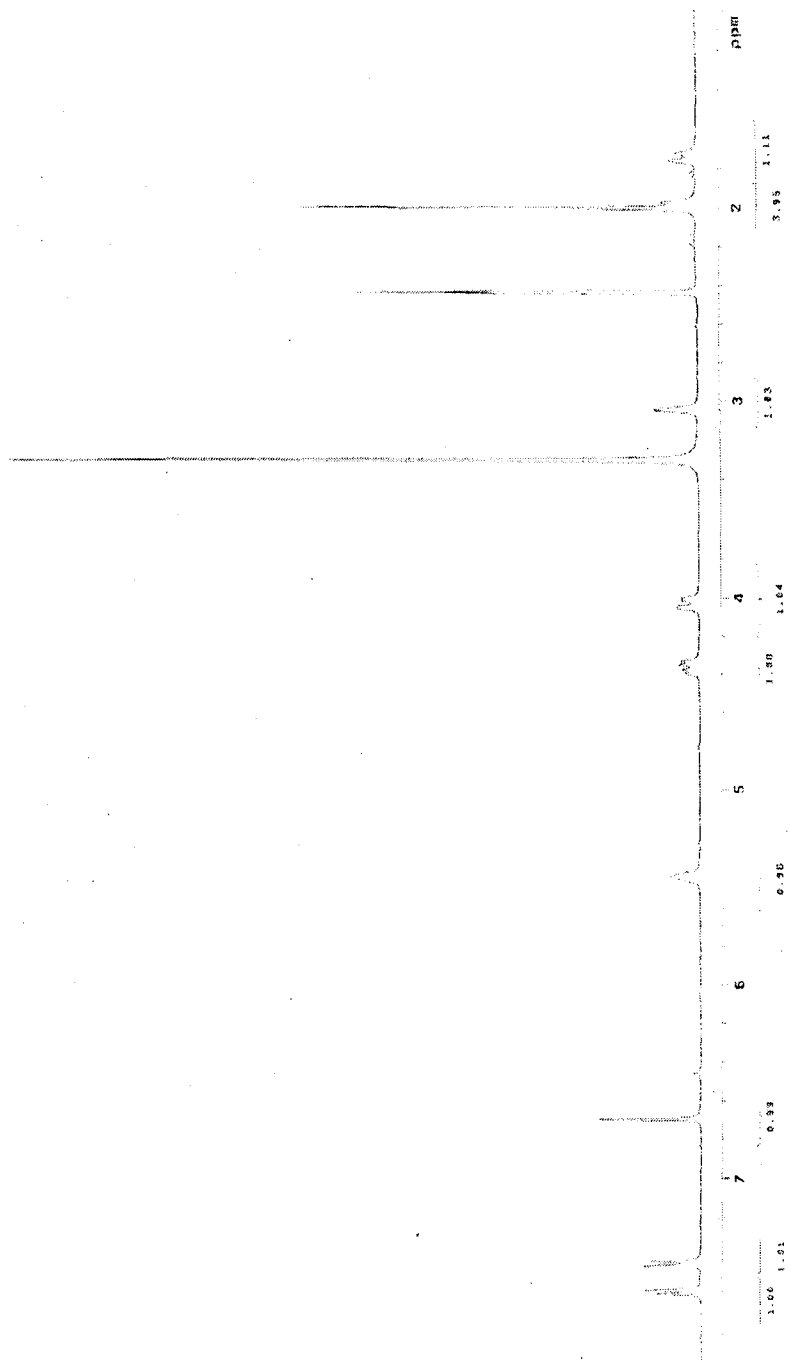
Mixture of [Fe(tach-4-Mepyr)]²⁺ and [Fe(tach-4-Mepyr-ox-2)]²⁺ from Disproportionation Reaction with Imine and Methyl peaks Integrated
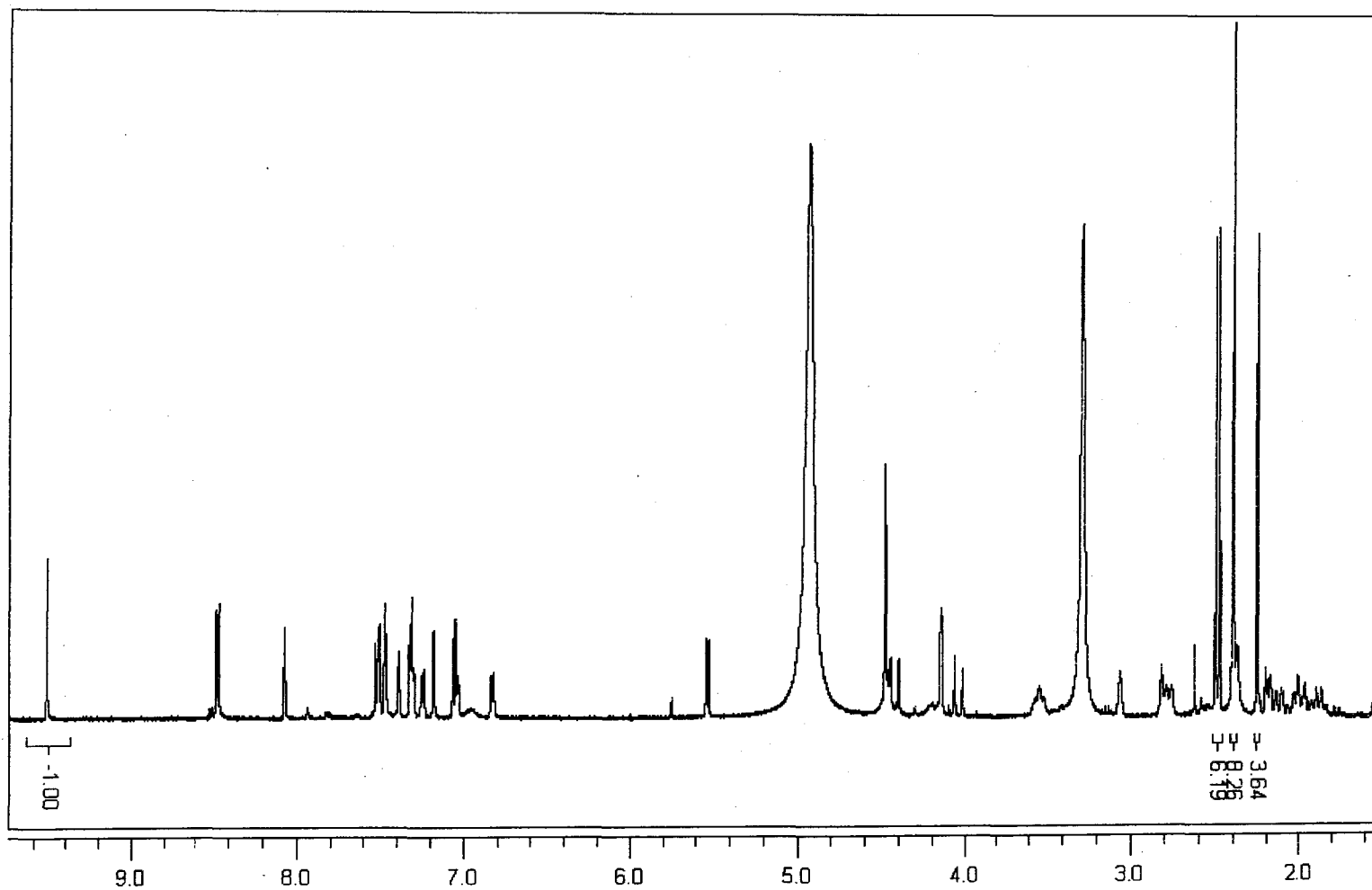
Disproportionation Reaction Mixture + Bipy (Inset is of Methyl Peaks)
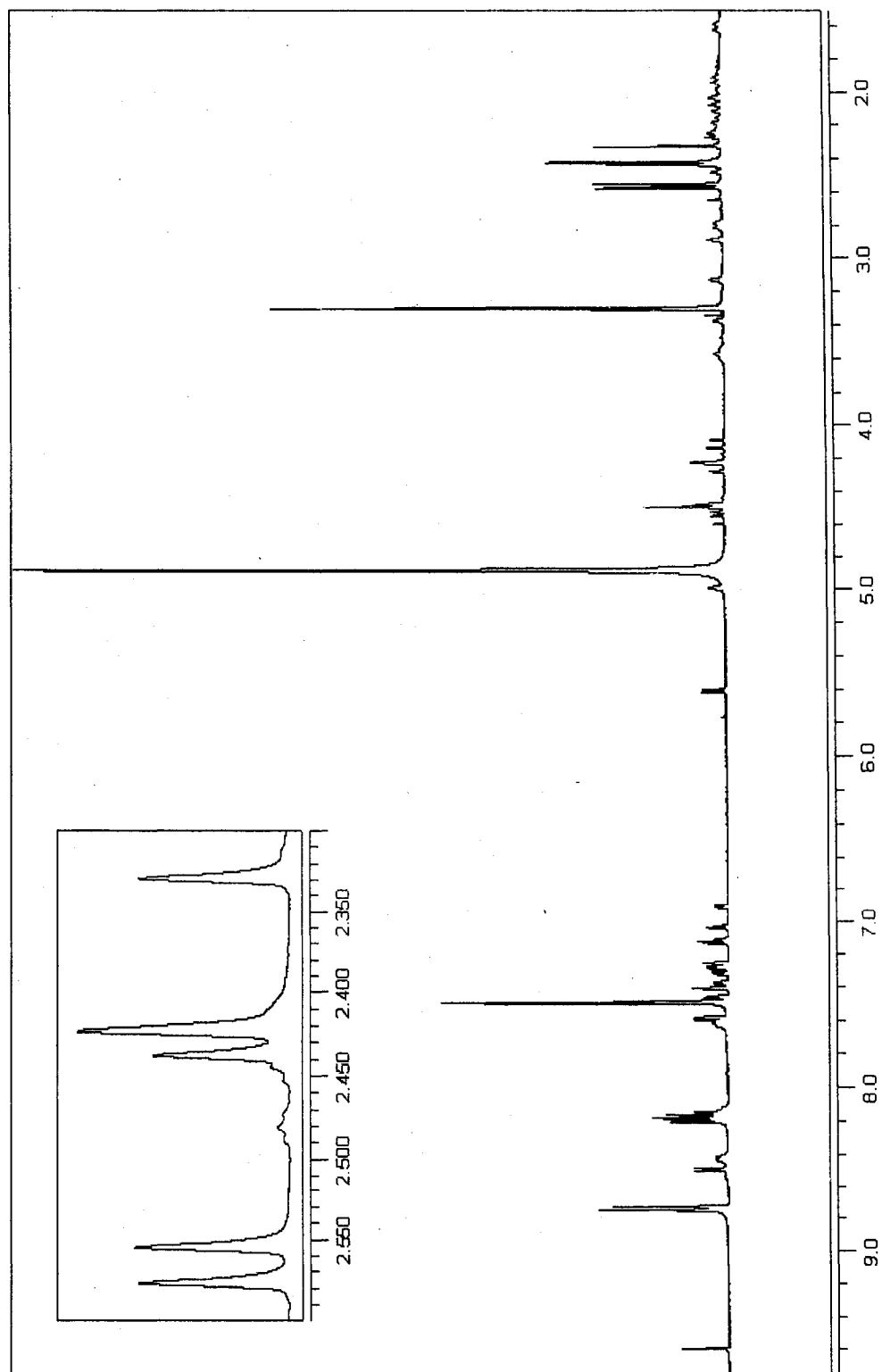
Disproportionation Reaction Mixture + Phen (Inset is of Methyl Peaks)

[Fe(tach-3-Mepyr-ox-4)]²⁺

130

[Fe(tach-3-Mepyr-ox-6)]$^{2+}$

131
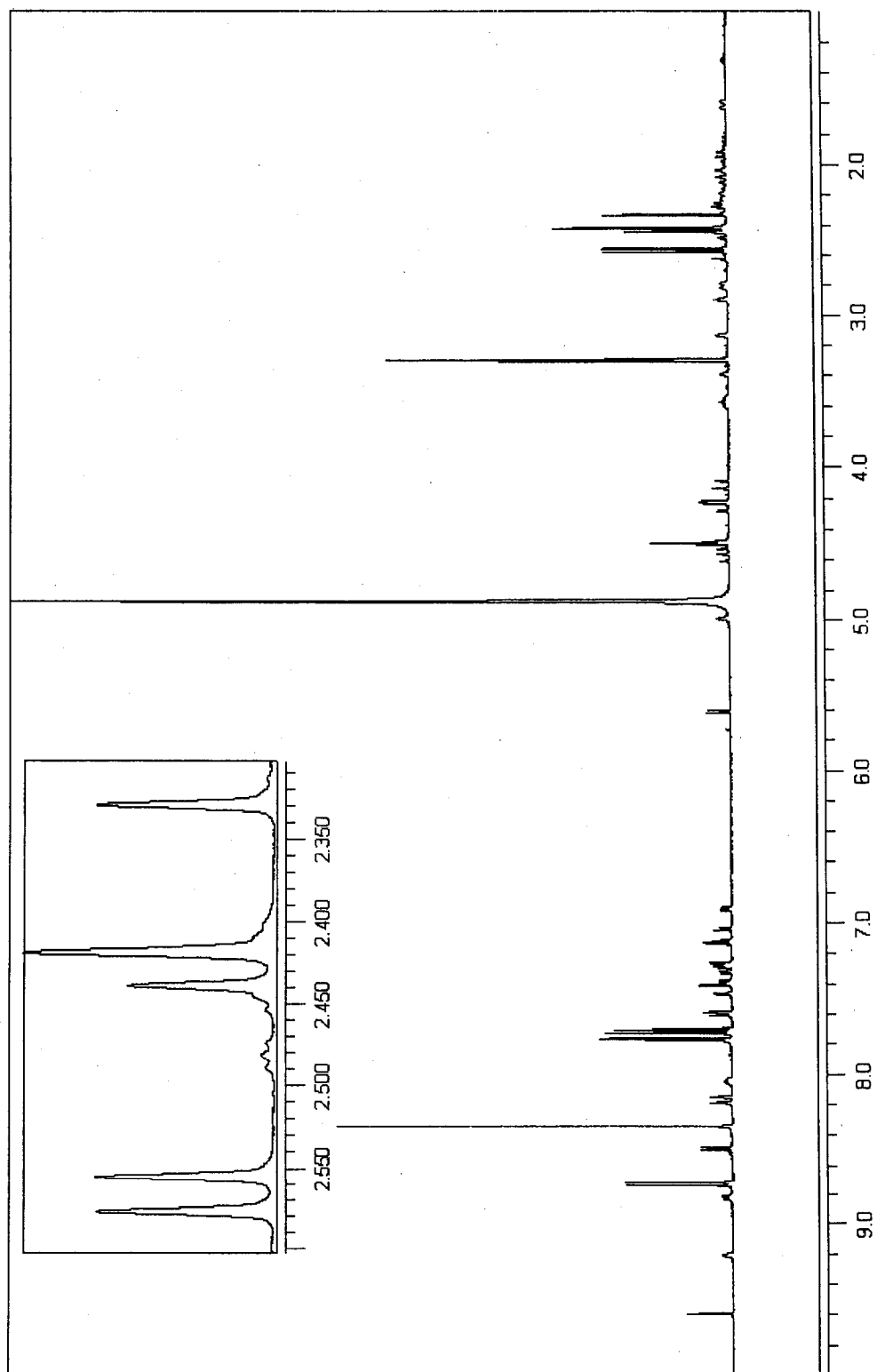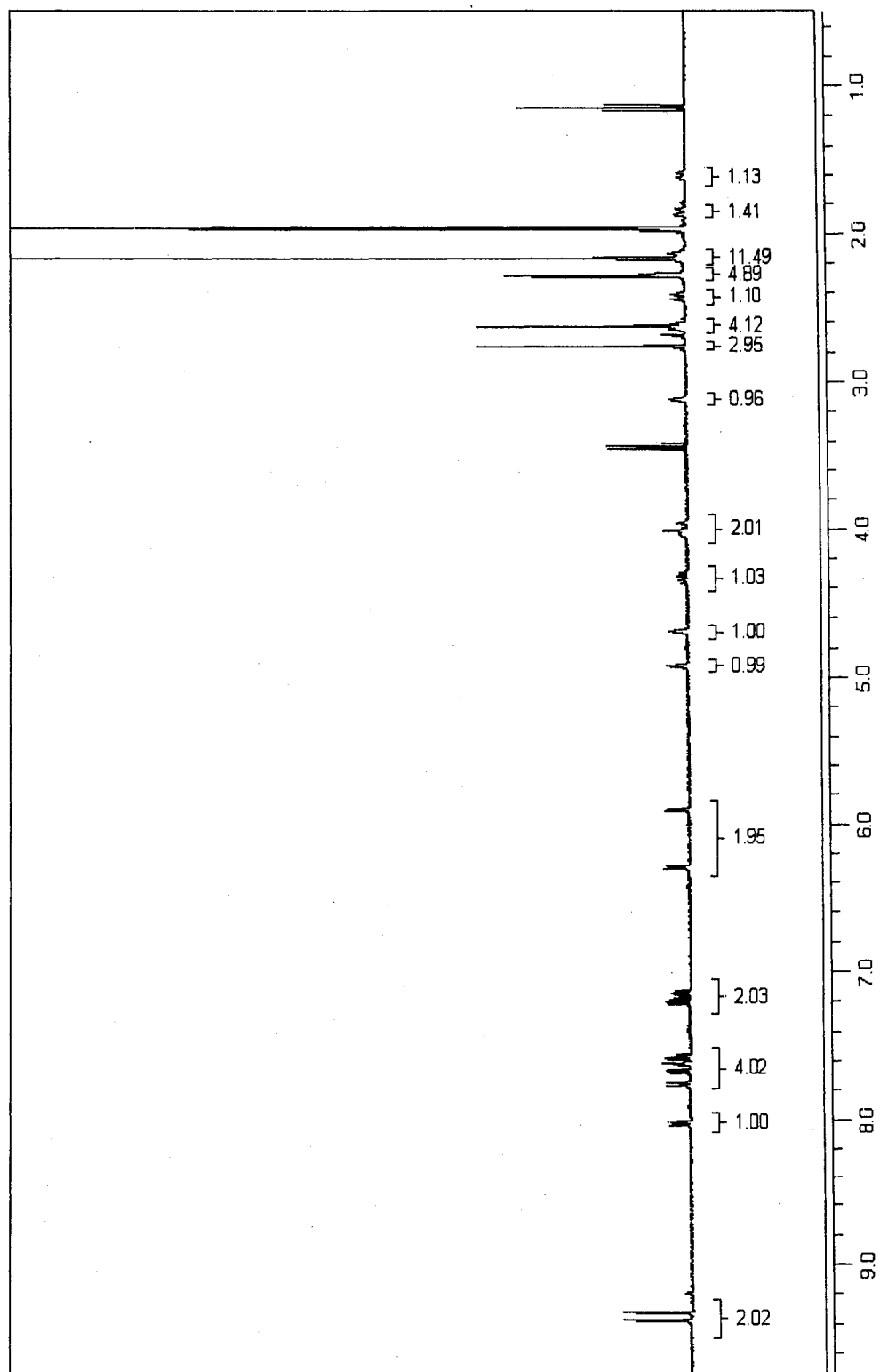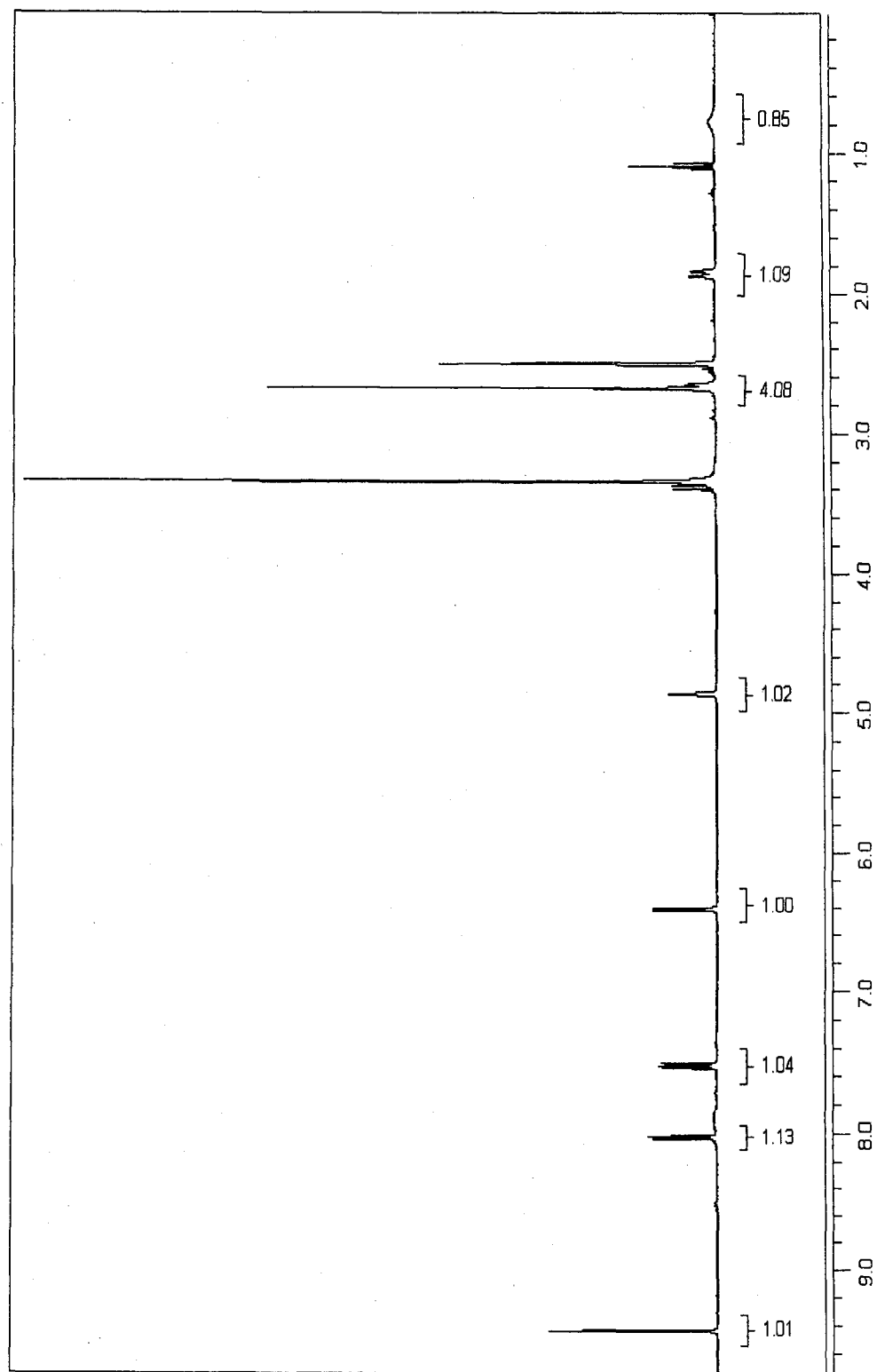
Oxidation of [Fe(tach-3-Mepyr)]²⁺ by air to [Fe(tach-3-Mepyr-ox-n)]²⁺ (n = 2 or 4)

132
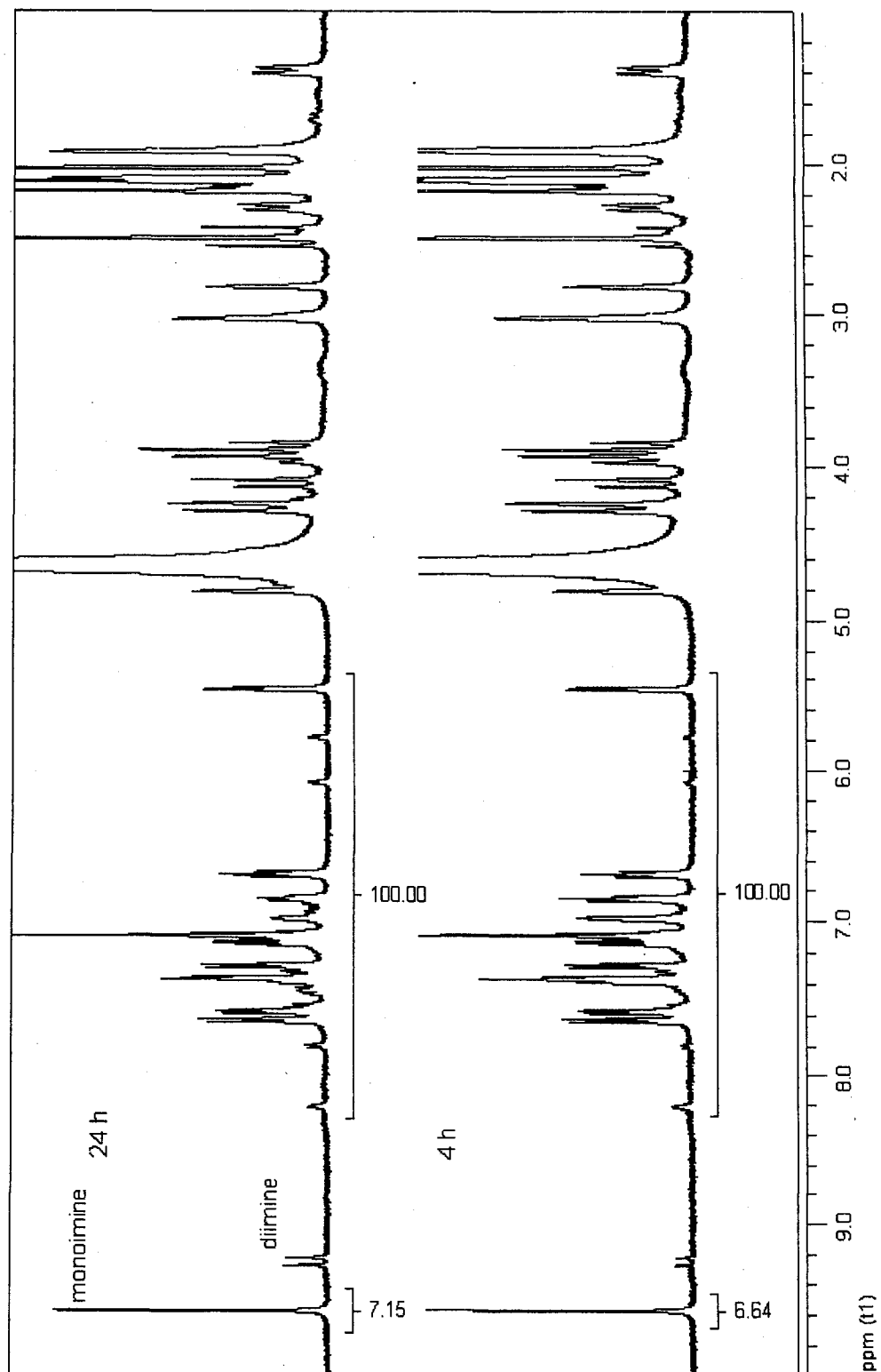
Oxidation of [Fe(tach-3-MeOpyr)]$^{2+}$ by air to [Fe(tach-3-Mepyr-ox-2)]$^{2+}$

133
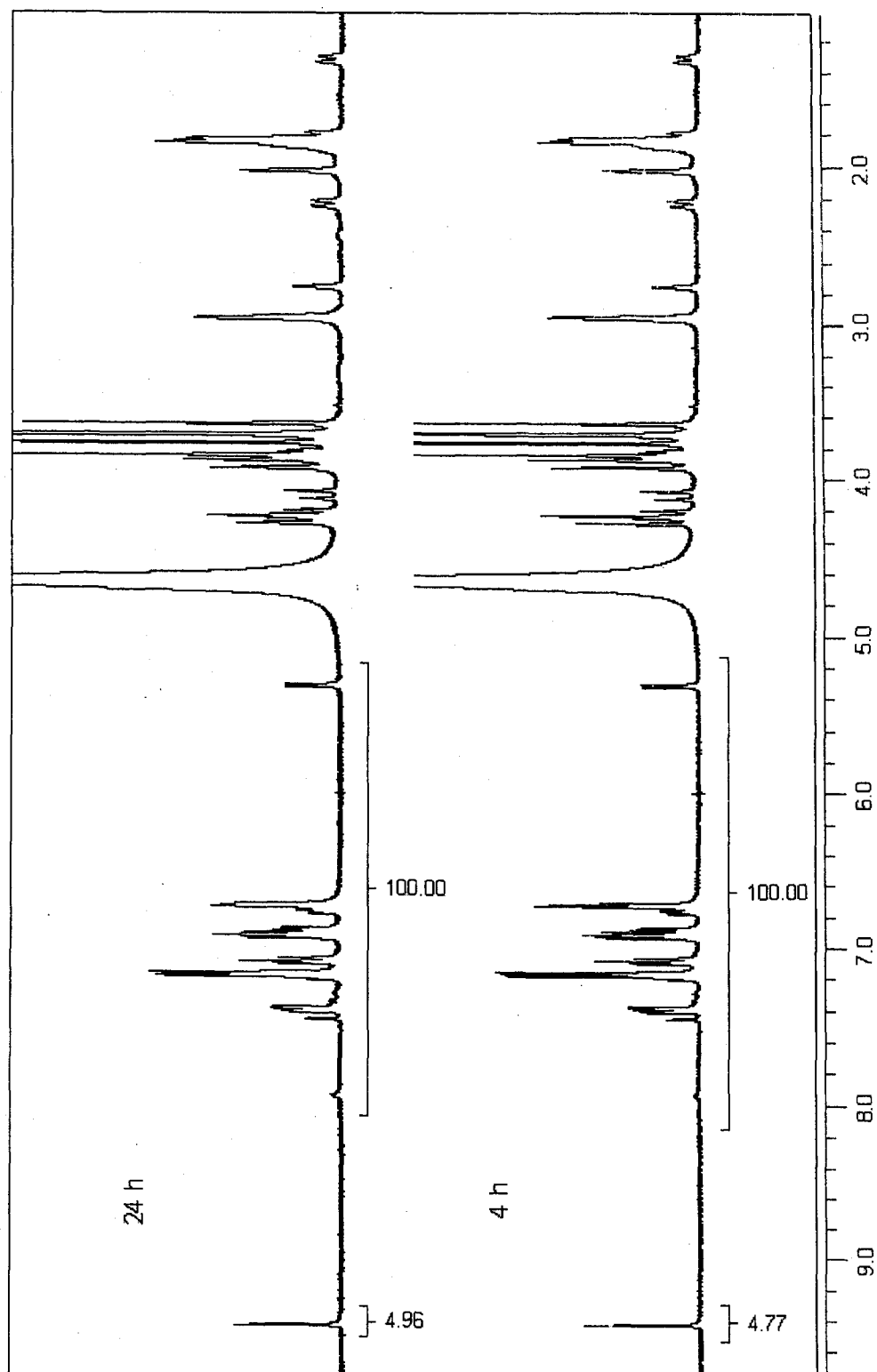
Oxidation of [Fe(tachpyr)]$^{2+}$ by air to [Fe(tachpyr-ox-n)]$^{2+}$ (n = 2 or 4)

24 h

100.00

5.64

4 h

100.00

4.77

134

bispicpn (L⁶)

135

bis6Mepicpn (L^7)

136
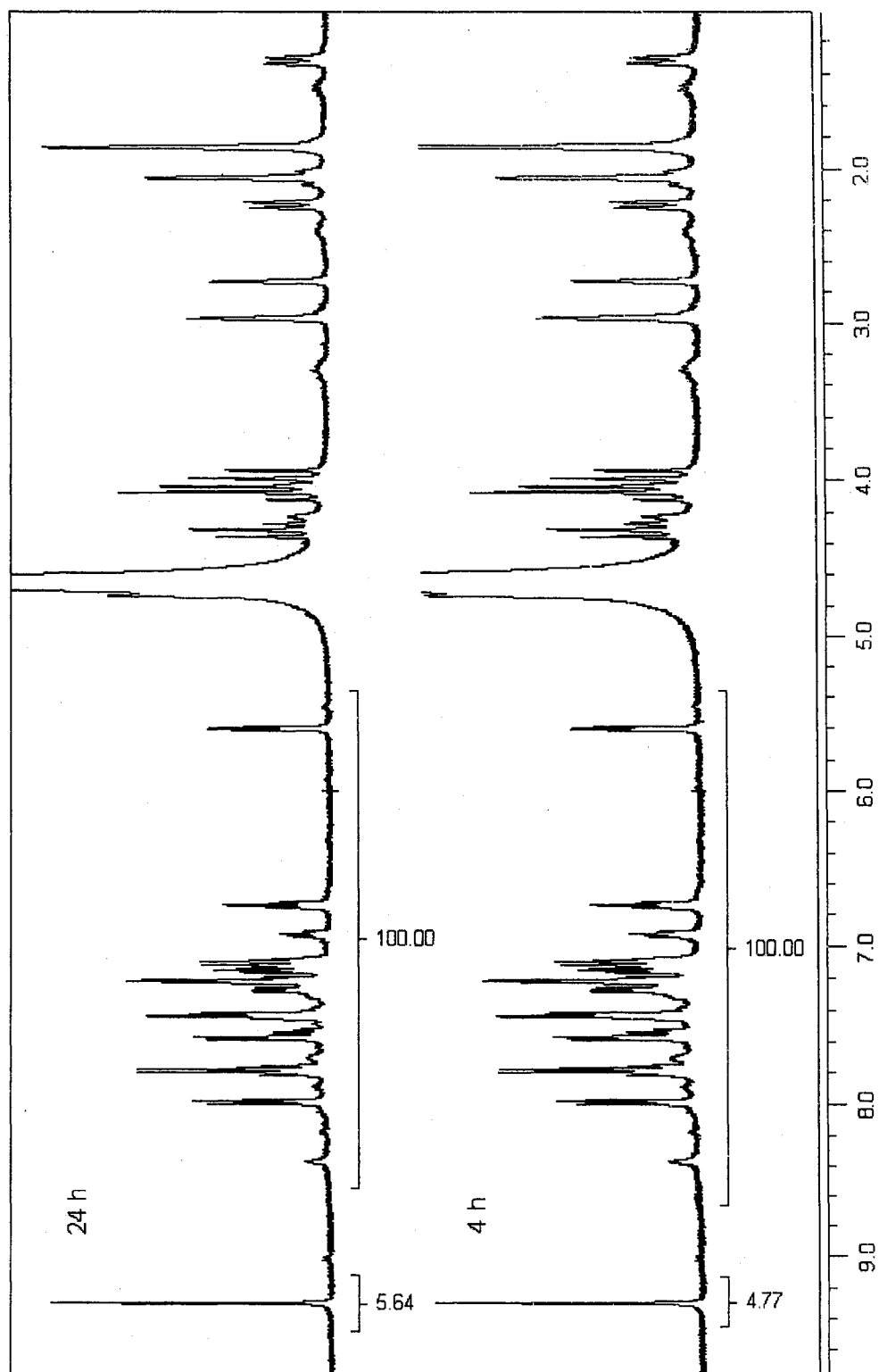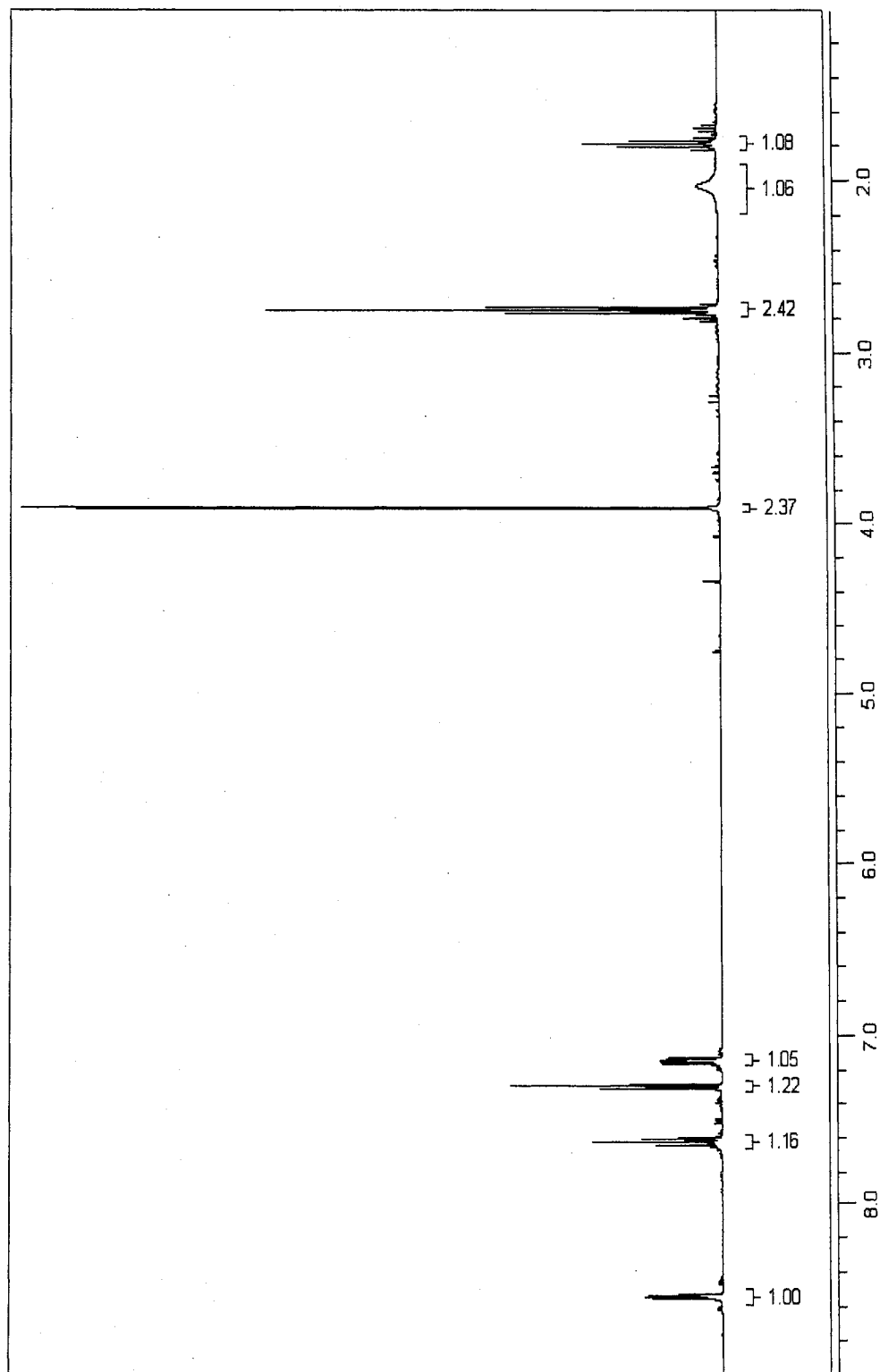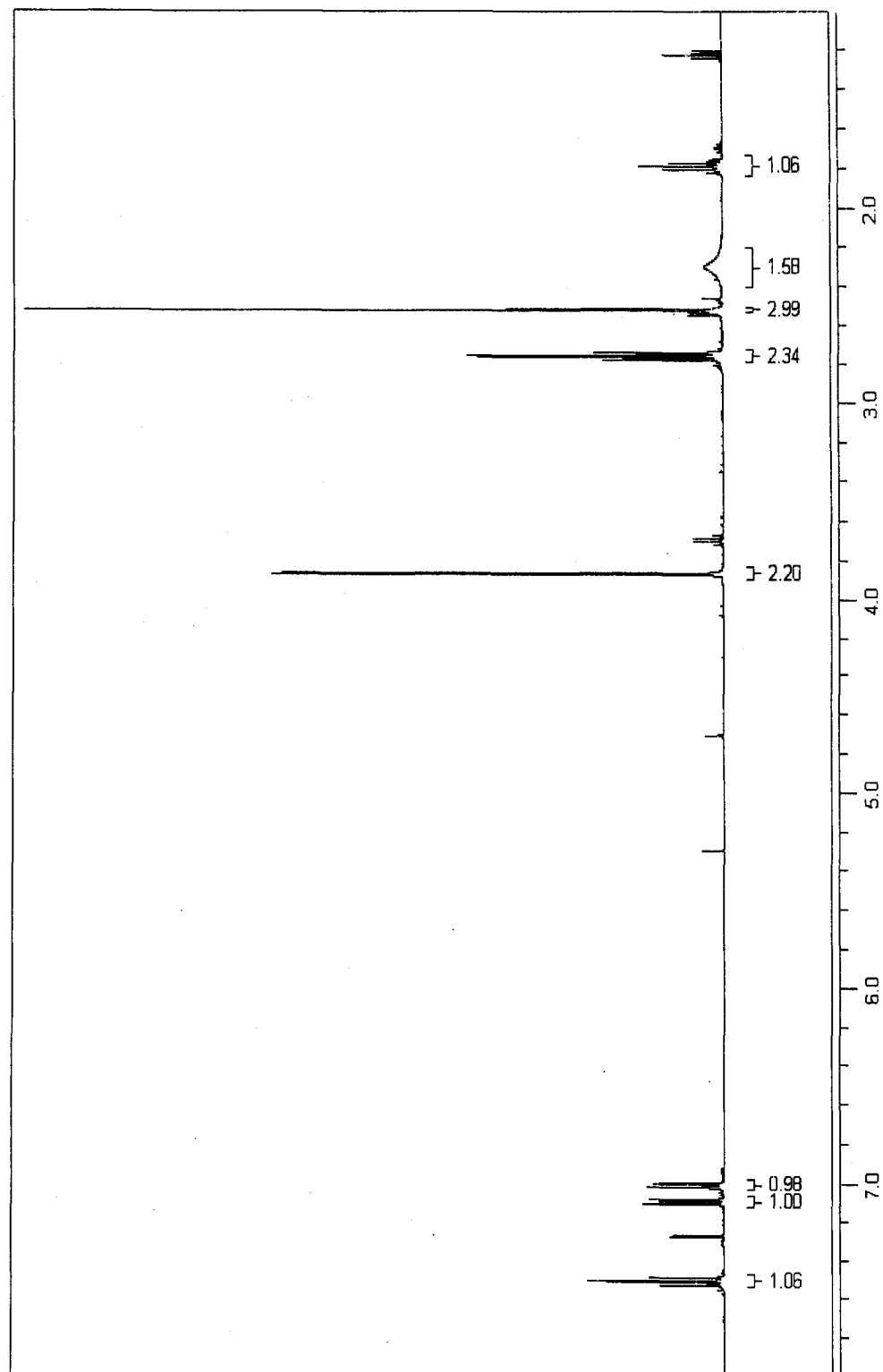
Tosylated 2-(2-aminoethyl)pyridine

137
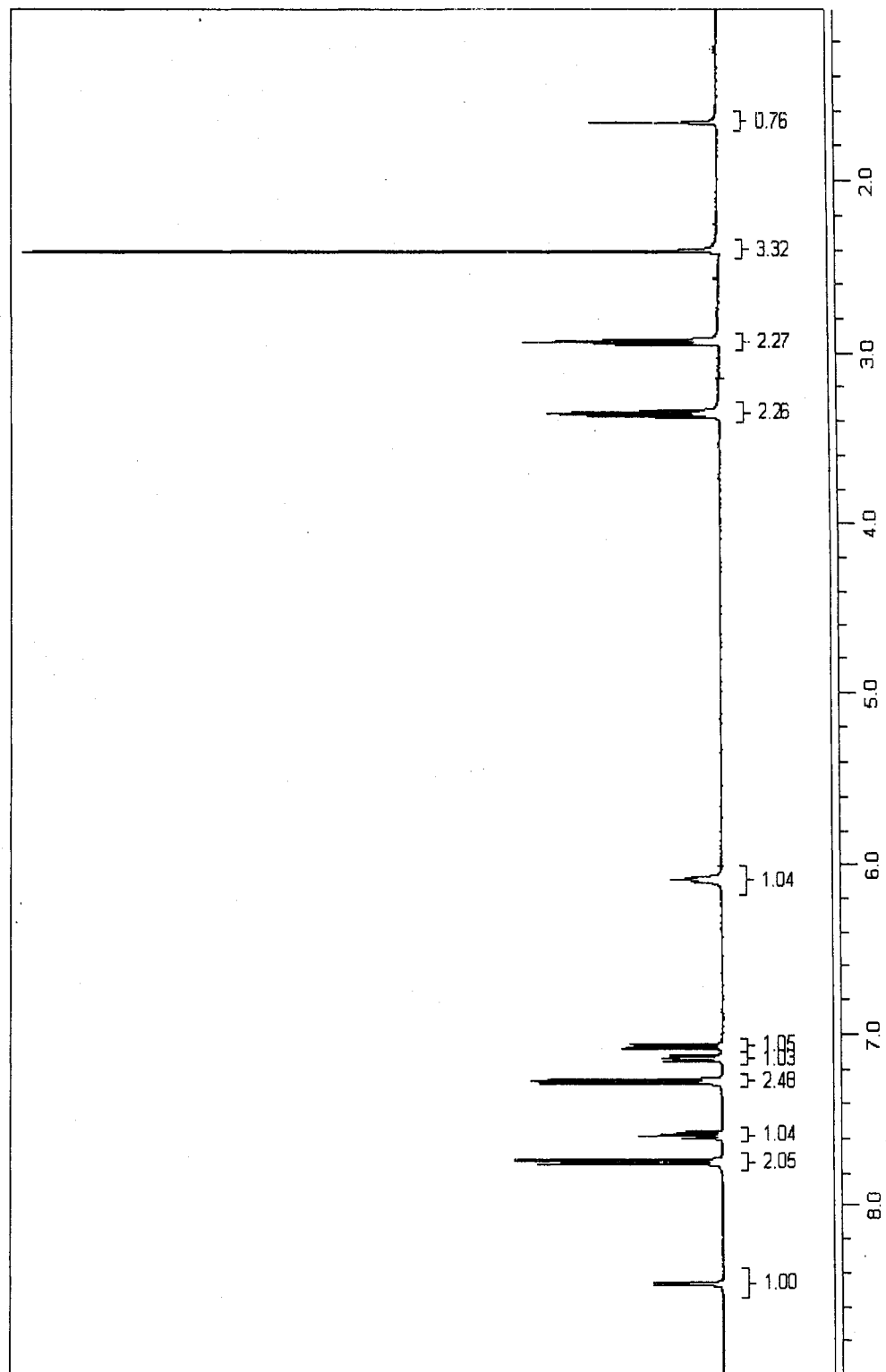
Tosylated 1,3-propanediol
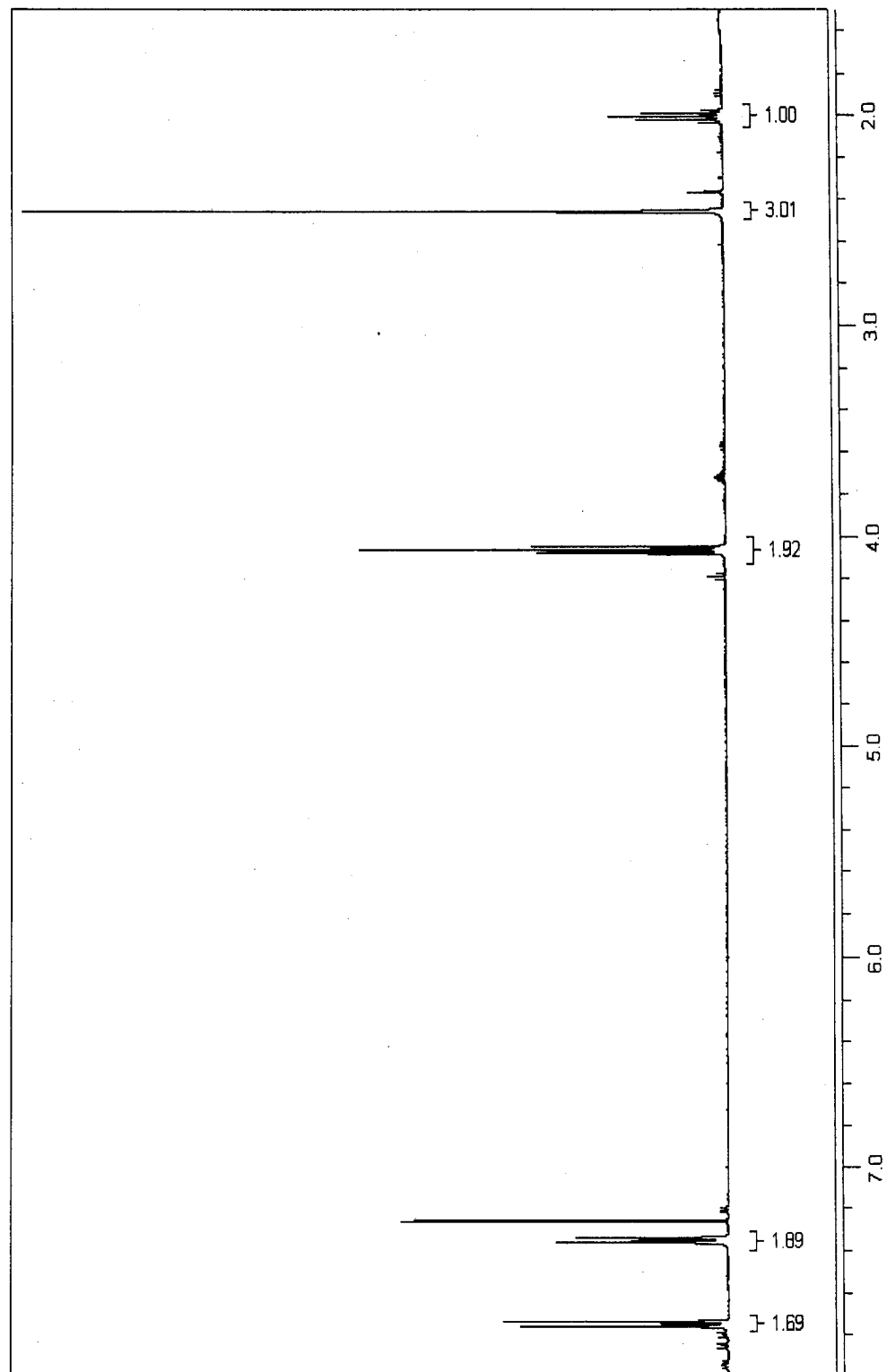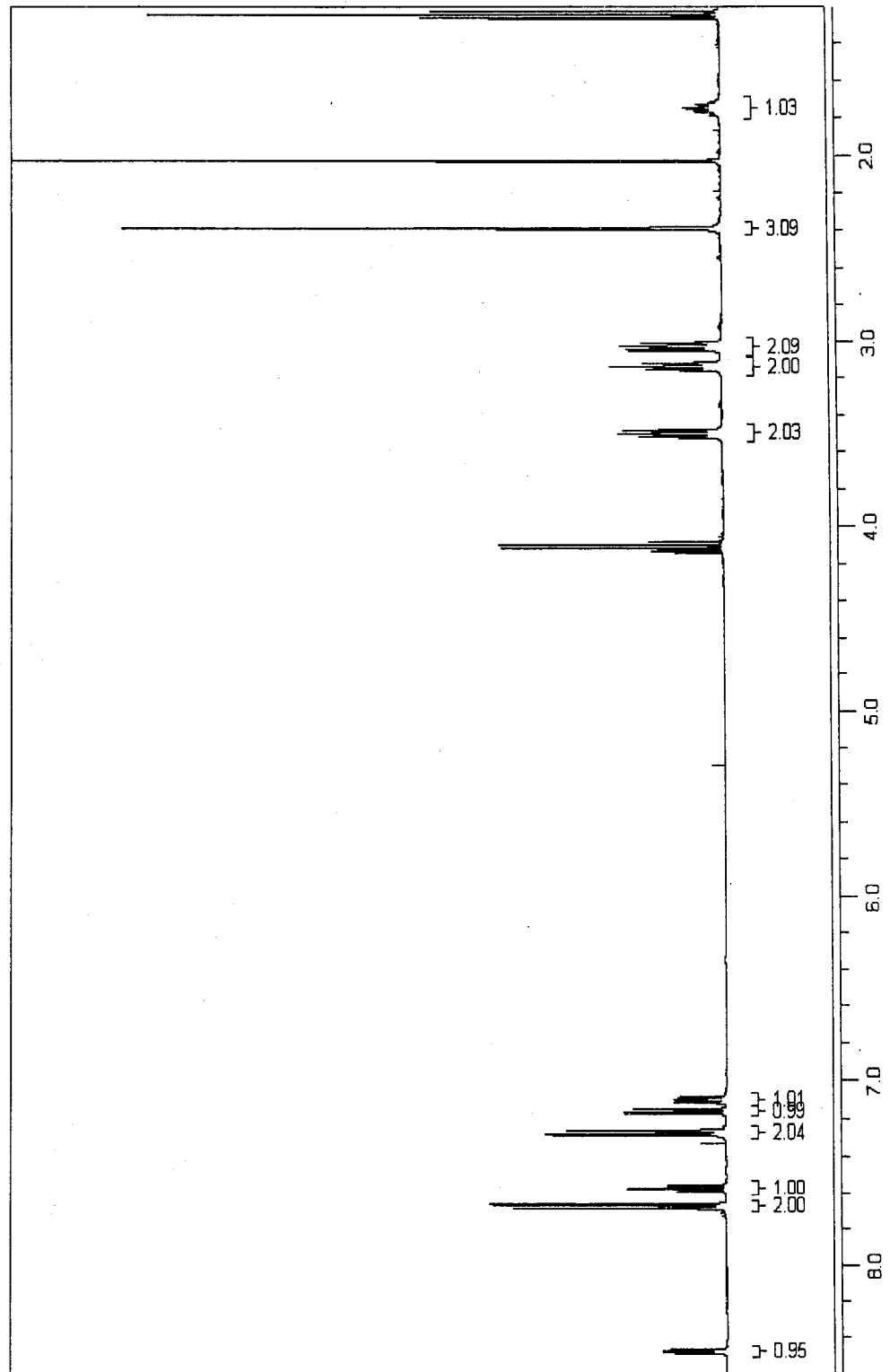
138

Tosylated bpdan

139

bpdan (L⁸)

140

Zn(NO₃)₂ + bispicpn

141

ZnCl$_2$ + bispicpn

142

Zn(ClO$_4$)$_2$ + bispicpn

NMR peak labels: 24.725, 27.325, 51.002, 51.742, 52.042, 124.150, 124.807, 125.237, 141.068, 141.648, 147.203, 147.986, 156.236, 156.547

143

Zn(OTf)$_2$ + bispicpn

24.731
27.340
50.984
51.704
51.998
124.072
124.731
124.779
126.156
141.017
141.577
147.188
148.009
156.251
156.591

50
100
150

2.0
3.0
4.0
5.0
6.0
7.0
8.0

144
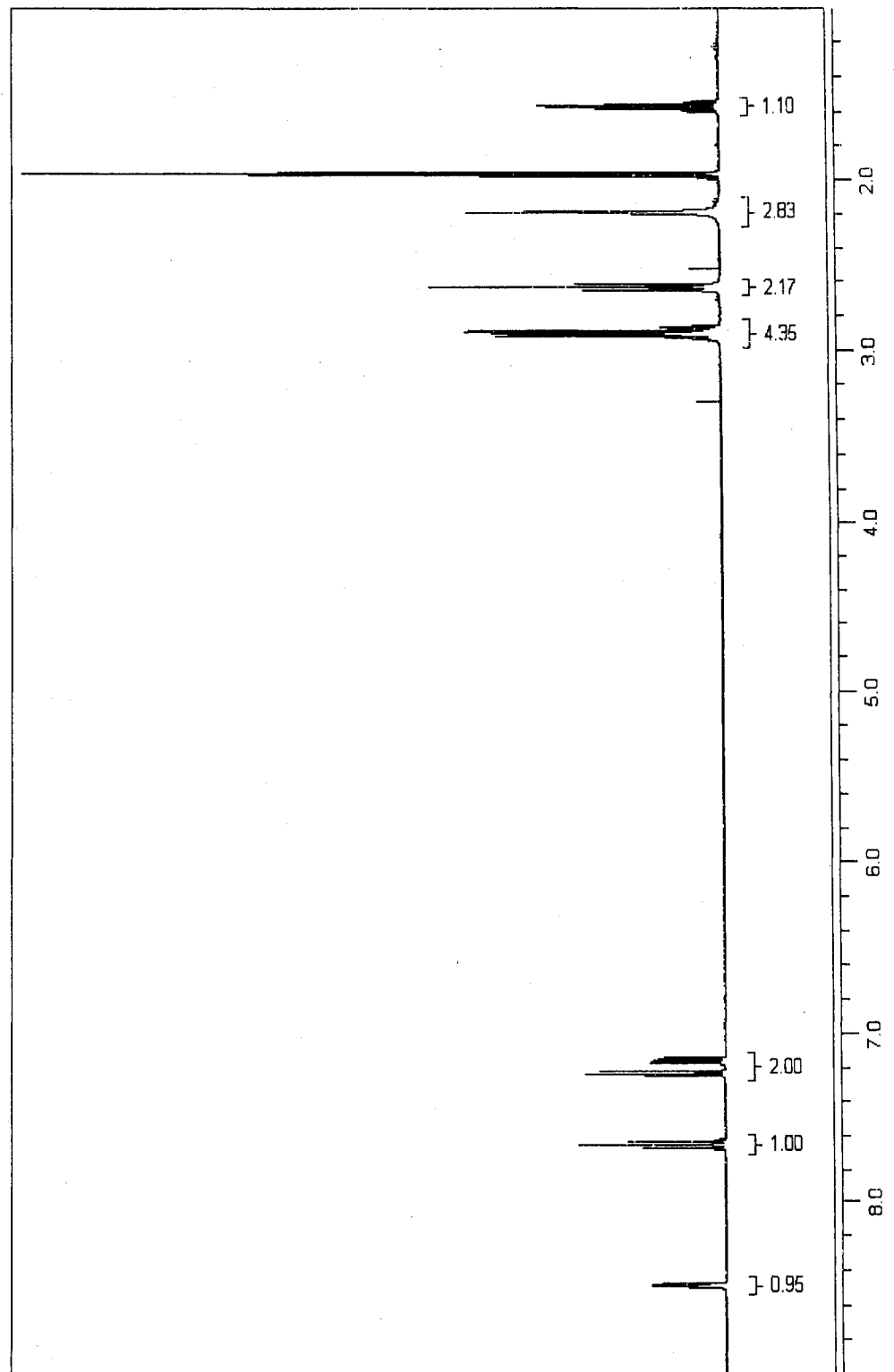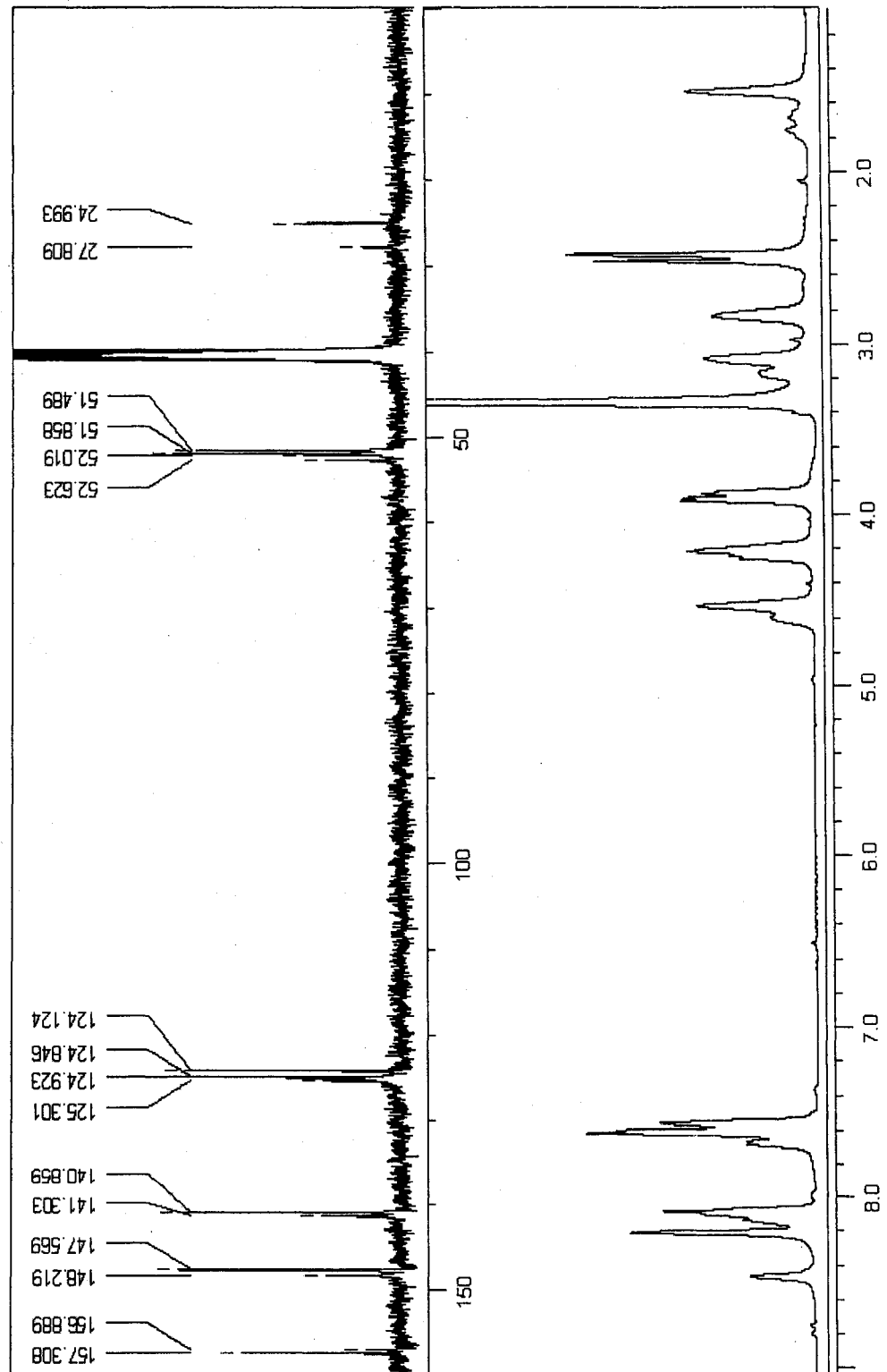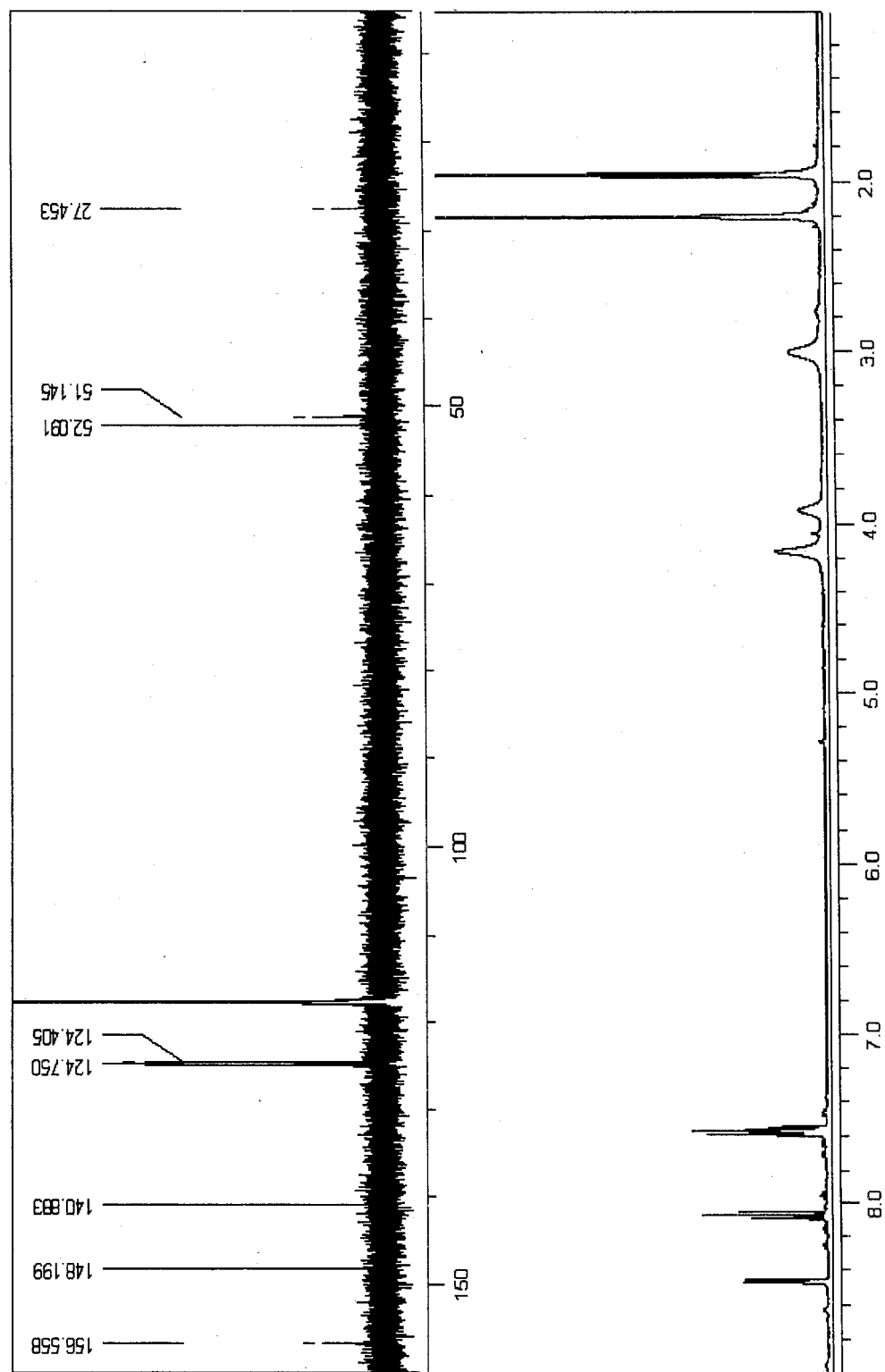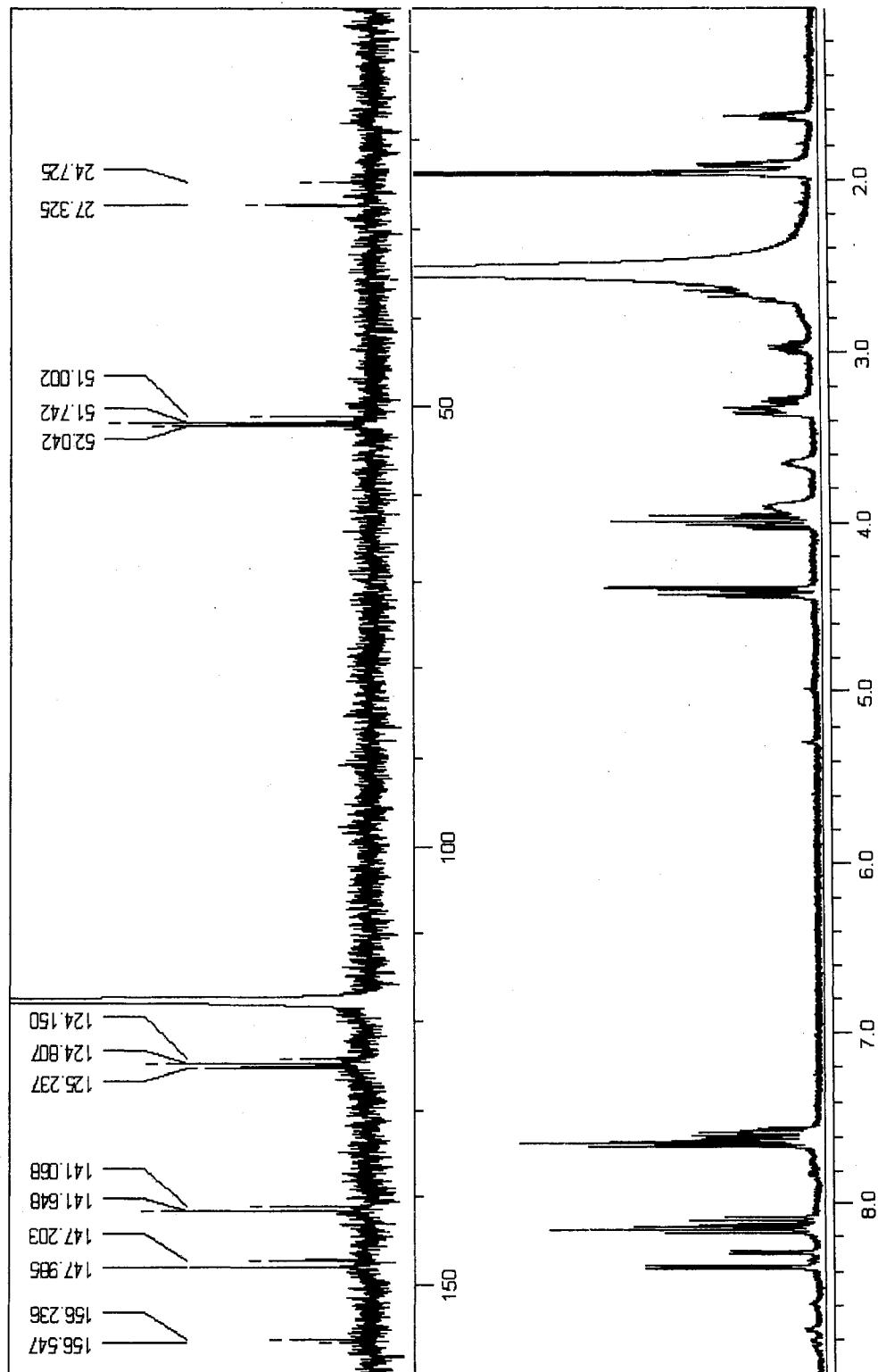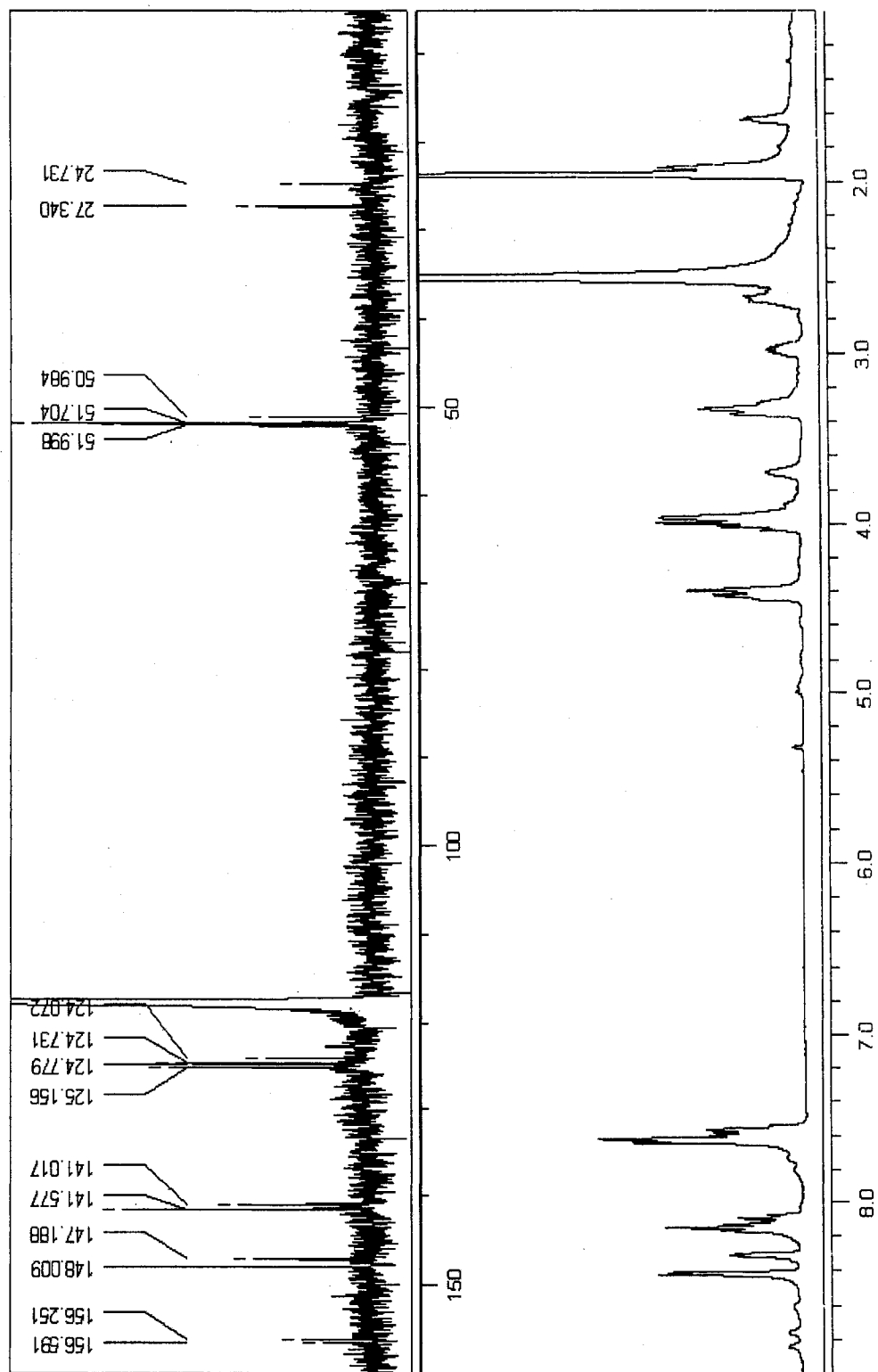
VT ^{1}H NMR of [Zn(bis6Mepicpn)]$^{2+}$ (19b) from 5.5 – 1.5 ppm

145
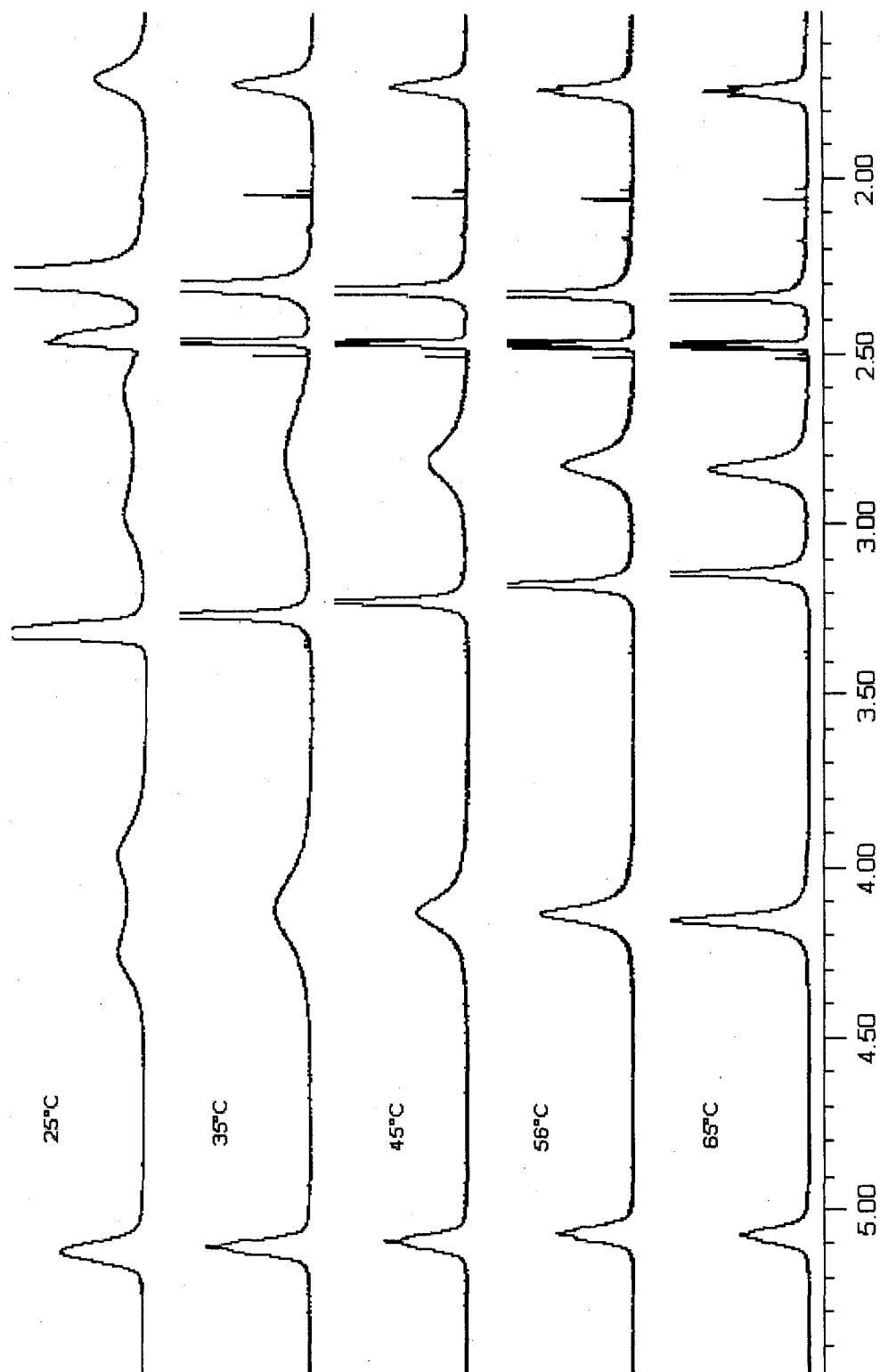
VT ^{13}C NMR of [Zn(bis6Mepicpn)]$^{2+}$ (19b) from 60 – 20 ppm

146

Zn(NO₃)₂ + bpdan

147

ZnCl₂ + bpdan

27.163
34.555
49.617
50.519
122.502
124.485
138.305
149.230
159.960

148

Zn(ClO₄)₂ + bpdan

149

Zn(OTf)$_2$ + bpdan

24.353
33.235
34.590
48.450
48.802
50.934
52.055
123.996
124.489
126.182
127.131
141.431
142.470
148.827
149.622
161.696

150
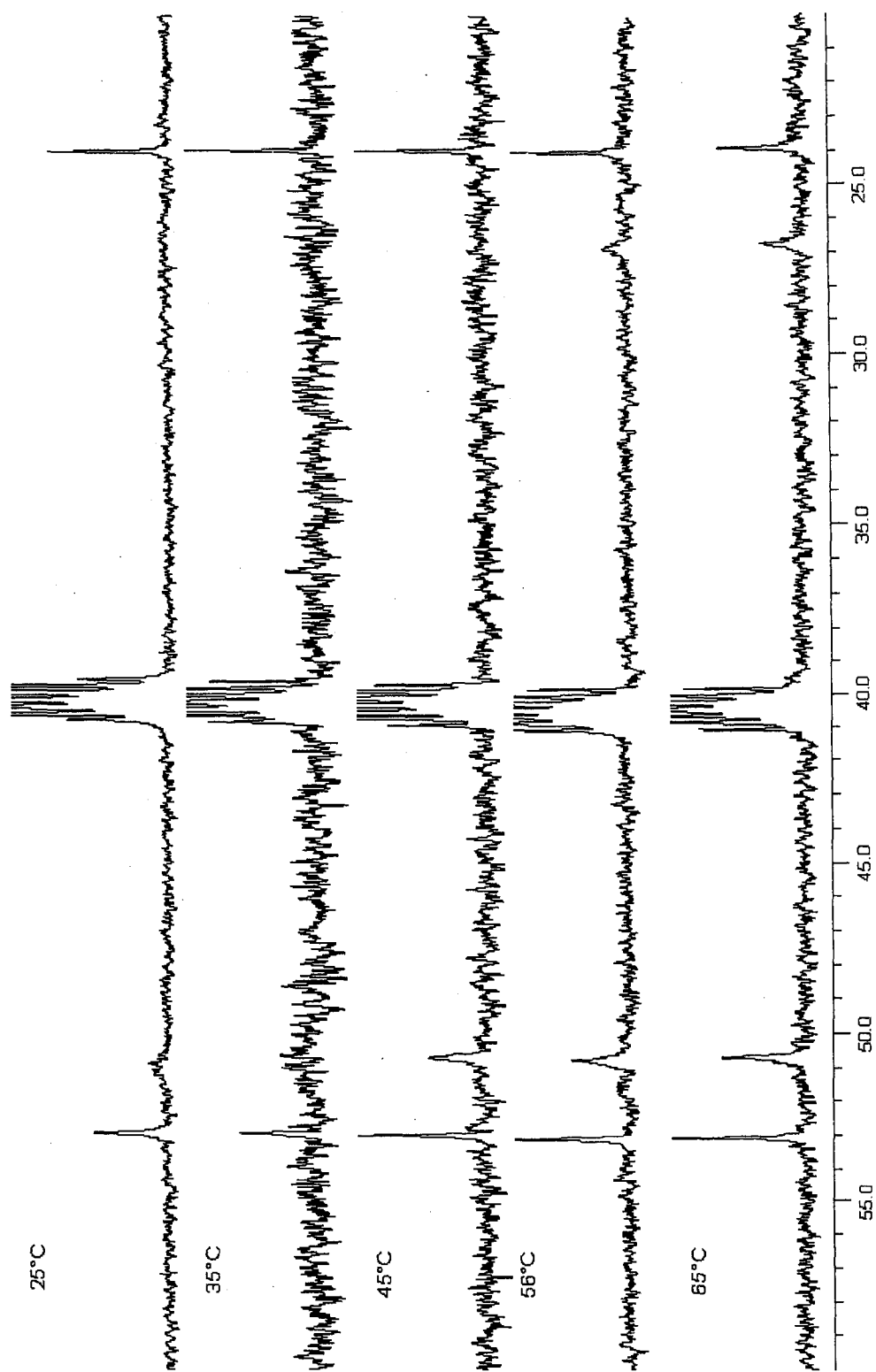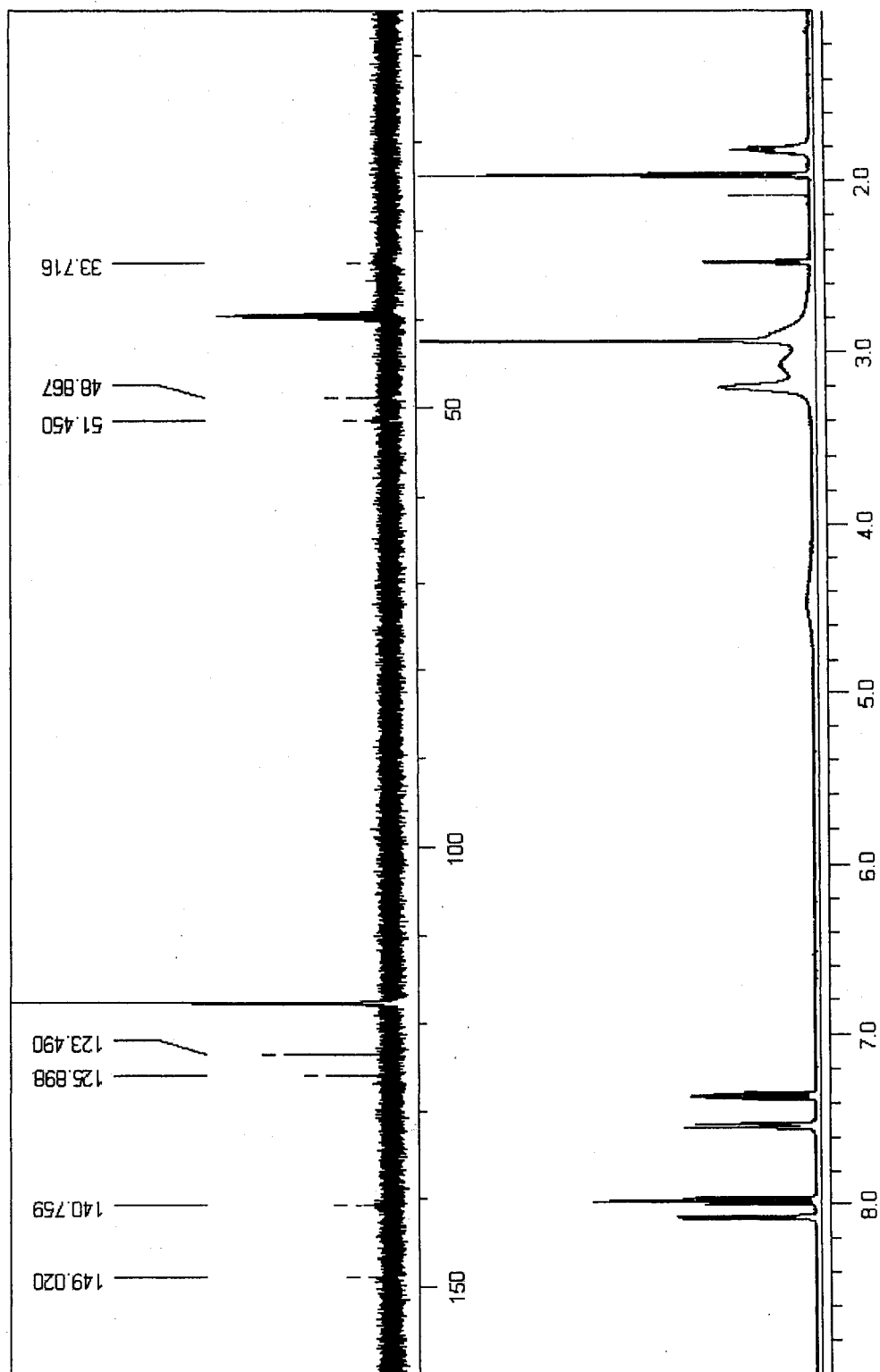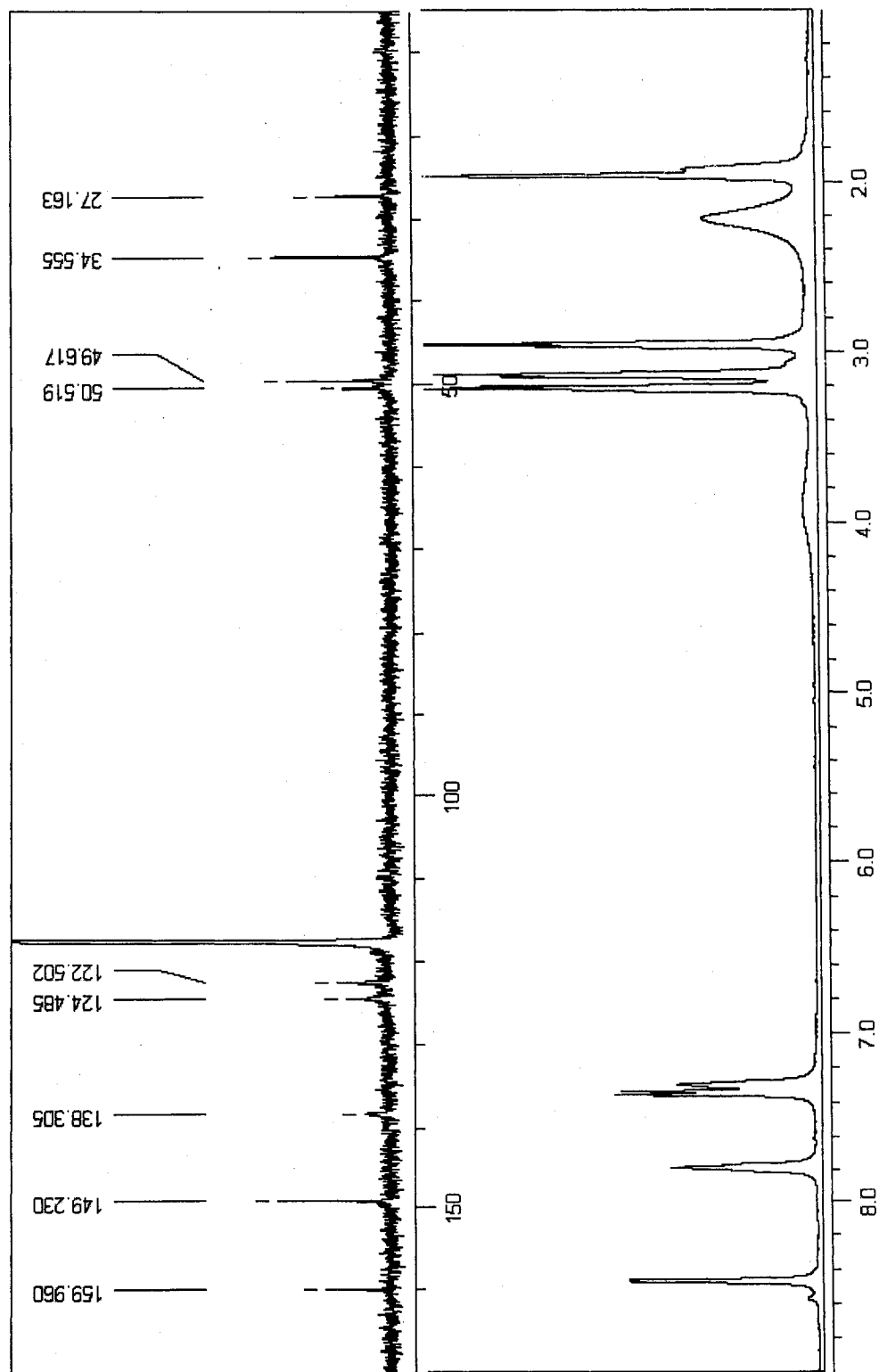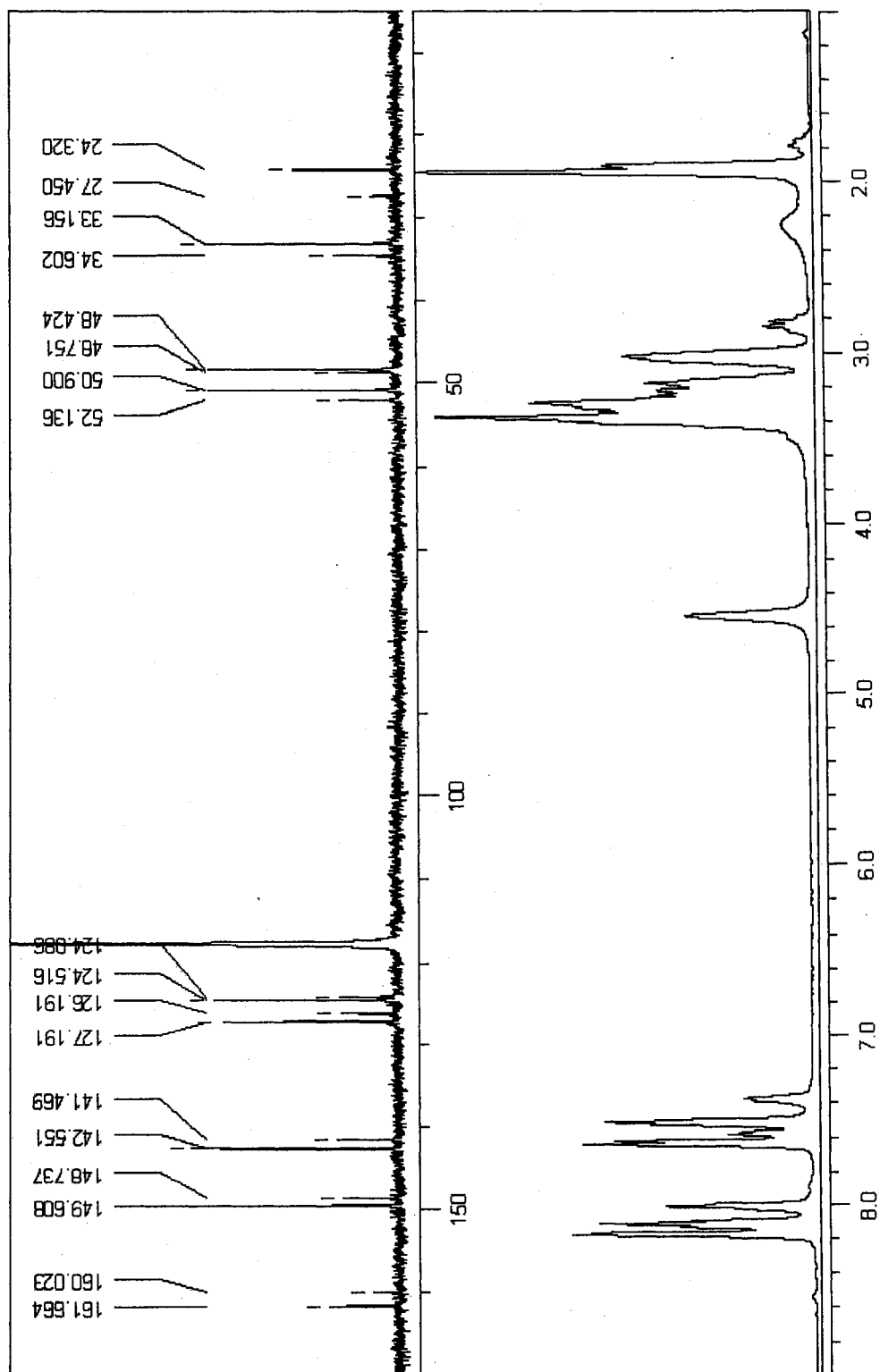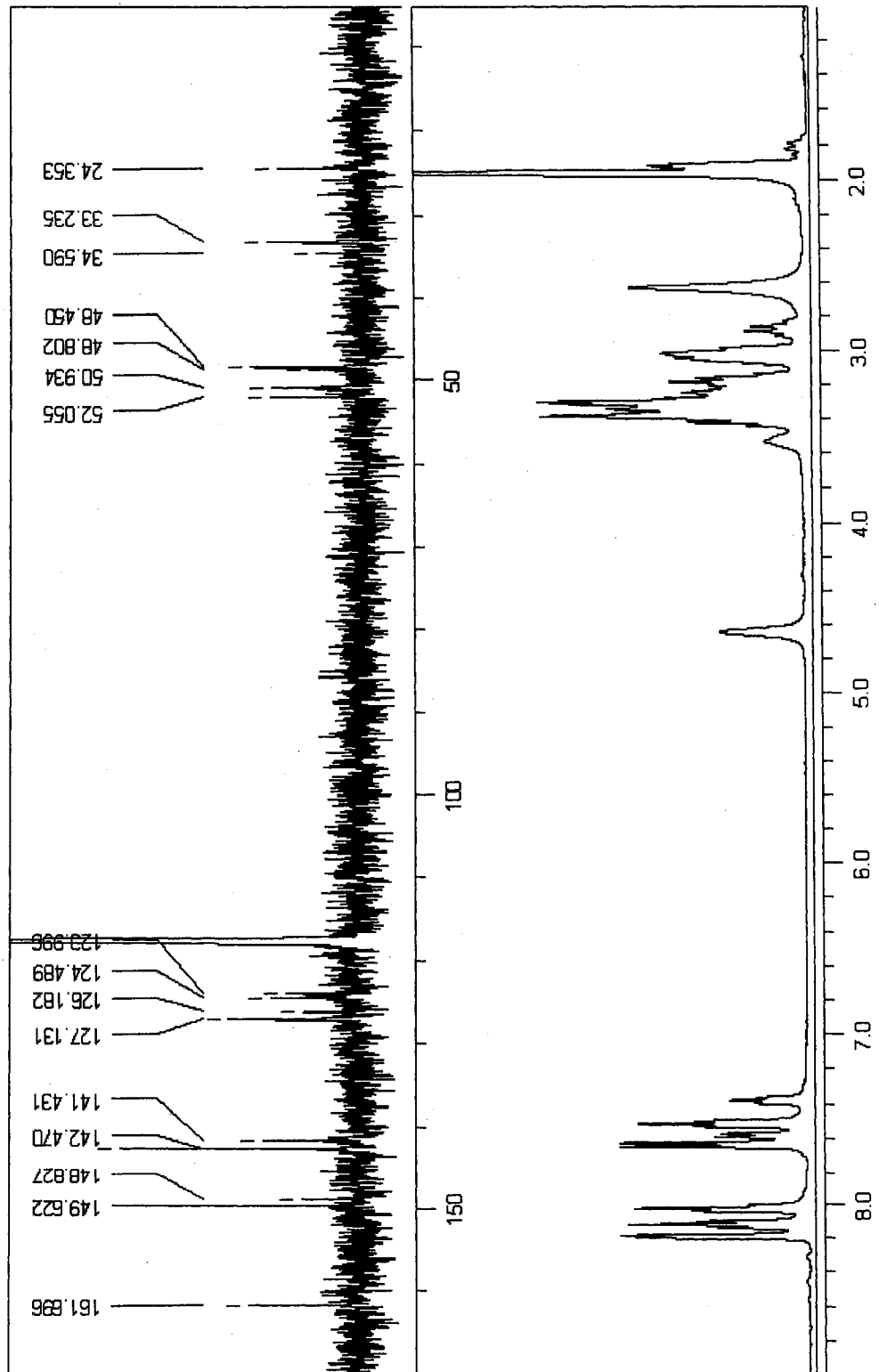
APPENDIX C: X-Ray Data Tables

151

	[Fe(tach-3-Mepyr)]Cl$_2$•1.5H$_2$O	[Fe(tach-6-Mepyr)](ClO$_4$)$_2$•H$_2$O•MeOH
Formula	C$_{29.50}$H$_{46}$Cl$_2$FeN$_6$O$_{2.50}$	C$_{55}$H$_{75}$Cl$_4$Fe$_2$N$_{12}$O$_{18}$
M$_w$	651.47	1445.77
Crystal system	monoclinic	triclinic
Space group	$P2_1/n$	P-1
a [Å]	10.9853(7)	9.5245(9)
b [Å]	13.5083(8)	17.4908(17)
c [Å]	21.1005(13)	19.0395(19)
α [°]	90	96.239(2)
β [°]	91.1420(10)	95.334(2)
γ [°]	90	95.093(2)
V [Å^3]	3130.5(3)	3123.7(5)
Z	4	4
Color	amber	dichroic/red plates
Crystal shape	block	plate
Crystal dimensions [mm^3]	0.25 x 0.25 x 0.20	0.40 x 0.30 x 0.08
D$_{calcd.}$ [gcm^{-3}]	1.382	1.924
μ [mm^{-1}]	0.692	1.383
λ [Å]	0.71073	0.71073
Refl. collected/unique	19145/7043	20964/12159
θ range [°]	1.79 – 28.19	1.69 – 26.00
Parameters	337	821
GOF	1.101	1.202
Final R indicies [$I > 2\sigma(I)$]	R = 0.0368 R_w = 0.0970	R = 0.0607 R$_w$ = 0.1648
$\Delta\rho_{max.}$ [eÅ^{-3}]	0.661	1.051

152

	[Fetach-3-Mepyr-ox-4)](PF$_6$)$_2$	[Zn(bispicpn)(NO$_3$)]NO$_3$
Formula	C$_{27}$H$_{32}$F$_{12}$FeN$_6$P$_2$	C$_{15}$H$_{20}$N$_6$O$_6$Zn
M$_w$	786.38	445.74
Crystal system	orthorhombic	monoclinic
Space group	Pca2(1)	P2(1)/c
a [Å]	14.003(6)	8.5671(6)
b [Å]	14.302(6)	26.0444(19)
c [Å]	15.046(6)	16.1609(12)
α [°]	90	90
β [°]	90	91.8990(10)
γ [°]	90	90
V [Å^3]	3013(2)	3603.9(5)
Z	4	8
Color	dark blue	colorless
Crystal shape	plate	cube
Crystal dimensions [mm^3]	0.15 x 0.15 x 0.07	0.30 x 0.30 x 0.20
D$_{calcd.}$ [gcm^{-3}]	1.733	1.643
μ [mm^{-1}]	0.714	1.411
λ [Å]	0.71073	0.71073
Refl. collected/unique	6881/6881	30804/8384
θ range [°]	2.44 – 28.22	1.48 – 28.20
Parameters	436	521
GOF	1.095	1.036
Final R indicies [$I > 2\sigma(I)$]	R = 0.0443 R$_w$ = 0.0894	R = 0.0328 R_w = 0.0809
$\Delta\rho_{max.}$ [eÅ^{-3}]	0.452	1.299

153

	[Zn(bis-6Mepicpn)(NO$_3$)]NO$_3$	[Zn(bpdan)(NO$_3$)]NO$_3$
Formula	C$_{17}$H$_{24}$N$_6$O$_6$Zn	C$_{17}$H$_{24}$N$_6$O$_6$Zn
M$_w$	473.81	473.79
Crystal system	monoclinic	triclinic
Space group	C2/c	P-1
a [Å]	23.758(4)	7.8064(7)
b [Å]	10.8160(18)	8.1160(7)
c [Å]	16.651(3)	15.8402(14)
α [°]	90	94.172(2)
β [°]	100.664(3)	100.8670(10)
γ [°]	90	94.383(2)
V [Å^3]	4182.1(12)	978.80(15)
Z	8	2
Color	colorless	colorless
Crystal shape	prism	prism
Crystal dimensions [mm^3]	0.20 x 0.20 x 0.20	0.10 x 0.10 x 0.10
D$_{calcd.}$ [gcm^{-3}]	1.505	1.608
μ [mm^{-1}]	1.221	1.304
λ [Å]	0.71073	0.71073
Refl. collected/unique	14313/4950	11845/4424
θ range [°]	2.08 – 28.28	2.53 – 27.97
Parameters	273	271
GOF	1.032	1.066
Final R indicies [$I > 2\sigma(I)$]	R = 0.0381	R = 0.0409
	R$_w$ = 0.1002	R$_w$ = 0.1085
$\Delta\rho_{max.}$ [eÅ^{-3}]	0.772	1.984

154